

SCIENCE OF TSUNAMI HAZARDS

Journal of Tsunami Society International

Volume 32

Number 4

2013

METHOD FOR THE ESTIMATION OF TSUNAMI RISK ALONG RUSSIA's FAR EAST 212

G. V. Shevchenko, D. E. Zolotukhin, I. N. Tikhonov

Institute of Marine Geology and Geophysics FEB RAS, Yuzhno-Sakhalinsk, RUSSIA

LATE HOLOCENE TSUNAMI DEPOSITS AT SALT CREEK, WASHINGTON, USA 221

Ian Hutchinson - Geography, Simon Fraser University, Burnaby, BC, **CANADA**

Curt D. Peterson - Geology, Portland State University, Portland, OR, **USA**

Sarah L. Sterling - Anthropology, Portland State University, Portland, OR, **USA**

A CRITICAL REVIEW AND EVALUATION OF APPLYING SEMI-VOLATILE ORGANIC COMPOUNDS (SVOCS) AS A GEOCHEMICAL TRACER TO INDICATE TSUNAMI BACKWASH: The Bilateral, Deutsche Forschungsgemeinschaft (DFG) and National Research Council of Thailand (NRCT) Funded Project "Tsunami Deposits in Near-Shore- and Coastal Waters of Thailand (TUNWAT)" 236

Siwatt Pongpiachan - *NIDA Center for Research & Development of Disaster Prevention & Management, School of Social and Environmental Development, National Institute of Development Administration (NIDA), 118 Moo-3, Sereethai Road, Klong-Chan, Bangkok, Bangkok 10240 THAILAND*

Klaus Schwarzer - *Institute of Geosciences Sedimentology, Coastal and Continental Shelf Research, Christian Albrechts University Kiel, Otto Hahn Platz 1, D - 24118 Kiel, GERMANY*

MARINE CONGLOMERATE AND REEF MEGACLASTS AT MAURITUS ISLAND: Evidence of a tsunami generated by a flank collapse of the PITON DE LA Fournaise volcano, Reunion Island? 281

R. Paris^{1,2}, K. Kelfoun^{1,2}, T. Giachetti³

¹*Clermont Université, Université Blaise Pascal, BP 10448, F-63000 Clermont-Ferrand, FRANCE*

²*CNRS, UMR 6524, Magmas et Volcans, F-63038 Clermont-Ferrand, FRANCE*

³*Department of Earth Science, Rice University, Houston, TX 77005, USA*

Copyright © 2013 - TSUNAMI SOCIETY INTERNATIONAL

WWW.TSUNAMISOCIETY.ORG

TSUNAMI SOCIETY INTERNATIONAL, 1741 Ala Moana Blvd. #70, Honolulu, HI 96815, USA.

SCIENCE OF TSUNAMI HAZARDS is a CERTIFIED OPEN ACCESS Journal included in the prestigious international academic journal database DOAJ, maintained by the University of Lund in Sweden with the support of the European Union. SCIENCE OF TSUNAMI HAZARDS is also preserved, archived and disseminated by the National Library, The Hague, NETHERLANDS, the Library of Congress, Washington D.C., USA, the Electronic Library of Los Alamos, National Laboratory, New Mexico, USA, the EBSCO Publishing databases and ELSEVIER Publishing in Amsterdam. The vast dissemination gives the journal additional global exposure and readership in 90% of the academic institutions worldwide, including nation-wide access to databases in more than 70 countries.

OBJECTIVE: Tsunami Society International publishes this interdisciplinary journal to increase and disseminate knowledge about tsunamis and their hazards.

DISCLAIMER: Although the articles in SCIENCE OF TSUNAMI HAZARDS have been technically reviewed by peers, Tsunami Society International is not responsible for the veracity of any statement, opinion or consequences.

EDITORIAL STAFF

Dr. George Pararas-Carayannis, Editor
<mailto:drgeorgepc@yahoo.com>

EDITORIAL BOARD

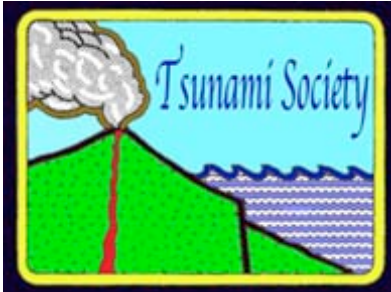
Dr. Charles MADER, Mader Consulting Co., Colorado, New Mexico, Hawaii, USA
Dr. Hermann FRITZ, Georgia Institute of Technology, USA
Prof. George CURTIS, University of Hawaii -Hilo, USA
Dr. Tad S. MURTY, University of Ottawa, CANADA
Dr. Zygmunt KOWALIK, University of Alaska, USA
Dr. Galen GISLER, NORWAY
Prof. Kam Tim CHAU, Hong Kong Polytechnic University, HONG KONG
Dr. Jochen BUNDSCHUH, (ICE) COSTA RICA, Royal Institute of Technology, SWEDEN
Dr. Yurii SHOKIN, Novosibirsk, RUSSIAN FEDERATION

TSUNAMI SOCIETY INTERNATIONAL, OFFICERS

Dr. George Pararas-Carayannis, President;
Dr. Tad Murty, Vice President;
Dr. Carolyn Forbes, Secretary/Treasurer.

Submit manuscripts of research papers, notes or letters to the Editor. If a research paper is accepted for publication the author(s) must submit a scan-ready manuscript, a Doc, TeX or a PDF file in the journal format. Issues of the journal are published electronically in PDF format. There is a minimal publication fee for authors who are members of Tsunami Society International for three years and slightly higher for non-members. Tsunami Society International members are notified by e-mail when a new issue is available. Permission to use figures, tables and brief excerpts from this journal in scientific and educational works is granted provided that the source is acknowledged.

Recent and all past journal issues are available at: <http://www.TsunamiSociety.org> CD-ROMs of past volumes may be purchased by contacting Tsunami Society International at postmaster@tsunamisociety.org Issues of the journal from 1982 thru 2005 are also available in PDF format at the U.S. Los Alamos National Laboratory Library <http://epubs.lanl.gov/tsunami/>



**A METHOD FOR THE ESTIMATION OF TSUNAMI RISK
ALONG RUSSIA'S FAR EAST**

G.V. Shevchenko, D. E. Zolotukhin, I. N. Tikhonov

Institute of Marine Geology and Geophysics FEB RAS, Yuzhno-Sakhalinsk, Russia

ABSTRACT

A simplified method was developed for estimating the tsunami risk for a coast for possible events having recurrence periods of 50 and 100 years. The method is based on readily available seismic data and the calculation of magnitudes of events with specified return periods. A classical Gumbel statistical method was used to estimate magnitudes of small probability events. The tsunami numerical modeling study used the average earthquake coordinates in the Kuril-Kamchatka high-seismic area. The verification and testing of the method were carried out using events from the North, Middle and South Kuril Islands – the most tsunami-risk areas of Russia's Far East. Also, the study used the regional Kuril-Kamchatka catalogue of earthquakes from 1900 to 2008 - which included earthquakes with magnitudes of at least $M=6$. The results of the study indicate that the proposed methodology provides reasonable estimates of tsunami risk.

Keywords: *tsunami risk, earthquake, magnitude, numerical modeling*

1. INTRODUCTION

As demonstrated by the tsunami of March 11, 2011, which had disastrous consequences for the northeast coast of Honshu, the risk of tsunami should be properly taken into account when planning of coastal areas development. Even a very good job of a tsunami warning service and a high degree of organization of the population did not help to avoid significant losses of life. This example shows the importance of reliable tsunami risk estimation - the calculation of possible tsunami heights with return periods of 50, 100 or another number of years.

Usually to get the reliable estimates of tsunami risk for the given stretch of the coast we need to conduct the expeditionary survey to assess the run-up heights of historical tsunamis (KAISTRENKO, 2011). The probability regional model of tsunami activity in the given area can be built on the base of these historical data. Numerical simulation of the strongest tsunami in the area required estimating the tsunami risk for the points in which historical data are absent or little. This method gives the reliable results, but it requires a lot of money and time. At the same time, it is often necessary to obtain quick preliminary estimates, although not that reliable.

As the simplified estimation of tsunami heights for the specified return period (H_T for return period of T years) we can take the results of numerical simulations with the corresponding earthquake parameters: estimated magnitude M_T for a given return period, the average focal depth and epicenter coordinates. This approach is based on the assumption of a linear relationship between the tsunami height at the source and magnitude of earthquakes, which is justified for the task.

2. METHODOLOGY

To solve a problem of preliminary tsunami risk estimates, the simplified method of tsunami risk estimation for the coast is developed. The method is based on the easily available seismological data and calculation of magnitudes for the specified return periods. A classical Gumbel (1962) statistical method was used to estimate magnitudes of small probability events. This method is based on a double exponential distribution:

$$1 - P(\dot{I}) = \exp(-\exp(-y)) \quad (1)$$

where $P(M)$ is a probability of exceeding the magnitude M , and y is the reduced variable, which is associated with the magnitude of the linear

$$\dot{I} = a y + b \quad (2)$$

or nonlinear dependence

$$y = k(\ln(v-\omega) - \ln(\omega-M)). \quad (3)$$

where k , v , and ω -unknown parameters to be determined from the observed values of M_i and their corresponding values of the reduced variable y_i . Here ω is the limiting magnitude that cannot be exceeded.

We analyzed the earthquake with a magnitude of at least 6.5, the weaker events of no interest for the problem of tsunami generation. Empirical probabilities for the ordered ascending series of magnitudes were determined by the modified Weibull formula (GUMBEL, 1962):

$$1 - P_i = iN / T(N + 1), \quad (4)$$

where N - the length of the data set, i - number of the magnitude in the ordered series, T - period of observations (in years).

In the case of linear dependence, the parameters a and b are determined by the least squares method. In the nonlinear case, we used an iterative procedure for determining the parameters of the distribution. First, we set the initial value of the limiting magnitude ω_1 ; values v_1 and k_1 can be determined by the least squares method from the resulting system of equations. Then for these values a new limiting magnitude ω_2 is calculated, etc. With the reasonable initial value, the iterative procedure converges rapidly.

For the series of the strongest earthquakes in each region, the average values of latitude φ and longitude λ of the epicenter were determined. It is possible to use these values as the source coordinates in the study area for tsunami numerical modeling. The standard deviations of epicenter coordinate σ_φ and σ_λ were also calculated, we used these values for the tsunami source shifting $\{\varphi \pm \sigma_\varphi; \lambda \pm \sigma_\lambda\}$ for two additional variants of numerical simulations. As a final assessment, we selected for each coastal point the maximum tsunami height from the three variants of the calculations, considering them equiprobable.

The method was tested on the example of the high-seismic areas adjacent to North, Middle and South Kuril Islands – the most tsunami-risk areas of the Russia's Far East (the location of these areas and epicenters of historical tsunamigenic earthquakes are shown in Fig. 1).

For the North and South Kuril Islands the maps of tsunami risk were constructed as previously (KAISTRENKO ET AL, 2009). This allows us to compare the results of our method with more precise estimations. For non-populated Middle Kuril islands the tsunami risk was not estimated.

The regional Kuril-Kamchatka catalogue of strong earthquakes for the period of 1900-2008 years (which included earthquakes with a magnitude of at least 6) was used.

2.1 Numerical modeling

We used a nonlinear shallow-water finite difference tsunami model by V.N. Kharmushin (POPLAVSKY, KHRAMUSHIN, 2008). The length of the fault and source length and width (axis of ellipse) are expressed through the magnitude M and focal depth of earthquakes h_0 as

$$L \text{ (km)} = 0.5 M - 1.8; \quad a \text{ (km)} = L/2 + h_0, \quad b \text{ (km)} = h_0. \quad (5)$$

Initial tsunami height in the center of the source we can find from the equation

$$\lg \xi = 0.97 (1.5M - 4.5 \lg h_0 - 4.45), \quad (6)$$

which is the empirical formula based on the statistical analysis of Kuril earthquakes. The typical focal depth of tsunamigenic earthquakes in the high-seismic Kuril-Kamchatka area equals $h_0=36$ km (POPLAVSKY, KHRAMUSHIN, 2008).

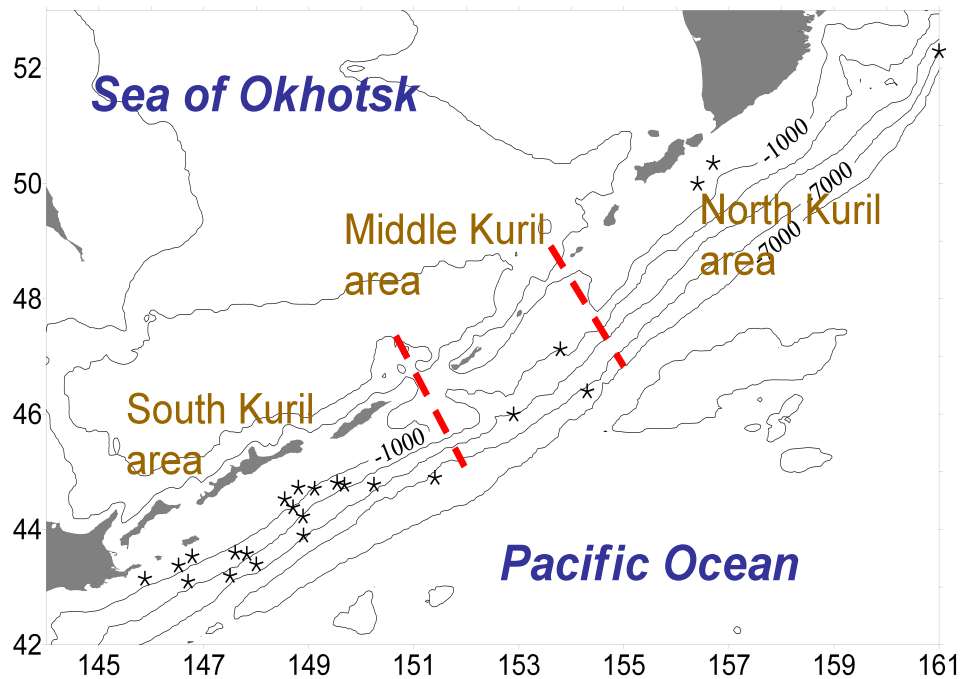


Figure 1. The location of the North, Middle and South Kurile areas. The epicenters of the strong tsunamigenic earthquakes in each area are marked by stars.

3. RESULTS AND DISCUSSION

For the area adjacent to the North Kurile Islands the linear function was well consistent with the empirical distribution of extreme magnitude (Fig. 2). The magnitude for return period 100 years equals 8.2. The magnitude of Great Kamchatka earthquake of November 5, 1952 ($M=8.5$) corresponds to return period about 200 years. According to magnitude $M_{100}=8.2$ and focal depth $h_0=36$, the length of the source equals 272 km (width=72 km), initial height $\xi=6.6$ m (Fig. 3). The calculated maximal tsunami heights 9 -11 m were obtained on the coast of the Second Kuril Strait (the results for the central position of the source are shown in Fig. 3). This is the most tsunami dangerous (and most populated) stretch of the coast in the North Kuril Islands; there is no settlement in the present time on the safe Okhotsk Sea Coast of Paramushir Island. Another area of relatively high tsunami risk (obtained for the southwestern position of the source) is located on the southeastern coast of the Island. These results are well consistent with more precise estimations (KAISTRENKO ET AL, 2009).

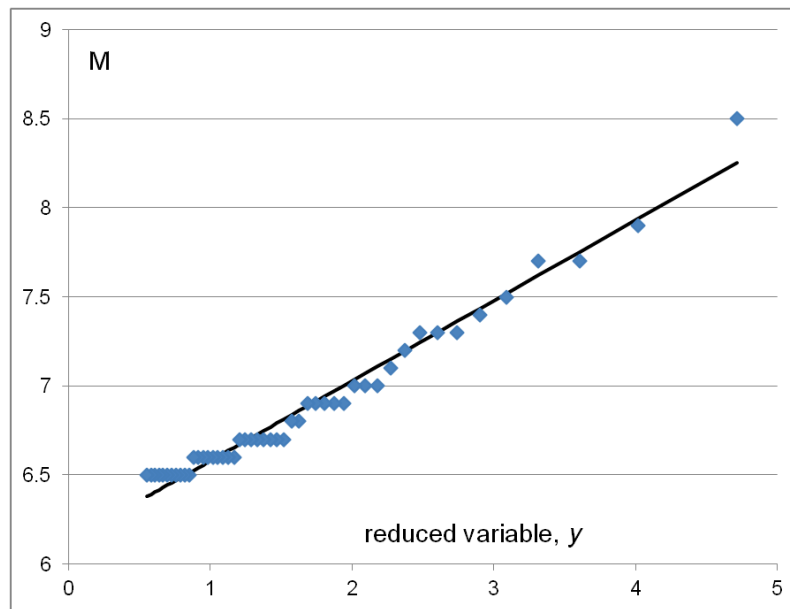


Figure 2. The empirical distribution of earthquake magnitudes and its approximation by linear dependence (2) for the area adjacent to the North Kuril Islands.

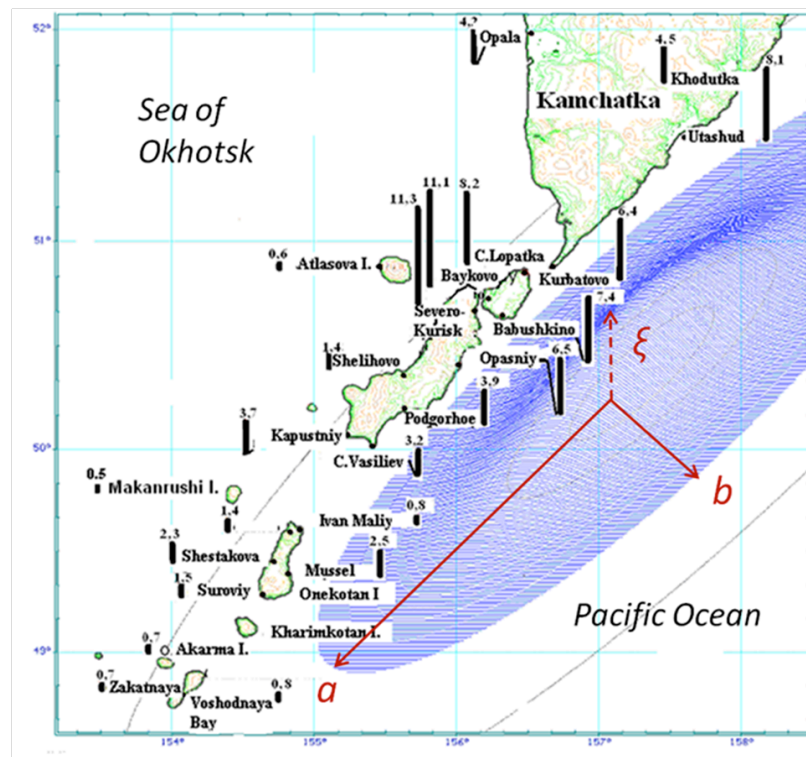


Figure 3. The central location of tsunami source and calculated tsunami heights on the coasts of North Kuril Islands and the southern part of Kamchatka Peninsula.

For the area adjacent to the Middle Kurile Islands the linear function was well consistent with the empirical distribution of extreme magnitude too (Fig. 4). The magnitude for return period of 100 years equals 8.1. This value corresponds to magnitude of strongest Simushir January 13, 2007 earthquake. According to $M_{100}=8.1$ and typical focal depth $h=36$ km, the length of the source equals 248 km and the initial height $\xi=5.4$ m. The calculated maximal tsunami heights 7 - 9 m were obtained on the coast of Simushir, Matua, and Ketoy Islands (Fig. 5a). The maximal historical tsunamis run-up of 12-15 m was found in the same areas after the Great Simushir tsunami of November 15, 2006 (LEVIN ET AL, 2008). However we think that we obtained reasonable results because this tsunami was unusually strong for the magnitude $M=8$ earthquake (some researchers have attributed the unusual intensity of the tsunami with an underwater landslide).

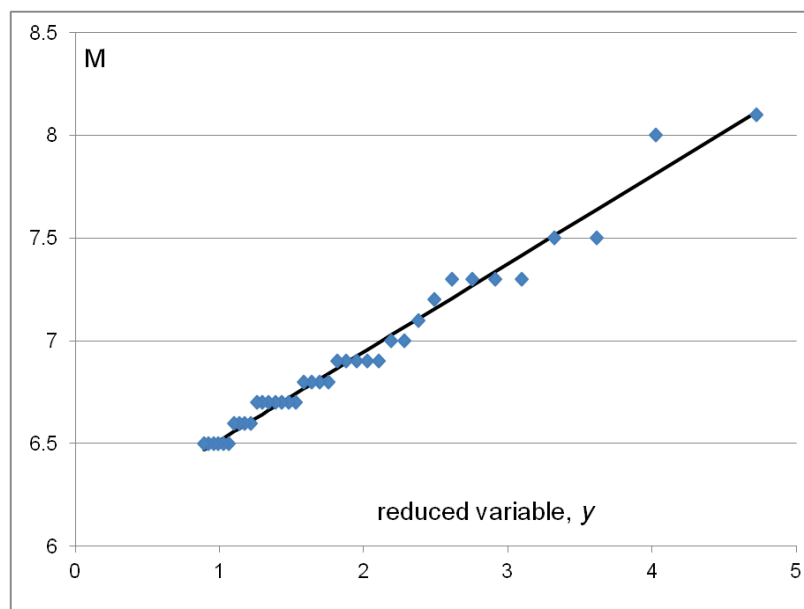


Figure 4. The empirical distribution of earthquake magnitudes and its approximation by linear dependence (2) for the area adjacent to the Middle Kuril Islands.

For the area adjacent to the South Kurile Islands the nonlinear function corresponds to empirical distribution of extreme magnitude, the magnitude for return period 100 years equals 8.3 ($M_{100}=8.5$ for liner model). According to $M=8.3$ and typical focal depth $h=36$ km, the length of the source equals 296, the initial height $\xi=9.2$ m.

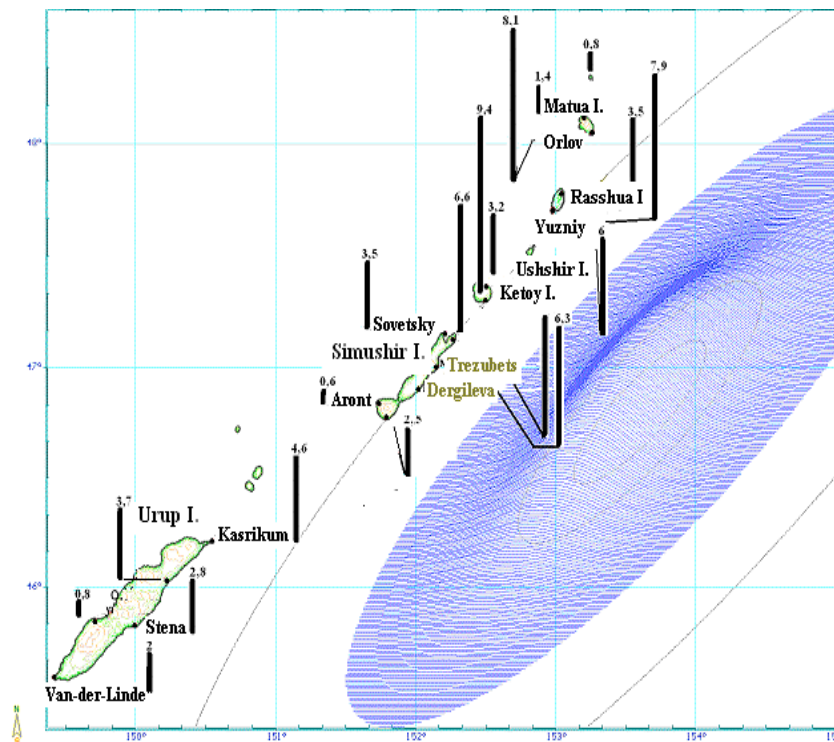


Figure 5a. The central position of tsunami source and spatial distribution of calculated tsunami heights on the coasts of the Middle Kuril Islands.

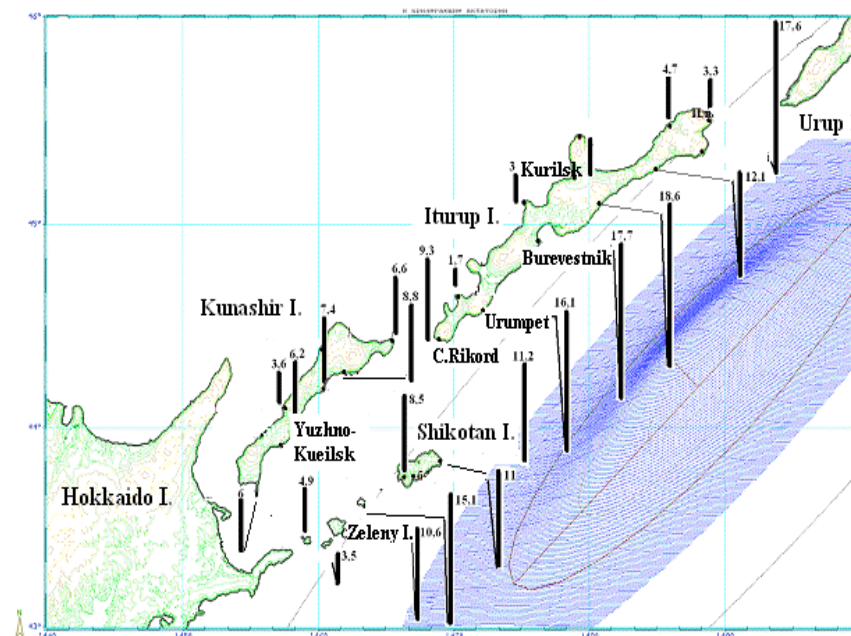


Figure 5b. The central position of tsunami source and spatial distribution of calculated tsunami heights on the coasts of the South Kuril Islands.

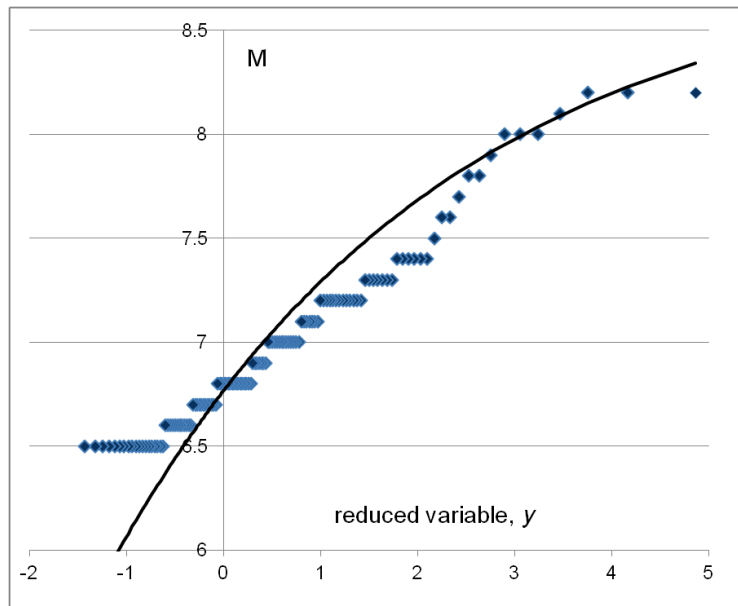


Figure 6. The empirical distribution of earthquake magnitudes and its approximation by nonlinear dependence (3) for the area adjacent to the South Kuril Islands.

To the Pacific coast of Iturup Island the estimated tsunami height were 16-18 m (Fig. 5b), which is significantly higher than for a more accurate method (KAISTRENKO, 2009) (8-10 m). The reason for this overestimation is the fact that earthquakes with $M = 8.3$ in the South Kuril Islands were not observed during the analyzed period. In addition, the sources of the strongest tsunami were not located in front of Iturup Island as in our model. The calculated maximal tsunami heights 15 -18 m for oceanic coast of Shikotan Island seems quite reasonable and realistic.

4. CONCLUSIONS

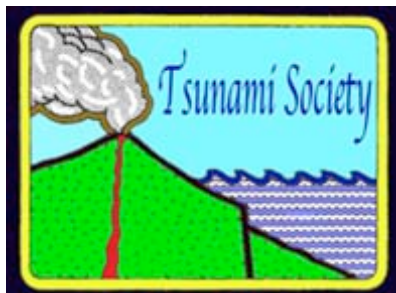
For the area adjacent to the North Kuril Islands, the linear function was determined to be in good agreement with the empirical distribution of extreme magnitude. The magnitude for return period 100 years equals 8.2. The calculated maximal tsunami heights 9 - 11 m were obtained for coastal areas bordering the Second Kuril Strait. This stretch of the coast is most vulnerable to tsunamis because of its higher population density. For area adjacent to the South Kuril Islands, the nonlinear function corresponds to empirical distribution of extreme magnitude. The magnitude for return period 100 years equals 8.3. For the Pacific Ocean coasts of Iturup and Shikotan Islands, the maximal tsunami heights were calculated to range from 15-to18 m. In summary, the calculations showed that reasonable estimates of tsunami risk can be obtained under the proposed approach.

5. ACKNOWLEDGEMENTS

This study was supported by a grant of the Russian Academy of Sciences (Far East Branch – Siberian Branch) No 12-II-0-08-003.

REFERENCES

- GUMBEL, E. (1962). Statistics of extremes, Columbia University press, New York, USA.
- KAISTRENKO, V. (2011). Tsunami recurrence versus tsunami height distribution along the coast // *Pure Appl. Geophys*, **168**, 2065-2069.
- KAISTRENKO, V., ZOLOTUKHIN, D. AND KHRAMUSHIN, V. (2009). Tsunami Zoning. Atlas of the Kuril Islands (ed. by N. Komedchikov), Russian Academy of Sciences press, Moscow-Vladivostok, 39-43. (in Russian)
- POPLAVSKY, A.A. AND KHRAMUSHIN, V.N. (2008). The methods of real-time tsunami and storm surge forecast. Dalnauka, Vladivostok, Russia (in Russian).



SCIENCE OF TSUNAMI HAZARDS

Journal of Tsunami Society International

Volume 32

Number 4

2013

LATE HOLOCENE TSUNAMI DEPOSITS AT SALT CREEK, WASHINGTON, USA

Ian Hutchinson

Geography, Simon Fraser University, Burnaby, BC, CANADA

Curt D. Peterson

Geology, Portland State University, Portland, OR, USA

Sarah L. Sterling

Anthropology, Portland State University, Portland, OR, USA

ABSTRACT

We interpret two thin sand layers in the estuarine marsh at Salt Creek, on the southern shore of the Strait of Juan de Fuca, as the products of tsunamis propagated by earthquakes at the Cascadia subduction zone. The sand layers extend for about 60 m along the left bank of the creek about 800 m from the mouth, and can be traced to the base of a nearby upland area. One layer is exposed in the creek bank about 400 m further upstream, but they are only patchily distributed in the rest of the central area of the marsh. Both layers contain brackish-marine epipsammic diatoms. The lower sand layer marks a sharp contact between intertidal peaty mud and overlying mud, perhaps reflecting modest coseismic subsidence in association with tsunami deposition, but little or no change in the bracketing sediment occurs in association with the upper sand layer. The ages of the sand layers are not closely constrained, but were most likely deposited by tsunamis generated by great earthquakes at the Cascadia subduction zone about 1650 and 1300 years ago. The Cascadia great earthquake of AD1700 may have induced slight subsidence in the marsh, but no tsunami deposit was detected at the inferred contact. The absence of deposits from the marsh immediately inland of the 4 m-high barrier beach indicates that the largest tsunamis in the late Holocene at this site have not overtopped the barrier, which suggests that these tsunamis were likely only 2-3 m high.

Key words: *tsunami deposits, diatoms, Cascadia subduction zone, Strait of Juan de Fuca, Washington*

1. INTRODUCTION

The geological characterization of the deposits left by prehistoric tsunamis has become one of the principal tools for assessing tsunami risk in susceptible areas. Mapping and analysis of the deposits can be used to establish the spatial extent of inundation, the height of wave run-up, the current velocity, and the frequency of occurrence of these hazards at a coastal site. In areas where few historical tsunamis have occurred these deposits serve as warnings, alerting local residents, in Weiss and Bourgeois' (2012) words, to the fact that "it can and has happened here".

The Cascadia subduction zone (extending from Cape Mendocino in northern California to Vancouver Island; Fig. 1A) is one area where the absence of major tsunamis during the historical period (AD 1778 —) engendered a false sense of security amongst coastal residents. Recent investigations of the distribution and character of palaeo-tsunami deposits in coastal marshes and near-shore lakes have revealed, however, that the shorelines of Cascadia are at considerable risk from tsunamis generated by ruptures at the interface of the Juan de Fuca and America plates (Fig. 1A).

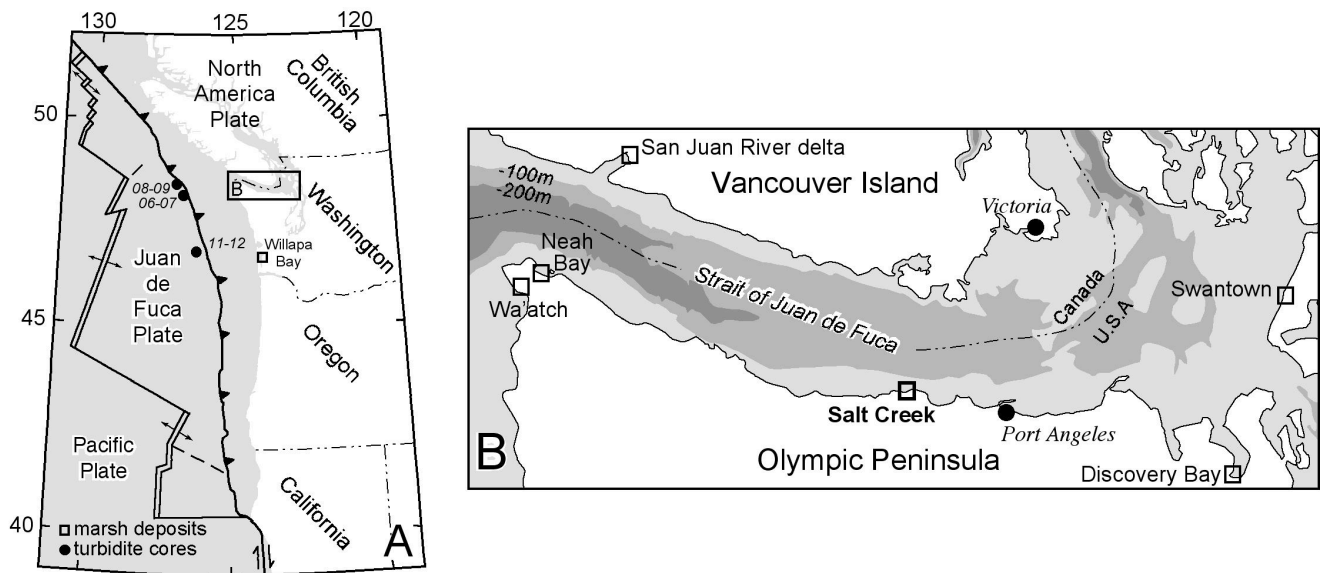


Fig. 1. (A) Major features of the Cascadia subduction zone, showing sites mentioned in the text, and (B) the Strait of Juan de Fuca, showing bathymetry and location of sites discussed in text. In A, the trace of the Cascadia thrust fault (dashed barbed line, barbs point down-dip) is placed at the bathymetric boundary between the continental slope and abyssal plain; double lines are spreading ridges, solid lines are strike-slip faults, and dashed lines are political boundaries.

Peters et al. (2003) listed 60 coastal sites in Cascadia that had been examined for evidence of tsunami inundation since the seismic potential of the Cascadia plate boundary was first recognized (Atwater, 1987; Heaton and Hartzell, 1987). The geographic distribution of these sites, however, is not uniform; whereas virtually all of the coastal marsh areas in southwestern Washington, Oregon and

California have been intensively investigated, and many of the marshes and lakes on the northwest and west-central coast of Vancouver Island have been examined, only a few sites (Williams and Hutchinson 2000, Williams et al. 2005, Peterson et al., 2013) have been investigated on the shores of the 160-km long Strait of Juan de Fuca, which connects the inland waters of Georgia Strait and Puget Sound to the Pacific Ocean (Fig. 1B).

In an attempt to remedy this situation, we describe the results of a search for paleotsunami deposits at an estuary on the southern shore of the strait, and place these results in the context of previous investigations of tsunami hazard in the region. We anticipate that these results will be of value in refining tsunami source models for the northern segment of the Cascadia subduction zone.

2. IDENTIFYING EPISODES OF COSEISMIC SUBMERGENCE AND PALEOTSUNAMI DEPOSITS

A variety of high-energy processes can leave anomalous elements in marsh deposits. Coarse-textured layers, such as sands or gravels, may be deposited by both fluvial and coastal processes. Material transported into a marsh by very large waves tends to have a characteristic sedimentary signature that distinguishes it from material left by river floods. Coarse layers left by tsunamis and storm surges tend to become finer and taper in thickness landward (Goto et al. 2012) and the number of layers diminishes landward as the inundation limit of individual events is passed. Moreover, these deposits commonly contain tell-tale microfossils reworked from offshore or neighboring beaches and tidal flats (Hemphill-Haley 1995, 1996). Distinguishing tsunami deposits from those left by storm surges is more difficult. Storms commonly leave thick washover deposits in the lee of overtopped beaches, and their deposits show more complex patterns of stratification than those of tsunamis (Morton et al. 2007, Peters and Jaffe 2010, Tuttle et al. 2004).

But the most compelling evidence of tsunami inundation is a layer of sand above a buried marsh soil that marks an episode of coseismic subsidence (e.g. Atwater 1997, Atwater et al. 2004). Plants growing in coastal marshes trap fine-grained sediment transported into the marsh by high tides. This material accumulates on the marsh surface, and the annual incorporation of decaying plant matter leads to the development of a peaty soil. If the subsidence accompanying a great earthquake locally exceeds about 0.5 m, the marsh surface may be lowered into the tidal flat zone, and the marsh soil is gradually buried by mud (e.g. Guilbault et al. 1996). A more modest amount of subsidence might lower the surface into the low marsh zone, characterized by the accumulation of slightly peaty mud. A regionally-coherent depositional sequence of buried marsh soils capped by mud layers (peat-mud couplets) is *prima facie* evidence of episodic coseismic deformation at subducting plate margins (Atwater 1997).

Not all the sandy layers at peat-mud contacts, however, are the products of tsunamis. Marsh deposits are commonly underlain by tidal flat sands, and these may be vented onto the marsh surface during major earthquakes. A liquefaction deposit may also contain marine microfossils, and can potentially be confused with tsunami-laid sands (Martin and Bourgeois 2012), particularly when sample cores are widely spaced.

3. STUDY SITE AND METHODS

The intertidal marsh at the mouth of Salt Creek on the south-central shore of the Strait of Juan de Fuca (48.16°N, 123.71°W; Fig 1B, 2A) currently occupies an area of about 22 ha. The marsh has developed in an intertidal embayment sheltered by a 4 m-high sandy barrier beach that is oriented WSW-ENE and is breached at its eastern end by the creek (Fig. 2B). Todd et al. (2006) note that the marsh was used as pasture in the decades following Euroamerican settlement, but disturbance was minor, and took the form of diking and ditching, particularly in the northwestern quadrant of the marsh.

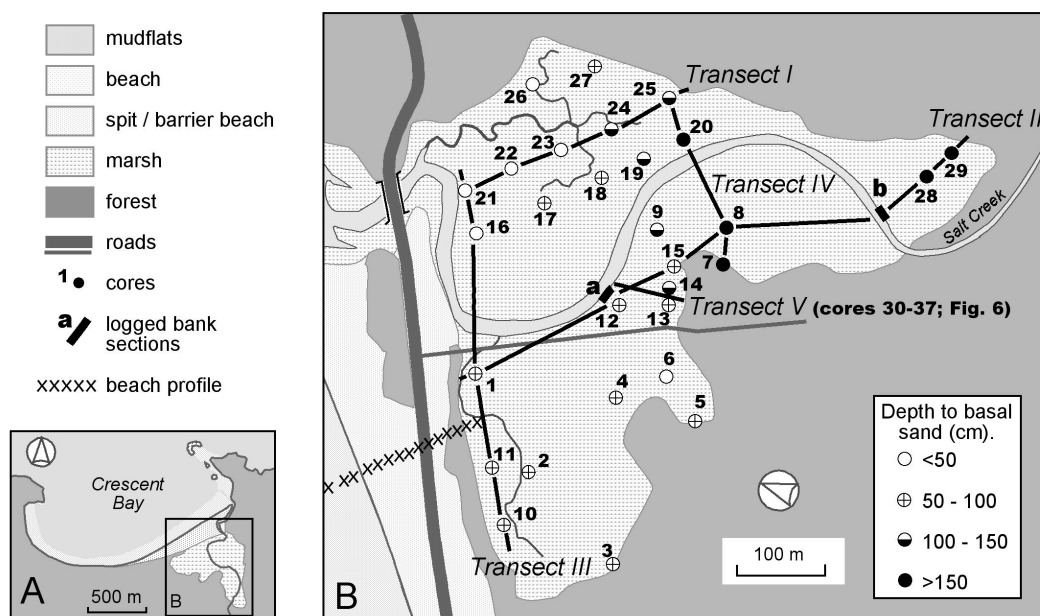


Fig. 2. (A) Salt Creek estuary and environs; (B) Salt Creek marsh, showing the location of core sites, the depth to basal sand in the cores and the location of the transects displayed in Figures 4 and 5.

We described the stratigraphy in the marsh deposits using a hand-driven gouge core (2m long, 2.5 cm wide) to retrieve samples, and examined exposures along the channel banks of Salt Creek for evidence of laterally continuous sand layers, focusing on two outcrops (Fig. 2B).

Three bench marks were established by RTK-GPS (± 5 cm) onsite. Core and bank outcrop locations were established by GPS using a Garmin 12-channel receiver with WASS real-time differential correction. A topographic profile was surveyed using a total station across the barrier beach and the eastern marsh to the upland margin. The barrier beach reaches a height of 4.0 m (NADV88 datum). The marsh surface lies just above MHHW in Crescent Bay, ranging in elevation from about 2.1 to 2.4 m at the core locations.

We collected samples of organic material (sticks, charcoal fragments, marsh peats) from cores and bank sections to date marsh initiation in the embayment and to constrain the age of paleotsunami

layers. Five samples were submitted to Beta Analytic for AMS dating. Conventional radiocarbon ages were calibrated with CALIB 6.0 using INTCAL09 data with the laboratory multiplier set to 1. The results (Table I) are rounded to the nearest decade.

Table I: AMS radiocarbon ages, Salt Creek marsh

core / outcrop	Depth (m)	Lab number (Beta-)	Material dated	14C age (yr BP)	Cal BP (2 sigma range)	significance
8	0.94	331750	plant material	940±30	930 — 790	rejected (root contamination)
a	0.60	355056	charcoal	1560±30	1530 — 1380	close maximum limiting age for upper sand at outcrop “a”
28	1.26	322473	peat	1590±30	1540 — 1410	maximum limiting age for marsh initiation near outcrop “b”
a	0.55	322471	peat	1790±30	1820 — 1620	maximum limiting age for upper sand at outcrop “a”
a	0.88	355055	stick	2330±30	2360 — 2330	maximum limiting age for marsh initiation and lower sand at outcrop “a”
a	0.69	322472	wood fragment	2440±30	2700 — 2360	maximum limiting age for lower sand at outcrop “a”

Samples for diatom analysis were collected from sand layers in the river bank and from a thick sand layer in one of the cores. A composite sample was taken from algal mats on sandy sediments in the vicinity of the mouth of the creek for comparative purposes. Organic matter in the samples was removed by H₂O₂ digestion. The remaining material was dispersed in 250 ml of distilled water, and, after repeated decanting and settling to remove fine sand to bring the solution to a near-neutral pH, aliquots of suspended material were dried on glass slides and mounted in Zrax. At least 300

specimens, or, in diatom-poor materials, the number of valves encountered on 10 random parallel traverses of the slide, were identified and counted for each sample (except the modern sample, which was qualitatively assessed). Identifications of taxa were principally based on descriptions in Hemphill-Haley (1993) and Witkowski (2000).

3.1 Paleoseismic and tsunami evidence at Salt Creek

River bank sections - Two thin but continuous layers of sand are readily evident on the left bank of Salt Creek, about 800 m from the mouth, as a result of etching by high tides. The sand layers extend from about 10 m downstream of site “a” to about 50 m upstream of the site (Fig. 3). They lie in the middle of the bank section, about 0.1 m apart (Fig. 4A). The sand layers are more-or-less horizontal, of uniform thickness, and display sharp contacts with the encasing fine-grained deposits (Fig. 4B).



Fig. 3. Left bank of Salt Creek upstream of riverbank section “a” (at right of photo). The two sand layers in the bank are visible as parallel etched lines [photo: Brian Atwater].

Along this section of the bank a basal channel or tidal flat sand at a depth of 1.2 m is sharply overlain by mud, with peaty mud and muddy peat phases becoming more prominent towards the top (Fig. 4A). The lower sand layer (at 0.7 m depth in the logged section) is underlain by a 3-cm thick layer of grayish-brown peaty mud, and overlain by a less peaty gray mud. The former likely represents an incipient high intertidal marsh, the latter a low marsh environment. The abrupt change from incipient high marsh to low marsh may signal a modest amount (<0.5 m) of submergence, either as a result of coseismic settling and compaction, or elastic tectonic subsidence.

There is a less pronounced change in the deposits bracketing the upper sand (at 0.6 m depth in the logged section), suggesting a smaller degree of coseismic subsidence. The only other potential subsidence event displayed in this section occurs at a depth of about 0.3 m, where a dark brown muddy peat is abruptly overlain by tan to yellowish brown mud, perhaps indicating a subsidence event equivalent to that recorded at in association with the lower sand layer.

Both sand layers were about 5 mm thick throughout this section of the river bank. Both were composed of fine to very fine sand. Their lateral extent and uniform thickness, and the absence of

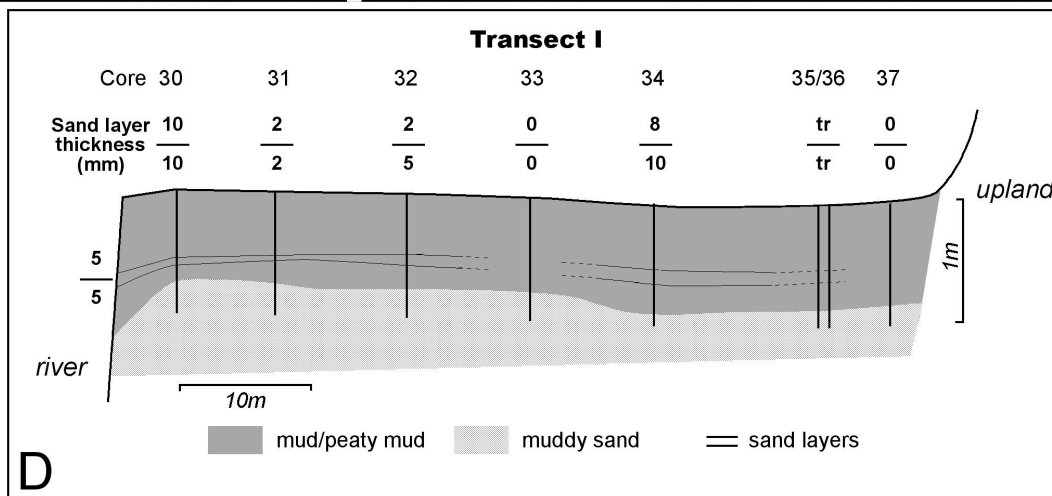
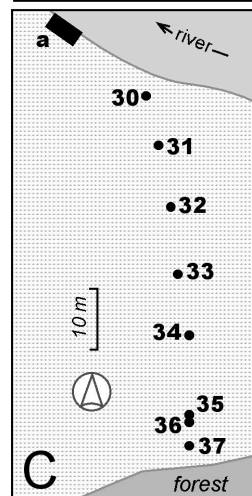
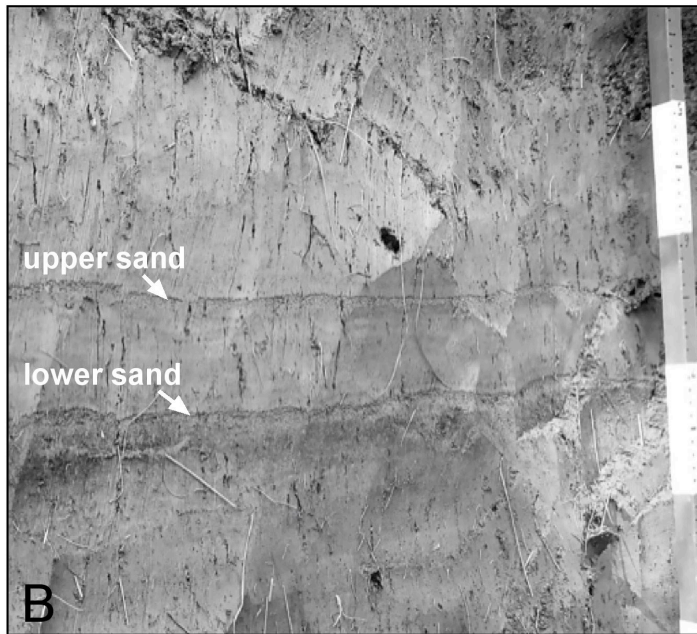
Figure 1 is a stratigraphic profile of the peat core from the Kamaishi Tidal Flat. The vertical axis represents Depth (m), ranging from 0.0 to 1.0+ meters. The core is divided into several layers, each with a distinct texture and color. The layers are labeled as follows:

- muddy peat (dark grey)
- peaty mud (medium grey)
- mud (light grey)
- muddy sand (dotted pattern)
- sand layer (horizontal lines)
- weathered *Triglochin* rhizomes (V-shaped symbols)
- tsunami sand (ts) (horizontal lines)

Radiocarbon dates (xxxx ± 30 ¹⁴C yr BP) are provided for specific depths:

- 1560 ± 30
- 1790 ± 30
- 2440 ± 30
- 2330 ± 30

A subsidence event is marked at approximately 0.35m depth. The profile is labeled 'A'.



Vol. 32, No. 4, page 227 (2013)

Both sand beds had similar assemblages of diatoms, with epipelagic marsh taxa dominant. The absence of freshwater species in the diatom assemblage shows that the sand beds are not fluvial deposits. The commonest species (~50-70% of the total count) is *Diploneis interrupta*. A large percentage of the frustules of this species were intact and unweathered. *Diploneis interrupta* is a salt marsh diatom with a large salinity tolerance range (Vos and de Wolf 1993), and although Hendey (1964) notes that it is also commonly found on sandy beaches, it was absent from the sample taken at the mouth of Salt Creek. That observation, the pristine condition of the frustules of *D. interrupta*, and the presence of *Cosmioneis pusilla* and *Caloneis westii*, which are also absent from the river-mouth sample, suggest that this assemblage is largely a product of post-depositional colonization of the surface of the sand by epipelagic marsh diatoms.

In addition to the epipelagic marsh taxa there are, however, small numbers (~5% of the total count) of brackish-marine epipsammic taxa (principally *Trachysphenia australis*, *Delphineis minutissima* and *Opephora mutabilis*) in both sand beds. These diatoms typically grow on sandy substrates in the lower intertidal or shallow subtidal zone (Vos and de Wolf 1993, Witter et al. 2009), and they may have been transported with the sand from near-shore habitats to the high marsh. Their presence supports our contention that the sand layers are the product of tsunami deposition. Their low relative abundance (compared, for example, to the results reported by Hemphill-Haley, 1996), is likely a product of not being able to sample the centre of these very thin sand beds, thereby including the post-depositional colonists.

The ages of the sand beds are constrained by four radiocarbon samples collected from the logged section and its immediate vicinity (Table I). These supply maximum limiting ages for the inferred tsunamis. A stick lying immediately above weathered rhizomes of *Triglochin maritima* at about 0.9 m depth (0.2 m below the lower sand layer) yielded an age of 2400 – 2300 cal. yr BP. Both sand layers therefore post-date this period. A charcoal fragment from the mud at the base of the upper sand indicates that this layer was deposited about, or shortly after, 1530–1380 cal. yr BP. The lower sand layer almost certainly dates from the intervening interval.

At riverbank site “b” (Fig. 2B), 400 m further upstream, a thin layer (5 – 15 mm thick) of fine to very fine sand occurs at 0.7 m depth (Fig. 5; Transect III), the same depth as the lower sand at site “a”. The correlation with the lower sand is tentative, however, because the continuity of the sand layers is interrupted by outcrops of point bar deposits in the channel banks between the two sites. A diatom sample from this sand was barren.

Stratigraphy: cores - We attempted to determine the inland extent of tsunami inundation in the vicinity of logged section “a” by tracing the two sand beds from the riverbank to the base of a small upland promontory about 60 m away (Fig. 2B; Transect I). The extent and thickness of the two sand layers in the rest of the marsh was determined from a further 29 cores (Fig. 2B).

A series of simplified sedimentary sections (Figs. 4C, 5) show the results of the coring program. In all the cores a basal tidal flat or channel sand fines up-core to mud, peaty mud, muddy peat, and, in a few instances, peat (>50% organic matter), marking the gradual infilling of the Salt Creek embayment in the late Holocene.

In Transect I the two sand layers can be traced from the riverbank for about 50 m inland in the 1 m-thick peaty mud facies that caps the intertidal sands. The sand beds are thickest (10 mm) in the core closest to the riverbank (Fig. 4C), and taper inland, but thicken again at one site in the lee of the raised

channel margin. They thin to single-grain thickness at the base of the upland, which likely marks the inundation limit.

In the northeast quadrant of the marsh (Fig. 5, Transect II) the cap of mud and peaty mud is <0.5 m thick, and no evidence of abrupt changes in facies or anomalous sand layers were detected in this area. About 200 m inland, however, the surficial mud and peaty mud units rapidly thicken, reaching 1.5 m close to the upland margin of the marsh. Cores close to this upland margin display abrupt but subtle changes in lithology, and very thin sand layers were noted at depths akin to those in logged section “a”.

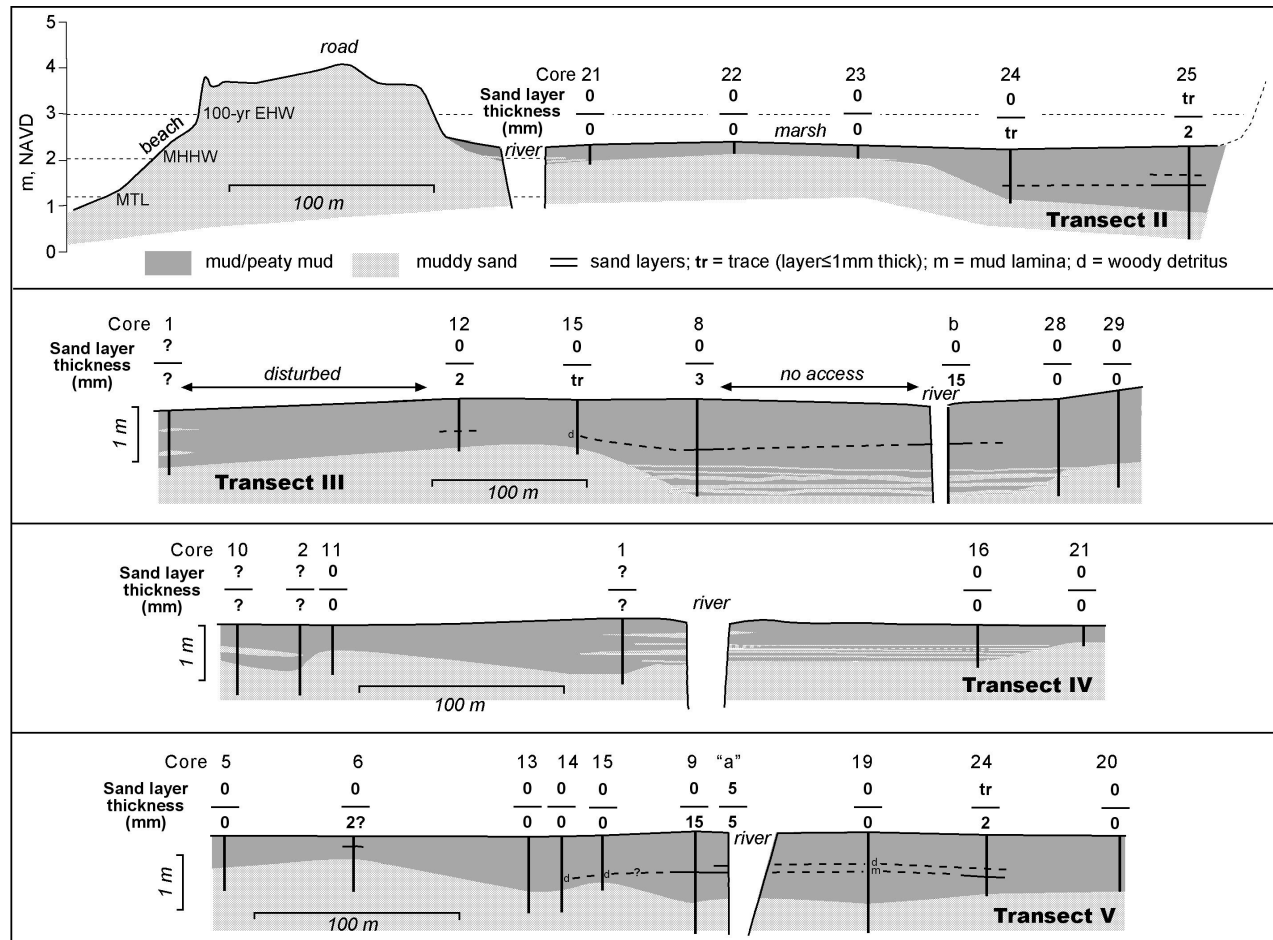


Fig. 5. Stratigraphy of cores along two shore-orthogonal transects (II and III), and two shore-parallel transects (IV and V), at Salt Creek marsh. The location of the transects is shown in Fig. 2B.

Transect III (Fig. 5) illustrates the variation in deposits in the western part of the marsh, and in a marsh embayment upstream. No sand beds were detected in the mud and muddy peaty units of the two cores landward of riverbank section “b” (Fig. 5; Transect III, cores 28, 29), but a thin sand bed occurs in the peaty mud facies in two of the cores close to section “a” (i.e. cores 12, 8). We noted a

layer of detrital wood fragments at an equivalent depth (0.7 m) in core 15. We tentatively correlate this sand-detritus bed with the lower sand in the nearby riverbank. A thicker layer of muddy sand occurs at 0.9 m depth in core 8. The few diatoms found in a sample from this layer were marsh and tidal flat taxa (Appendix II), and we consider this layer to be the uppermost of a series of channel/tidal flat sand deposits that interdigitate with mud at depths > 1m in core 8, riverbank section “b”, and core 28.

The basal sand in the cores along the shore-parallel transect immediately landward of the barrier beach (Fig. 5; Transect IV) typically lies at a depth of 0.6 —1.0 m. This fines into a thick mud or slightly peaty mud, which is capped by a thin dark brown peaty mud or peat. Two of the cores along this transect display anomalous sand layers (cores 1, 2) at similar depths. In core 1, a 3-cm thick sand layer lies at a depth of about 0.2 m below the surface, and a 9-cm thick layer of muddy sand lies at a depth of about 0.65 m, underlain by mud. The upper layer may be a product of disturbance associated with ditching of the marsh in this area, but the lower sand layer may be correlative with one of the two inferred tsunami layers in the logged riverbank section.

In core 2 this lower muddy sand layer is 6-cm thick and grades upwards into mud. The diatom assemblage in the muddy sand unit is dominated by species that live on muddy sandy shoals in the intertidal zone (*Planothidium delicatulum*, *P. hauckiana*, *Fallacia oculiformis*, *Opephora* spp., *Paralia sulcata*), so we consider it unlikely to be a tsunami deposit. The abrupt change between the sand layer and the underlying mud may therefore be a product of changes in the position of the meandering channel of Salt Creek, but it may also correlate with the subsidence event associated with the lower sand layer in the logged riverbank section.

Two of the cores discussed previously (cores 8, 25) are end-members of Transect V (Figure 5). The two intervening cores (7, 20) both show possible evidence of at least one weak subsidence event, and, in the case of core 7, a very thin (0.2-cm thick) sand layer at a depth of about 1.0 m that may correlate with the lower sand in the riverbank.

3. CONCLUSIONS AND IMPLICATIONS

In the near-shore areas of the Salt Creek marsh, extending landward for a distance of about 200 m from the inland margin of the barrier beach, the cap of muds and peaty muds above the tidal-flat deposits is thin, and has accumulated recently, most probably in the historic period. With one possible exception (Fig. 5; Transect V, core 1) the sedimentary archives in this area do not display evidence of the effects of prehistoric great earthquakes at the Cascadia subduction zone. The area that lies >600 m from the barrier beach also appears to be devoid of coseismic evidence, likely because the amount of subsidence at Salt Creek is too small to produce discernable changes in the character of the sediment in marsh areas close to the extreme limit of tides.

Facies changes are evident, however, in the intervening marsh area, primarily in the vicinity of the river channel. At least two such buried marsh soils can be detected in the logged riverbank section at Salt Creek. The lower horizon dates from the 2300 – 1530 cal yr. BP interval. The upper buried soil (at 0.3 m depth) is undated, but sharp facies changes at the same depth in the Wa’atch wetlands (Peterson et al., 2013) and on the San Juan River delta (Clague et al. 2000) date from the last plate-boundary earthquake in AD 1700, and we conjecture that the upper buried soil in the riverbank at Salt Creek also dates from this event.

The two sand layers identified in riverbank section “a” at Salt Creek as tsunami deposits are generally thicker than their counterparts in the cores from the rest of the marsh. This indicates that both tsunamis likely surged upriver, overtopped the channel banks, and spread across the marsh surface, leaving thin and patchy layers of sand and organic detritus in their wake.

We have no evidence to suggest that the 4 m-high barrier beach was overtopped by these waves. This implies that the maximum wave height did not exceed 3 m if the state of tide was close to MTL (~1 m NAVD88) when the biggest waves arrived, but must have exceeded 2 m in order to inundate the marsh surface. Tsunami simulation models developed by Cherniawsky et al. (2007) and AECOM Canada Ltd. (2013) generate maximum wave heights in the vicinity of Crescent Bay of about 2.5 m, which accords with our estimate.

If the two sand layers at Salt Creek are indeed the products of tsunamis prompted by ruptures at the Juan de Fuca – North America plate boundary, which events were responsible? Correlating the age of the inferred tsunami deposits at Salt Creek with the great-earthquake chronologies developed from buried marsh soil sequences in Willapa Bay (Fig. 1; Atwater and Hemphill-Haley, 1997), and turbidite sequences in Juan de Fuca and Barkley canyons (Fig. 1; Goldfinger et al., 2012), is complicated by the relatively poor dating control at Salt Creek, but it seems most likely (see Fig. 6) that the sand layers are products of plate-boundary earthquakes about 1650 years ago (event S in the Willapa Bay sequence), and about 1300 years ago (event U in the Willapa Bay sequence). These events are also the only well-documented tsunami deposits at Swantown marsh at the eastern end of the Strait of Juan de Fuca (Fig. 1B).

It is not surprising that deposits associated with the tsunami generated by the plate-boundary earthquake about 1650 years ago are widespread in marshes on the shores of the Strait of Juan de Fuca (Fig. 6). This earthquake followed a protracted period (about 1000 years) of strain build-up at the northern end of the Cascadia subduction zone, and the resultant thrust event was almost certainly larger than any other in the late Holocene.

The subsequent earthquake, however, followed only about 350 years of strain at the plate interface. Why are tsunami deposits attributable to this event found at Salt Creek, but those of subsequent plate ruptures not, despite the fact that they are encountered at Wa’atch – Neah Bay and Discovery Bay?

We suggest two possible reasons for this, operating singly or in concert:

1. The 1300 cal yr. BP tsunami coincided with high tide at Salt Creek; more recent tsunamis did not;
2. Changes in the morphology of the barrier beach in Crescent Bay led to narrowing of the river mouth within the last millennium, inhibiting tsunami incursion.

Tidal state – The last great earthquake at the Cascadia subduction zone is reliably dated to the January 26, AD 1700, at about 2100 h local time. Mofjeld et al. (1997) reconstructed the tidal state at that time, and concluded that the earthquake occurred during a low neap tide, which may explain the absence of a tsunami deposit from this event both at Salt Creek and Swantown marsh. The presence of tsunami deposits from the AD 1700 earthquake and preceding events at an intervening site (Discovery Bay) is almost certainly the result of wave amplification in that embayment (Cherniawsky et al., 2007).

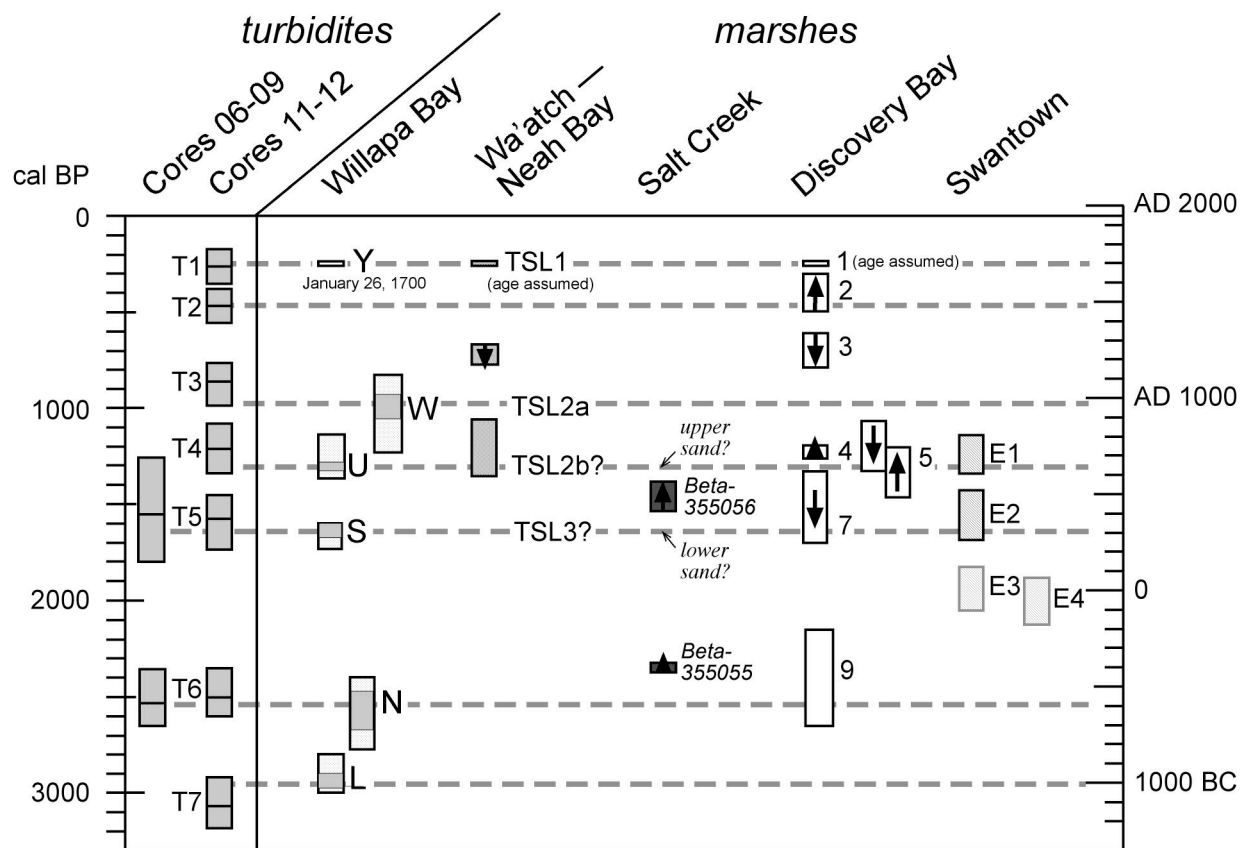


Fig. 6. Correlations between inferred paleotsunami events at Salt Creek marsh with paleoseismic and paleotsunami evidence from elsewhere in the Strait of Juan de Fuca and vicinity. Upward-pointing arrows indicate maximal ages; downward-pointing arrows indicate minimal ages. Data: turbidite cores (Goldfinger et al., 2012); Willapa Bay buried marsh soils (Atwater et al., 2004); Wa'atch – Neah Bay (Peterson et al., 2013); Discovery Bay (Williams et al., 2005), and Swantown marsh (Williams and Hutchinson, 2000).

Estuarine palaeogeography – Tsunami incursion up-channel at Salt Creek in the late Holocene has undoubtedly been influenced by the position and morphology of the barrier beach and the position and width of the mouth of Salt Creek. These in turn are influenced by regional climate (e.g. changes in storminess or river flooding regime), and relative sea level.

Relative sea level along the Cascadia littoral rises and falls as stress is built-up and released at the interface of the Juan de Fuca and North America plates. Incomplete release of stress in the earthquake phase of the cycle may have led to gradual tectonic uplift and lowering of local sea level, or, if the rate of uplift was more modest, offset of the eustatic sea level rise in the late Holocene and sea-level stabilization. Both of these scenarios would lead, in turn, to infilling of the back-barrier lagoon, reduction of the tidal prism, narrowing of the river mouth, and reduced tsunami access.

ACKNOWLEDGEMENTS

This project was funded by a Portland State University Faculty Enhancement Grant to Sarah Sterling. Thanks to our field assistants, Andrew Huff and Christopher Milton, and to the PSU Geology students (Charles Davidshofer, Scott Lunski, Molly Pontifex, Ann Stransberry, Emily Jenkins, Tamara Linde, Elizabeth Westby, Al Mowbray, and Craig Annsa) who undertook the elevation survey. Nan Feagin, Bud Taggart, the Luthers, the Palzers, and the Novaks allowed access to their land, and Anne Schaffer and Dave Parks gave us access, data, and encouragement. We particularly appreciate Brian Atwater's insights and guidance in the field, Josef Cherniawsky's sharing of tsunami model output, and Ian Miller's outreach efforts.

REFERENCES

- AECOM Canada Ltd. 2013. Modelling of Potential Tsunami Inundation Limits and Run-up. Report prepared for the Capital Regional District. Available online at <http://www.crd.bc.ca/media/documents/20130424-TsunamiFullreport.pdf> (accessed 13 August 2013).
- Atwater B. F. 1987. Evidence for great Holocene earthquakes along the outer coast of Washington State. *Science* 236:942-944.
- Atwater, B. F. 1997. Coastal evidence for great earthquakes in western Washington. U.S. Geological Survey, Professional Paper 1560:77-90.
- Atwater, B. F., and E. Hemphill-Haley. 1997. Recurrence intervals for great earthquakes of the past 3,500 years at northwestern Willapa Bay, Washington. U.S. Geological Survey, Professional Paper 1576.
- Atwater, B. F., M. P. Tuttle, E. S. Schweig, C. M. Rubin, D. K. Yamaguchi, and E. Hemphill-Haley. 2004. Earthquake recurrence inferred from paleoseismology. *Developments in Quaternary Science* 1:331-350.
- Clague, J.J., P. T. Bobrowsky, and I. Hutchinson, I., 2000. A review of geological records of large tsunamis at Vancouver Island, British Columbia, and implications for hazard. *Quaternary Science Reviews* 19:849–863.
- Cherniawsky J. Y., V. V. Titov, K. Wang, and J.-Y. Li. 2007. Numerical simulations of tsunami waves and currents for southern Vancouver Island from a Cascadia megathrust earthquake. *Pure and Applied Geophysics* 164:465–492.
- Goldfinger, C., C. H. Nelson, A. E. Morey, J. E. Johnson, J. R. Patton, E. Karabanov, J. Gutiérrez-Pastor, A. T. Eriksson, E. Gràcia, G. Dunhill, R. J. Enkin, A. Dallimore, and T. Vallier. 2012. Turbidite event history – methods and implications for Holocene palaeoseismicity of the Cascadia subduction zone. U.S. Geological Survey, Open-File Report 1661-F.

Goto, K., C. Chague-Goff, J. Goff, and B. Jaffe. 2012. The future of tsunami research following the 2011 Tohoku-oki event. *Sedimentary Geology* 282:1-13.

Guilbault, J. P., J. J. Clague, and M. Lapointe. 1996. Foraminiferal evidence for the amount of coseismic subsidence during a late Holocene earthquake on Vancouver Island, west coast of Canada. *Quaternary Science Review* 15:913-937.

Heaton, T. H., and S.H. Hartzell. 1987. Seismic hazards on the Cascadia subduction zone. *Science* 236:162-168.

Hendey, N. I. 1964. An Introductory Account of the Smaller Algae of British Coastal Waters. Part V: Bacillariophyceae (Diatoms). Ministry of Agriculture, Fisheries and Food, Fisheries Investigations Series IV. London.

Hemphill-Haley, E. 1993. Taxonomy of recent and fossil (Holocene) diatoms (Bacillariophyta) from northern Willapa Bay, Washington. U.S. Geological Survey, Open-File Report 93-289.

Hemphill-Haley, E. 1995. Diatom evidence for earthquake-induced subsidence and tsunami 300 yr ago in southern coastal Washington. *Bulletin of the Geological Society of America* 107:367-378.

Hemphill-Haley, E. 1996. Diatoms as an aid in identifying tsunami deposits. *The Holocene* 6:439-448

Martin, M. E., and J. Bourgeois. 2012. Vented sediments and tsunami deposits in the Puget lowland, Washington – differentiating sedimentary processes. *Sedimentology* 59:419-444

Mofjeld, H. O., M. G. G. Foreman, and A. Ruffman. 1997. West Coast tides during Cascadia subduction zone tsunamis. *Geophysical Research Letters* 24:2215-2218.

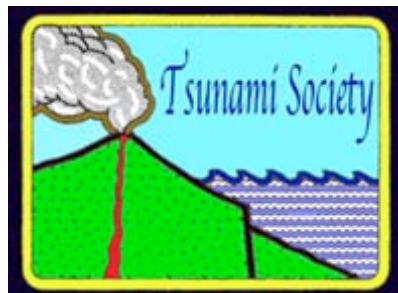
Morton, R. A., G. Gelfenbaum, and B. E. Jaffe. 2007. Physical criteria for distinguishing sandy tsunami and storm deposits using modern examples. *Sedimentary Geology* 200:184-207.

Peters, R., B. Jaffe, G. Gelfenbaum, and C. Peterson. 2003. Cascadia tsunami deposit database. U.S. Geological Survey, Open-File Report 03-13.

Peters, R., and B. Jaffe. 2010. Identification of tsunami deposits in the geologic record: developing criteria using recent tsunami deposits. U.S. Geological Survey, Open-File Report 2010-1239.

Peterson, C. D., K. M. Cruikshank, M. E. Darienzo, G. C. Wessen, V. L. Butler, and S. L. Sterling. 2013. Coseismic subsidence and paleotsunami run-up records from latest Holocene deposits in the Waatch Valley, Neah Bay, northwest Washington, U.S.A.: links to great earthquakes in the northern Cascadia margin. *Journal of Coastal Research* 29:157-172.

- Todd, S., N. Fitzpatrick, A. Carter-Mortimer, and C. Weller C. 2006. Historical changes to estuaries, spits, and associated tidal wetland habitats in the Hood Canal and Strait of Juan de Fuca regions of Washington State: Final Report. Appendix B2--central Strait region. PNPTC Technical Report 06-1, Point No Point Treaty Council, Kingston, Washington. Available online at http://www.pnptc.org/PNPTC_Web_data/Publications/habitat/GIS/Historic%20Changes%20Main%20Report.pdf (accessed 26 August 2012)
- Tuttle, M. P., A. Ruffman, T. Anderson, and H. Jeter. 2004. Distinguishing tsunami from storm deposits in eastern North America: the 1929 Grand Banks tsunami versus the 1991 Halloween storm. *Seismological Research Letters* 75:117-131.
- Vos, P., and H. de Wolf. 1993. Diatoms as a tool for reconstructing sediment environments in coastal wetlands – methodological aspects. *Hydrobiologia*, 269/270:285-296.
- Weiss, R., and J. Bourgeois. 2012. Understanding sediments – reducing tsunami risk. *Science* 336:1117.
- Williams, H., and I. Hutchinson. 2000. Stratigraphic and microfossil evidence for late Holocene tsunamis at Swantown marsh, Whidbey Island, Washington. *Quaternary Research* 54:218-227.
- Williams, H. F. L., I. Hutchinson, and A. Nelson. 2005. Multiple sources for late-Holocene tsunamis at Discovery Bay, Washington State, USA. *The Holocene* 15:60–73
- Witkowski, A., H. Lange-Bertalot, and D. Metzeltin. 2000. Diatom Flora of Marine Coasts I. *Iconographica Diatomologica* (volume 7), Koeltz Scientific, Koenigstein.
- Witter, R. C., E. Hemphill-Haley, R. Hart, and L. Gay. 2009. Tracking prehistoric Cascadia tsunami deposits at Nestucca Bay, Oregon. Final Technical Report, U.S. Geological Survey, National Earthquake Hazards Reduction Program, Award No. 08HQGR0076.



SCIENCE OF TSUNAMI HAZARDS

Journal of Tsunami Society International

Volume 32

Number 4

2013

A CRITICAL REVIEW AND EVALUATION OF APPLYING SEMI-VOLATILE ORGANIC COMPOUNDS (SVOCS) AS A GEOCHEMICAL TRACER TO INDICATE TSUNAMI BACKWASH: The Bilateral, Deutsche Forschungsgemeinschaft (DFG) and National Research Council of Thailand (NRCT) Funded Project “Tsunami Deposits in Near-Shore- and Coastal Waters of Thailand (TUNWAT)”

Siwatt Pongpiachan¹ & Klaus Schwarzer²

¹*NIDA Center for Research & Development of Disaster Prevention & Management, School of Social and Environmental Development, National Institute of Development Administration (NIDA), 118 Moo-3, Sereethai Road, Klong-Chan, Bangkok, Bangkok 10240 Thailand**

Corresponding author phone: (66) 2727-3090; mobile phone: (66) 819751456; fax: (66) 27273747; e-mail: pongpiajun@gmail.com

²*Institute of Geosciences Sedimentology, Coastal and Continental Shelf Research, Christian Albrechts University Kiel, Otto Hahn Platz 1, D - 24118 Kiel, Germany*

ABSTRACT

Tsunamis symbolize one of the most harmful natural disasters for low-lying coastal zones and their residents, due to both its destructive power and irregularity. The 2004 Boxing Day tsunami, which attack the Andaman Sea coast of Thailand, resulted 5,395 of deaths and inestimable casualties, interrupted economies and social well-being in numerous coastal villages and caused in extreme alterations of both onshore and offshore coastal morphology. The Great Indian Ocean tsunami also highlighted that there are many missing jigsaw puzzle pieces in scientific knowledge, starting from the generating of tsunamis offshore to the countless influences to the marine ecosystems on the continental shelf, coastal areas and on land and to the economic and social systems consequences. As with all deposits that do not have a direct physical link to their causative sources, marine tsunami deposits must be distinguished from other deposits through regional correlation, dating and criteria for recognition within the deposits themselves. This study aims to provide comprehensive reviews on using Polycyclic Aromatic Hydrocarbons (PAHs) as a chemical proxy to discriminate tsunami related

deposits from typical marine sediments. The advantages and disadvantages of this chemical tracer will be critically reviewed and further discussed.

Keywords: *Tsunami Deposits, Marine Sediments, Polycyclic Aromatic Hydrocarbons (PAHs), Andaman Sea*

1. INTRODUCTION

Tsunamis has been a cause of concern all over the world for their tremendous destructive power. This destruction was particularly great in Asia where tsunamis have occurred often throughout history. The 2004 Indian Ocean earthquake is generally recognized as one of the world's largest and deadliest natural disasters in modern times, responsible for estimated US\$ 10 billions of damages including the number of deaths approximately 230,000 people. Since tsunamis dominate natural catastrophe statistics in term of causing casualties and damaging constructions, a large number of studies have been performed over the last three decades to assess the alteration of geological and sedimentological features related to tsunami impact around the world (Atwater, 1987; Benson et al., 1997; Bondevik et al., 1997; Choowong et al., 2007, 2008a, 2008b, 2009; Clague and Bobrowsky, 1994; Dawson et al., 1988, 1991; Gelfenbaum and Jaffe, 2003; Pinegina and Bourgeois, 2001; Szczuciński et al., 2005, 2006, 2007). Tsunamis are recorded since historical times and numerous investigations have been done about their origin, wave distribution and energy release along coastlines, potential for coastal changes as well as on sediment deposition further inland (Bryant, 2001). Tsunamis have been compared to storms even if they are two genetically unrelated phenomena. Both are remarkably similar in their physical power and in their ability to transport sediment across the shelf and to deposit it in deeper water environments, but there is some difference between large storms with long wave periods and the effects of tsunamis in terms of hydrodynamics on the shelf (Bryant, 2001). The differences exist in (i) the capacity of eroding sediments from the sea-floor and the beach-face and to carry and to deposit this material onshore if there are suitable topographic conditions existing and (ii) in the tremendous backflow of tsunami water masses from the inundated areas carrying land-borne material offshore. While it is accepted that storm surges result in the deposition of discrete sedimentary units, tsunami waves generally result in deposition of sediment sheets over relatively wide areas and considerable distances inland (Dawson, 1999). According to a recent review by Gusiakov (2005), 688 tsunamis occurred in the tsunamigenic regions of the Indo-Pacific including Indonesia during 1901 – 2000 and at least 100 megatsunamis have occurred during the past 2000 years worldwide (Scheffers and Kelletat 2003). In historical times 5 Tsunamis hit the coast of Sumatra (1797, 1833, 1843, 1861 and 1883) and might have affected the coast of Thailand as well (Department of Mineral Resources, 2005).

Most of the knowledge about offshore, shallow marine tsunami deposits results from onshore outcrops of ancient lithified strata (Cantalamessa and Di Celma, 2005). Indicators of backrush flow in Miocene sediments are described by le Roux and Vargas (2005). They consider sandstone injections and dikes associated with intraclasts, penetrating underlying strata, as well as debris flow including “wave-smoothed” beach material, as the most reliable evidence. Poor knowledge exists about the

deposition on the upper and lower shore face induced by tsunami across-shelf backwash, which might produce sediment aprons, sand bars or large sediment waves. Only very few investigations have been made on submerged unconsolidated Holocene marine deposits (Le Roux and Vargas, 2005, Vargas et al. 2005). The successive run-up and backwash of tsunami waves can produce strong seaward currents causing additional erosion and sediment re-deposition, depending on the nature of the coastal topography and bathymetry (Bondevik et al., 1997; Shi et al., 1998; Dawson and Shaozhong, 2000). Also, large objects (boulders, coral blocks and human artifacts) may be dragged or deposited on the seafloor producing a debris field and other evidence on the seafloor. Einsele (1988), who proposed diagnostic criteria for tsunami deposits, noted that the backflow of tsunamis is commonly focused by the coastal geomorphology into channelized flows. Due to this channeling, the velocity of the backwash flow is more erosive and powerful than the run-up flow. Le Roux and Vargas (2005) show that the backrush of the 1960 tsunami, which hit the coastline of Chile with up to 14 m high waves, developed as kind of rip currents. In short cores obtained from water depth between 75 – 100 m Vargas et al (2005) observed features and sediment material in two layers originating from areas shallower than 50 m. They relate these deposits to the tsunami backwash. By dating with radioisotopes and lateral correlation they inferred ages as between A.D.1409 – 1449 and A.D.1754 – 1789.

As tsunami backflows advance offshore from the coastline, they will undergo several changes known as flow transformation (Fisher 1983). Flow channelization seems to play an important role in lateral flow transformations leading to unusual deposits. Hyper concentrated flow conditions may therefore develop within the morphologically deepest channel zones, accompanied by intraclasts ripped up from the substrate. Very dense sediment-water mixtures, which the backrush might be, may initially behave as Bingham Fluids dominated by frictional grain interactions and shearing, so that shear carpets may develop at their base. According to Nittrouer and Wright (1994) the midshelf region is in many cases the dead end for many of the particles transported across continental shelves due to storm events. Besides the investigations of Le Roux and Vargas (2005) to our knowledge nothing is known about the fate and the area where most of the tsunami related material is deposited offshore. However, Shanmugam (2005) assumes that tsunami-related deposits should be volumetrically important in coastal, shallow-water and deep-water environments.

For a long time it was neglected that on wave dominated coastal and shelf areas the impact of tsunami waves on shore-face deposits can be preserved in modern sediments. However recent investigations based on modern high resolution remote sensing mapping techniques for marine areas revealed that even in highly dynamic areas and even if the perturbed shore face is in a disequilibrium state, a preservation potential of sediment distribution patterns and shore face geomorphology exist for decades (Schwarzer et al., 2003; Murray & Thielert, 2004; Ferrini & Flood, 2005; Diesing et al. 2006). Conceivably, on the deeper parts of the lower shore face and inner shelf the elevated water level may induce deposition (similar to the classic "Bruun Rule" response) if there is sufficient accommodation space. Thus, the initial morphological response of the shore face to the tsunami is hypothesized to have a pattern of sediment deposition on the lower shore face and inner shelf, erosion on the upper shore face and beach face, and deposition landward of the beach.

1.1 General background of Tsunami Deposits in Near-Shore- and Coastal Waters of Thailand (TUNWAT) Project

In the months following the tsunami disaster, consultations between the National Research Council of Thailand (NRCT) and the German Research Foundation (DFG) resulted in a general agreement for a bilateral cooperation, which was focused on tsunami-related research. Backed by discussions during a joint NRCT-DFG workshop in Bangkok in July 2006, German and Thai scientists agreed to propose research projects, which specifically address scientific issues dealing with tsunami triggering, tsunami wave development and interaction with the sea-bottom and the impacts, alterations and risks to gain a better understanding of tsunamis, their origin, propagation, physical-, social- and economic impacts, resulting destructions and long-term effects and, thus, to improve risk management in the Andaman Sea Region (see Fig.1-3).

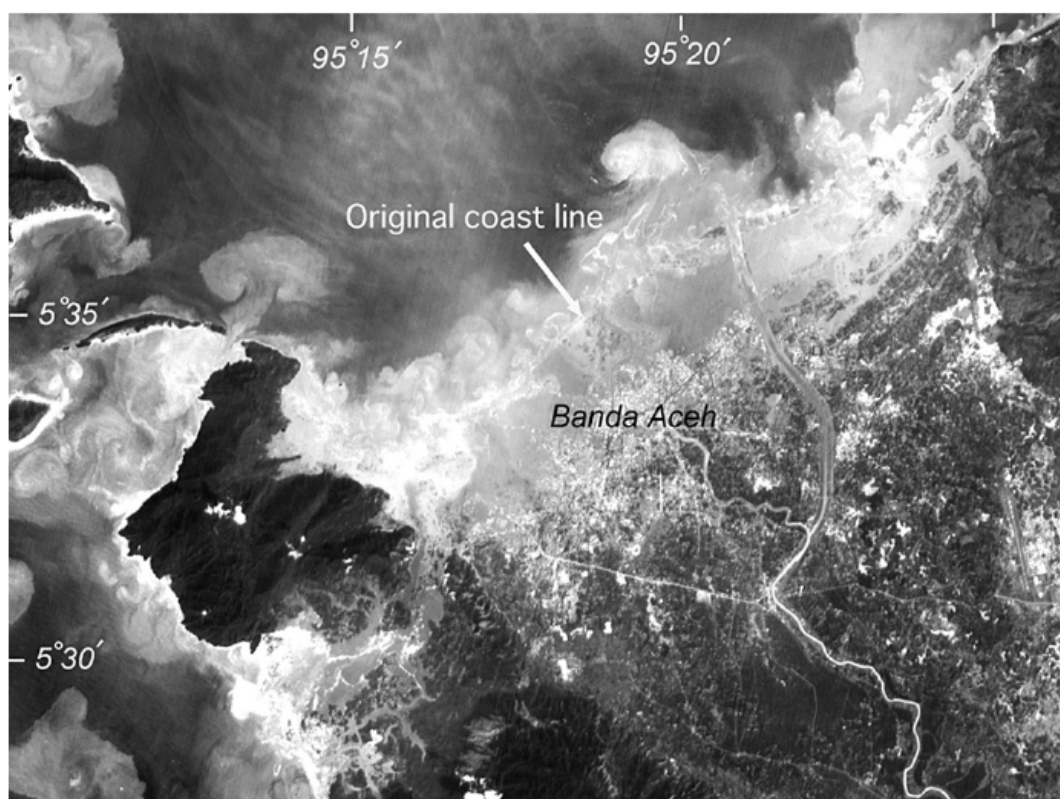


Figure 1. Inundation and tsunami flow of the Banda Ache Plain shown in the SPOT2 image. The image was taken about 4 h after the earthquake. (Includes material from CNES2005, Distribution Spot Image S.A., France, all rights reserved). Taken from Umitu, M. et al., 2006. Own comment: Rip current eddies can be observed along the whole coastline.

Within the framework of this theme, several topics have been brought forth. As there is a common focus on tsunamis and impacts, the research issues of the individual projects are interlinked by the fact

that they are aiming at providing complementary answers to key questions about tsunamis in the study region and their potential impacts. These major questions can be described as follows; (i) Where and how can tsunamis be triggered in the Andaman Sea? (ii) How often have tsunamis struck this coast in the recent past? (iii) How does a tsunami wave propagate from offshore (deep water) via the shelf and near-shore zone onto the adjacent low-lying land areas? (iv) What are the impacts of tsunami waves to the seafloor topography, to the sediment cover and to the marine & littoral ecosystems while progressing onshore? (v) How does the land-sea loaded backflow influence the marine abiotic and biotic system? (vi) How is tsunami wave energy attenuated in the near shore zone, beachfront and hinterland and how is this attenuation influenced by the presence of natural barriers such as coastal forests? (vii) What factors determine the tsunami-related vulnerability of low-lying coastal areas, their population, communities and economies? (viii) Which kind of socio-economic, institutional and/or other factors make coastal societies or communities resilient against tsunami impacts? (ix) How can risk management, including early warning, be improved to prevent or mitigate future tsunami disasters along this coast?

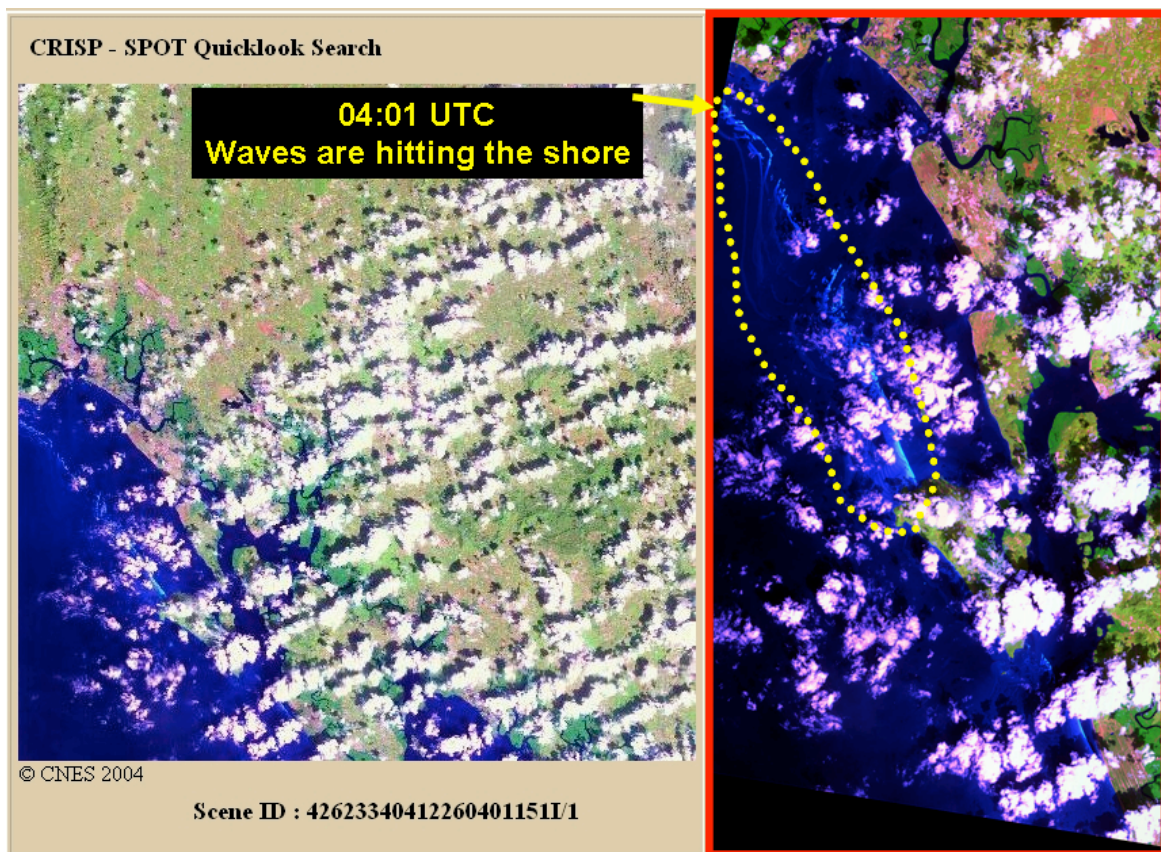


Figure 2. The coastal area of Thailand when the Tsunami waves hit the shore. Far offshore the influence of the sea bottom to the tsunami waves becomes obvious when due to bottom friction by wave transformation and wave-breaking occurs (Source: <http://www.crisp.nus.edu.sg/tsunami/tsunami.html>).

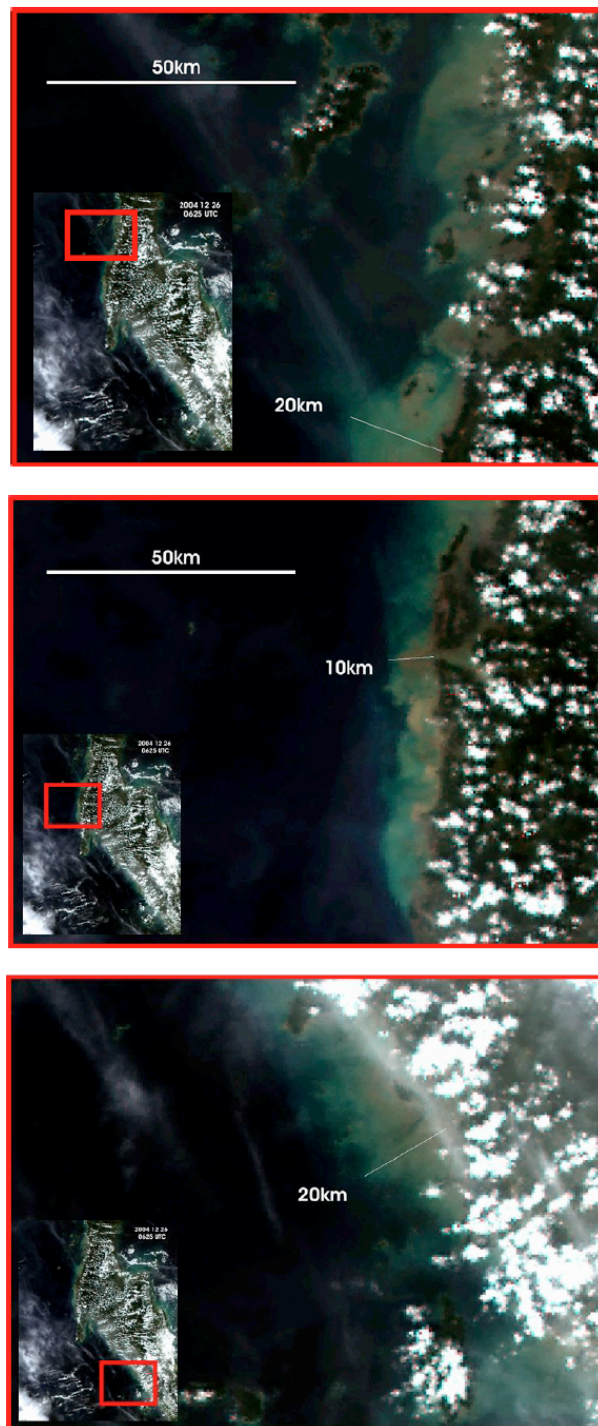


Figure 3. The coast of Thailand 2 hours after the tsunami hit the coast on December 26th, 2004 at 06:25 UTC. The suspension load plume of the backrush extends approximately 20 km offshore.
 (Source: <http://www.crisp.nus.edu.sg/tsunami/tsunami.html>).

The questions above provide a feasible basis for addressing key issues of regional tsunami research. They also outline some spatial structure, as the planned projects may be seen as lining up along an offshore – onshore transect from the deep Andaman ocean across the shelf, near shore and beach zone into the coastal hinterland as far as a mega-tsunami can reach. While in the offshore domain natural processes dominate, towards onshore and especially on land anthropogenic influences increase and trigger the vulnerability. Consequently, the intention of the group is to establish a German – Thai tsunami research network in which project data ought to be exchanged and results ought to be generated/synthesized as to contribute to the enhancement of the region's ability to cope with tsunami risks.

Based on this concept of interlinked and spatially adherent projects the German-Thai research group attempts to focus on the following issues:

- Analyze the possibility of tsunami-triggering by slides / slumps at the continental margin of the Andaman Sea;
- Detecting changes in seafloor topography and sediment pathways by use of remote sensing methods (satellite image investigation, mapping by multi-beam and side scan sonar techniques), sediment coring, sampling and dating by radio isotopes;
- Detection and reconstruction of previous tsunami events in order to determine the long-term history of tsunamis along this coast;
- Numerical modeling of wave propagation and run-up during the Dec. 26, 2004 tsunami. Validation of different models by comparing measured tsunami run-up characteristics with results from numerical model simulations;
- Determining the influence of coastal ecosystems, in particular coastal forests and mangroves, on the physical impacts of tsunami waves along the whole western coast of Thailand;
- Generating a scientific knowledge base and developing/validating prediction models for the tsunami attenuation performance of coastal forests;
- Assessment and evaluation of tsunami risks in flood-prone coastal areas and communities. Assisted by remote sensing techniques and field surveys, quantitative indicators are to be derived for ecologic, economic and social vulnerability as well as for local resilience;
- Comparing local and global interactions in disaster prevention and recovery in two regions strongly hit by the 2004 tsunami: Khao Lak, Thailand and Aceh, Indonesia;
-

The main objective of the proposed sub-projects is to complement individual research issues in such a way that a clear picture can be drawn about the destructive forces and processes of the recent tsunami and past tsunamis and to elaborate and to suggest measures how to avoid or mitigate future tsunami impacts and destructions in Thailand. Most of the deposits that are known to occur or may occur in marine environments require improvements in the criteria for recognition. Developments of such criteria are best done when there are deposits of unquestioned origin. The recognition of deposits of this tsunami gives the opportunity to extend the relatively short or non-existent historical record of tsunamis in this area. Presently most of the literature regarding marine tsunami deposits comes from ancient geologic record and cannot be tested. The December 2004 Sumatra-India earthquake and following tsunami represents an opportunity to catalogue geomarine effects from a very well recorded series of events, many of which are unknown or poorly known at present. A modern deposit of

unquestioned origin is invaluable for defining the palaeo record. This event represents the best-recorded mega-tsunami in human history and offers a unique opportunity to collect data, which have been never recorded yet. Even if offshore records offer the potential of good preservation, good spatial coverage and long-term span, data should be collected as soon as possible after this event as much of the information may be altered or destroyed over time.

Numerous field surveys have been carried out to measure the inundation, run up and deposition of marine derived sediment onshore caused by tsunamis, but no systematically detailed study exist up to now to measure geomorphological, sedimentological and geological alterations offshore beyond the upper shore face. This project aims to assess the impact of tsunami waves on changes and/or offsets of large-scale bed forms, on changes and/or offsets of shelf sediment distribution patterns and on estimating the spatial extension of erosion as well as on deposition by the backwash. The following offshore impacts are expected:

- Erosion by the onshore moving tsunami wave;
- Erosion by the channelized backwash currents;
- Transport of huge sediment plumes offshore and deposition from the shore face to the mid- or outer shelf.

Therefore the scientific questions in detail are:

- How do incoming tsunami waves influence sediments and sea bottom topography on the shelf and in near shore waters?
- How does the offshore flowing backrush influence sediments and sea bottom topography on the shelf and in near shore waters?
- Are there distinguished conduits for the sediment backflow?
- At which water-depth and at which offshore distance can a tsunami triggered alteration of the seafloor be observed?
- How will offshore tsunami deposits look like?
- How does an archive record of tsunami affected shelf deposits look like?
- How far offshore sediments are transported by the tsunami backwash?
- Was more sediment transported and deposited onshore or offshore?

To achieve the objectives of this project a multidisciplinary approach is required combining remote sensing methods, geophysical and sedimentological methods and geochemical methods.

1.2. Concept of using Semi-Volatile Organic Compounds (SVOCs) as geochemical tracers to characterize tsunami backwash deposits

Geochemical tracers have been extensively used as environmental tools to investigate the behavior and fate of target compounds in the environment (Pongpiachan et al., 2012a,b). While onshore tsunami deposits are supposed to contain organic and inorganic material of marine origin, offshore transported material should contain tracer-material originating from land, depending on landforms and

deposits, which are exposed in the areas, which were hit by the tsunami waves. For decades, both PAHs and aliphatics have been used as a “proxy” to distinguish the anthropogenic source and biogenic source. In this study we make the assumption that (i) terrestrial soils contain many anthropogenic PAHs coupling with aliphatics from terrestrial plants and (ii) marine sediments contain many of phytoplankton derived biomarkers. By analyzing these organic tracers from different points coupling with careful statistical treatments, it should be possible to investigate the impact of the tsunami to the distribution of terrestrial sediments in the recent deposits of the Andaman Sea.

Understanding the mechanisms and spatial variations of tsunami backwash sediment distribution patterns and burial within the offshore area of the Andaman Sea requires an ability to discriminate between terrigenous and marine components of organic compounds. Furthermore, the role of the shelf as a source area must be distinguished from those of basins, as sink areas and the coupling between the two should also be understood as well. A number of approaches have been used to distinguish between marine and terrigenous components in marine sediments including SVOCs such as PAHs, hopanes and cholestanes (Westerhom et al., 1992; Yunker et al., 2002, 2003; Kalaitzoglou et al., 2004). SVOCs have the advantage that they are all released into the atmosphere by imperfect combustion of organic matters and thus can be used as indicators to identify anthropogenic combustion sources (i.e. traffic emissions, industrial activities, incinerators etc) from natural combustion sources (i.e. forest fires, volcano activities, re-evaporization, etc.) by using specific binary ratios (Pongpiachan, 2013a,b,c; Pongpiachan et al., 2013c,d; Tipmanee et al., 2012; Yunker et al., 2002). Those areas which were most affected by the backrush of tsunami waters should contain more terrigenous sediments and thus as well relatively higher proportions of anthropogenic source derived organic compounds. Specific organic biomarkers such as 17 α (H) -22,29,30-Tris (Tm), 17 β (H), 21 β (H) -hopane, 17 β (H), 21 α (H) -30-northpane (Isoadiatane), 17 β (H), 21 α (H) -hopane (Moretane), 17 α (H), 21 β (H) -hopane, 18 α (H), 22,29,30-Trisnorneohopane (Ts), on the other hand, often yield clear evidence of sources (terrigenous and marine) even though they represent only a small proportion of the total organic material found in the sediments (Belicka et al., 2004). Furthermore, the value of CPI1 (Carbon Preference Index 1), CPI2 (Carbon Preference Index 2), CPI3 (Carbon Preference Index 3), ACL (Average Carbon Length), C_{max} (Carbon Maximum Number), Pristane and Phytane can be used as biomarkers to distinguish between terrigenous and marine derived sources of sediments (Yunker et al., 2002, 2003). By calculating SVOC concentrations against background values the spatial extension of the sediment load of the tsunami backrush can be estimated. In addition, there are other alternative analytical tools such as Attenuated Total Reflectance Fourier Transform Infrared Spectroscopy (ATR-FTIR) and micro-beam synchrotron X-Ray Fluorescence (μ -SXRF) that can be used to characterize the tsunami backwash deposits (Pongpiachan et al., 2013a,b).

1.3. Physicochemical properties, fates and environmental risks of PAHs

PAHs are a class of very stable organic molecules made up of only carbon and hydrogen and contain two to eight fused aromatic rings. PAHs are formed during incomplete combustion of organic materials such as fossil fuels, coke and wood. By definition as organic compounds with vapor pressure ranging from 10^{-3} – 10^{-7} Pa (see Table 1), PAHs, alkanes, cholestanes, hopanes and anthropogenic sourced chemicals like organochlorine pesticides, polychlorinated biphenyls (PCBs),

dioxins can be termed as SVOCs (Paasivirta *et al.*, 1999). These molecules were oriented horizontal to the surface, with each carbon having three neighboring atoms much like graphite (see Table 2-5). The structures of a variety of representative PAHs can be seen in Table 2. In order to reduce the atmospheric concentration of SVOCs, the UK's Expert Panel on Air Quality Standard (EPAQS) has selected benzo[*a*]pyrene (B[*a*]P) as a marker for levels of ambient PAHs in recognition of its carcinogenicity and mutagenicity. An annual mean of 0.25 ng m⁻³ has been set. However, this value exceeded the annual mean concentration of B[*a*]P measured in a number of UK cities since 1997. The long term monitoring of SVOCs in urban air, therefore, is a significant approach to investigate the annual trends and seasonal variations of targeted compounds. However, the environmental persistence and a wide range of vapor pressure of SVOCs have made this group of organic compounds globally ubiquitous and thus subject to unique atmospheric fate/behavior. The complexity of its existence in the atmospheric environment together with varieties of emission sources attributed the uncertainties in source apportionment of these specific compounds. Since SVOCs can be measured in the most remote areas like Antarctica, the worldwide concerns are also focused on the long-range atmospheric transportation (LRAT).

Epidemiological evidence suggests that human exposures to PAHs, especially B[*a*]P are high risk factors for carcinogenic and mutagenic effects. There are hundreds of PAH compounds in the environment, but only 16 of them are included in the priority pollutants list of US EPA (EPA, 2003). Many PAHs have also been identified as cancer-inducing chemicals for animals and/or humans (IARC, 1983). In 1775, the British surgeon, Percival Pott, was the first to consider PAHs as toxic chemicals with the high incidence of scrotal cancer in chimney sweep apprentices (IARC, 1985). Occupational exposure of workers by inhalation of PAH-both volatile and bound to respirable particulate matter- and by dermal contact with PAH-containing materials, occurs at high levels during coke production, coal gasification, and iron and steel founding. Coke oven workers have a 3- to 7-fold risk increase for developing lung cancer (IARC, 1984 and IARC, 1987). For this reason, the monitoring of PAHs in environmental media is a reasonable approach to assess the risk for adverse health effects. Since the fate of PAHs in the natural environment is mainly governed by its physiochemical properties, the study of general properties of the compounds is of great concern. In spite of a large number of publications related to the environmental fates of PAHs around the world, there are only few studies conducted in Thailand (Boonyatumanond *et al.*, 2007; Chetwittayachan *et al.*, 2002; Pongpiachan *et al.*, 2009; Pongpiachan, 2013b,c; Pongpiachan *et al.*, 2013c,d, e; Ruchirawat *et al.*, 2002, 2005, 2007; Tipmanee *et al.*, 2012).

In this study, the authors hypothesize that the employment of PAHs coupled with various analogies of statistical analysis assist in a better understanding of offshore terrestrial deposit distribution pattern, which can be subject to erosion by tsunami/monsoon waves and surface runoff by heavy rain in the tsunami-affected coastal areas of Andaman Sea, Thailand. Note that it is the purpose of this paper to critically review both the advantages and disadvantages of using SVOCs as an innovative proxy to separate the terrestrial deposit from the background sediment in tsunami-affected coastal areas. Neither the source apportionment, nor the analysis of spatial variation of SVOCs in sediments is the main focus of this study. In addition, the risks and possibilities of applying other geochemical tracers as an alternative extreme event proxy will be reviewed and discussed.

2. Source characterization of SVOCs

2.1 Source characterization of PAHs

The binary ratio method for PAH source identification, involves comparing ratios between pairs of frequently found PAH compound characteristics of different sources. Stationary source combustion emissions from the use of coal, oil and wood are low in coronene (Cor) relative to B[a]P, while mobile source combustion emissions from diesel and petroleum use are high in B[g,h,i]P and Cor relative to B[a]P (Stenberg et al., 1979). The ratio of these PAHs can be used to distinguish between traffic dominated PAH profiles and other sources (Brasser, 1980; Mainwaring and Stirling, 1981). Lim et al., (1999) used two methods in evaluation of PAH traffic contribution. Both of methods were adapted from Nielsen (Nielsen, 1996). Equation 1 based on the assumption that all Cor is traffic-generated, the concentration of B[e]P which is traffic generated is given by

$$B[e]P_{traffic} = \frac{Cor_{concentration}}{\frac{\delta Cor}{\delta B[e]P}}$$

Equation 1

Crucial to this method is the assumption that all Cor is traffic generated. Although this is likely to be an oversimplification, many studies have shown a high correlation between Cor and vehicular emissions. In addition, the ratios of B[g,h,i]P/B[e]P and Cor/B[e]P can also be used as traffic indicators, since both B[g,h,i]P and Cor have been reported to correlate closely with traffic emissions. Other PAHs such as retene (Ret) is also considered as a common biomarker of coniferous wood combustion, and resin acids such as abietic acid commonly found in smoke samples.

Since PAHs contents in atmosphere are sensitive to both anthropogenic and natural emissions, a more effective marker of traffic emissions is substantially required. Another potential index to distinguish the traffic emission is the use of inorganic tracers. It is widely known that particles from road dust appear to contain Pb, Fe, Mn, Ca and sometimes Zn, (Harrison et al., 1996). This can be explained by the attrition of road surfaces, resuspension of street dirt and soil dust (i.e. source of Ca and Mn; Pierson and Brachaczek, 1993), particles from tyre wear (i.e. source of Zn; Ondov et al., 1992), brake-drum abrasion, and debris from wear and rusting. In order to investigate the contributions of traffic related pollutants, several attempts were made for source apportionment of PAHs in Birmingham air by using inorganic source markers such as Cu, Fe, Pb, Zn and Mn. Lim et al (1999) reported high loading on higher MW PAHs (B[a]A to Cor) and moderate loading on BNT and Ph and the gasoline powered vehicle marker, Pb.

Based on size distribution of various elements at a road site location in Birmingham (BROS), Fe, Cu, Mg, Sr, Mo, Ce and Ba were found to be the major components in the traffic related coarse particle (i.e. 2 – 10 µm aerodynamic diameter, Harrison et al., 2003). Whilst strong correlations of Cu ($r^2 > 0.74$), Mo ($r^2 > 0.54$), Ba ($r^2 > 0.73$), Pb ($r^2 > 0.68$), Mn ($r^2 > 0.54$) and Zn ($r^2 > 0.61$) with NO_x indicated that these elements probably originate in road site particles. Until 1997, Pb and Br had been

widely employed as indicators of road traffic emissions (Harrison et al., 1997). Lead (Pb) is added to petrol in the form of an organic tetramethyl lead, an anti-knock agent, and is emitted by the exhaust stream in inorganic particulate forms, predominantly as PbClBr and $2\text{PbClBr}\cdot\text{NH}_4\text{Cl}$. Thus, the combination of Pb with Br can be used as classical marker elements for traffic emissions. However, the worldwide decline of Pb concentrations in the atmosphere has been observed due to the introduction of unleaded gasoline into the market in 1989 (Salma, et al., 2000). As a consequence, the Br/Pb ratio for determining the automotive contribution to the atmospheric lead burden may not be possible. In this study, *n*-alkanes and petroleum biomarkers such as hopanes and cholestanes had been introduced into the receptor models instead of inorganic marker elements like Pb. Alternatively, hopanes and cholestanes can be used as petroleum biomarkers, because: (i) these organic compounds are found mainly in exhausted gas from petroleum combustion and thus overlap PAHs combustion profiles, (ii) these organic compounds are not formed by atmospheric chemical reactions, (iii) these organic compounds are continuously released to the atmosphere by automotive emissions, and (iv) these organic compounds are prone to degradation in the environment. Because of these unique characteristics, hopanes and cholestanes have been widely used to define both the fossil origin and geological source of petroleum residues, (Rogge et al., 1993; Simoneit, 1984).

2.1.1 PAHs in aerosols from different countries

2.1.1.1 UK

PAH monitoring campaign was performed at two sites in London by Kendall et al (2001). The first sampling site was located at Bounds Green (BG) in North London. The second sampling site was positioned at St Paul's Cathedral (SP) in Central London. The annual means of the majority of the individual PAH compounds and ΣPAHs was higher at SP (7.24 ng m^{-3}) than at BG (4.27 ng m^{-3}). Both sites showed the same seasonal pattern of the lowest concentration during the summer and the highest average concentration during the autumn. B[g,h,i]P was the most abundant PAH at both London sites, followed by B[a]A and Chry, and these three PAHs dominated during all four seasons. The highest concentrations of these compounds were measured during the sampling week containing Bonfire Night at BG and during January at SP. Concentrations of these three compounds contributed over 50% of the ΣPAHs . In London, the winter ΣPAHs concentrations were only approximately twice the summer concentrations, possibly reflecting the small number of PAHs sources in London, with vehicles dominating PAHs production.

2.1.1.2 Indonesia

The burning of biomass as a method to clear and fertilise land is practiced in Indonesia every year by farmers and forestry companies. In 1997, Indonesia had been extremely dry due to El Nino, and what is now known as the Indonesia forest fire started to get out of control in the middle part of June. Emissions from biomass burning can vary widely because the material and the burning conditions can differ greatly. In a forest fire of this duration and magnitude, the burning material and conditions can vary from time to time as well as location to location. The ΣPAHs concentration ranged from 7 ng m^{-3} to 46 ng m^{-3} (Fang et al., 1999). The highest value of B[a]P was measured in Pudu on 27-09-97 at 3 ng m^{-3} while the lowest was at the same site on 04-09-97 at 0.1 ng m^{-3} . These values are comparable to those measured in Hong Kong, and the highest value matches some of the street-level monitoring

results (Fang et al., 1996). The concentration increase in Σ PAHs from the early to late September samples was the lowest. Retene, a common biomarker of coniferous wood combustion, and resin acids such as abietic acid commonly found in smoke samples in controlled studies, were not found in any of the samples in this study. This may be due to the transformation occurring in the long distance transportation of the aerosols, although retene was found to be relatively stable in sediments and did not vary in the same way as other PAHs (Ramdahl, 1983).

2.1.1.3 Greece

The field campaign took place in a conifer forest of central, continental Greece. Measurements were taken as part of the European Commission project, "Aerosols formation from biogenic organic carbon" (AEROBIC), during the period of 20 July-12 August, 1997. PAHs and oxy-PAHs detected in the Greek aerosols present an increase of concentrations with the number of benzene rings, with a dominance of PAHs with more than 5 rings. Σ PAHs concentrations (0.1 ng m^{-3} - 18.5 ng m^{-3}) were, in general, higher compared to that reported for a Portuguese forest, 0.1 ng m^{-3} - 0.9 ng m^{-3} (Kavouras et al., 1999), and other rural area of Greece, 0.2 ng m^{-3} - 2.0 ng m^{-3} (Gogou et al., 1996). However, these levels are lower than those presented for urban aerosols of a Greek island, 21.4 ng m^{-3} - 59.0 ng m^{-3} (Gogou et al., 1996).

2.1.1.4 Hong Kong

Hong Kong, with an area of 1092 km^2 and over 6.5 million in population, is surrounded by the South China Sea to the south and east, Pearl River Estuary on the west, and the landmass with complicated terrain on the north. It is also under the influence of the Asian Monsoon System. The summer monsoon brings in clean oceanic aerosols while a polluted air mass from the mainland comes with the northeasterly wind in the winter season. Thus the characteristics of Hong Kong's aerosols are represented by outside sources superimposed on very strong local emissions. Σ PAHs concentration was in the range of 0.7 ng m^{-3} - 12.2 ng m^{-3} (Zheng et al., 2000). In general, higher PAHs concentrations were found in the winter $\text{PM}_{2.5}$ samples. Other studies show that the changes in emission patterns (stationary and vehicular) and meteorological conditions (including less daylight hours, reduced ambient temperatures, and lower volatilization and photochemical activity) contribute to the higher PAHs levels during winter (Ramdahl et al., 1982, 1983; Freeman and Cattell, 1990; Baek et al., 1991a,b). The association of B[g,h,i]P with vehicle exhaust has long been established (Baek et al., 1991a,b), and a good correlation with total PAHs was obtained in this study. This suggests that vehicular emission was the dominant source of PAHs in the $\text{PM}_{2.5}$ cut of the aerosols in Hong Kong. The low molecular weight (LMW) PAHs such as Phe, Fluo and Pyr were enriched in the fall and winter samples. Comparing the spring and summer samples, the winter and fall samples contained more LMW PAHs. The LMW PAHs tend to be more concentrated in the vapour phase while the higher molecular weight ones are often associated with particulates. In addition, more details of PAHs in aerosols around the world are displayed in Table 6.

2.2 Source characterization of aliphatics

The enormous range of organic compounds detected in urban particles may be divided into two major source groups; primary condensates and oxidized hydrocarbons. Primary condensates (alkanes (C_{17} -

C₃₆), alkenes) originate directly from the incomplete combustion of fossil fuels and are sorbed onto the surface of particulate matter. Oxidized hydrocarbons (carboxylic acids, aldehydes, ketones, quinines, esters and phenols) may either be attached to the particulate as a primary condensate or may be produced during atmospheric oxidation reactions (Cautreels, 1978). Bray and Evans (1961) developed the carbon preference index (CPI) as an indicator of the extent of odd or even carbon number homologues within a sample. The CPI is expressed as a summation of the odd number homologues within a specified range of carbon numbers divided by a summation of the even number homologues within the same range. This inter-sample comparison is useful in identifying sources and establishing dominant sources of aerosol organic matter, as certain biologically produced *n*-alkanes show a pronounced predominance of odd carbon numbers (Bray and Evans, 1961). For example, organic matter of recent biogenic origin shows a preference for odd carbon numbered *n*-alkanes with CPI_{odd} values of 6-9 and more. Hydrocarbons of abiological origin (e.g. fossil fuels) typically show no carbon number preference or tend towards low CPI values (i.e. CPI < 1). To reconcile sources of organic species, CPI was calculated as follows (Tarek et al., 1996):

$$CPI_1 = \frac{\sum (C_{15} - C_{31})}{\sum (C_{14} - C_{32})}$$

Equation 2

CPI₁ represents whole range for *n*-alkanes

$$CPI_2 = \frac{\sum (C_{15} - C_{25})}{\sum (C_{14} - C_{24})}$$

Equation 3

CPI₂ represents petrogenic *n*-alkanes

$$CPI_3 = \frac{\sum (C_{25} - C_{31})}{\sum (C_{26} - C_{32})}$$

Equation 4

CPI₃ represents biogenic *n*-alkanes

The biogenic “wax” concentration of *n*-alkanes was calculated as follows:

$$Wax - n - Alkane = [C_n] - \left[\frac{(C_{n+1} - C_{n-1})}{2} \right]$$

Equation 5

Note that wax* has traditionally referred to a substance that is secreted by bees (i.e. beeswax) and used them in constructing their honeycombs. Additionally waxes may be natural or artificial. In this context, wax is natural oily substance. Chemically, a wax may be a combination of other fatty alcohols with fatty acids.

Scalan and Smith (1970) proposed the *odd-to-even* predominance n -C₂₉ OEP ratios by using the following equation;

$$n - C_{29}OEP = \frac{(C_{27} + 6C_{29} + C_{31})}{(4C_{28} + 4C_{30})}$$

Equation 6

OEP values were plotted against carbon chain length to construct the OEP curves. The pattern of the OEP curve is determined by the source of n -alkanes, which indicates the potential fingerprint for source apportionment. U:R is a good indicator of petroleum residue contribution. Under the resolved peaks in a typical n -alkane gas chromatogram, there is an unresolved complex mixture (UCM) in the form of an envelope, which contains branched and cyclic hydrocarbons. The UCM is also termed as the “hump” and is believed to be the contribution from fossil fuel residue. U:R is the ratio of the areas of the unresolved to resolved components (peaks) and is an indicator of the contamination by anthropogenic sources (Mei, 2000).

Hopanes are widespread in both recent and ancient sediments. The origin of most hopane is the bacterial C₃₅ tetratetrahydroxybacteriohopane. Hopane hydrocarbons present in sediments range from C₃₅ and down to C₂₇, usually with the C₃₀ isomers as the predominant. Hopanoid are produced by most living organism with $\beta\beta$ -configuration (17 β (H),21 β (H)). Increasing maturity leads to the more thermodynamically stable $\alpha\beta$ -hopanes and $\beta\alpha$ -hopanes, with the former being the predominant isomer. Molecular calculations have shown that the $\alpha\alpha$ -isomers are less stable than the $\alpha\beta$ -hopanes and $\beta\alpha$ -hopanes, but more stable than $\beta\beta$ -isomer (Philip et al., 1984). Most hopanoids are bio-synthesized with the 17 β (H),21 β (H) stereochemistry. C₂₉ and higher homologues of hopane are isomerized to 17 α (H),21 β (H) at any early stage of diagenesis. The degree of maturation can be calculated as follows:

$$\frac{17\alpha(H),21\beta(H)}{17\beta(H),21\beta(H) + 17\alpha(H),21\beta(H)} = \frac{\alpha\beta}{\beta\beta + \alpha\beta}$$

Equation 7

The ratio of equation 1.7 usually reach one simultaneously with the disappearance of 17 β (H),21 β (H). Furthermore, maturation enhances the content of 17 α (H),21 β (H) relative to 17 β (H),21 α (H). C₂₇-Hopanes have no side-chain and the conversion of 17 β (H) to 17 α (H) (T_m) reaches completion at maturity between the disappearance of 17 β (H),21 β (H) hopanes and 17 α (H),21 β (H) hopanes, that is prior to the onset of intense hydrocarbon generation. As illustrated in Figure 1.2, 18 α (H)-Trisnorhopane (T_s) is not affected by maturity changes, and the ratio: T_m/T_s can thus be used as a maturity indicator (Yunker et al., 2003). Recent studies have highlighted on the heterogeneous nature of hopane and sterane biomarkers in several river-dominated margins (Yunker et al., 2003 and Mudge, 2002). In the last two decades these petroleum biomarker parameters have been developed by organic geochemists to differentiate between oils, and determine their source in the aquatic environment and to trace their point sources (Zakaria et al., 2001).

For decades, pristane and phytane have been considered as biodegradable and thus these ratios might be valuable in the early stages of biodegradation (Prince et al., 1994). In particular, Burns and Teal (1979) stated that the branched alkanes extracted from marsh sediments at the West Falmouth site were completely degraded within the first seven years after the oil spill. These findings were based first on measurements of the pristane/phytane ratios. It was found that this ratio was 1.5 in the original Florida oil and that it decreased over a period of six years to 0.2. This is in contrast to another recent finding that have shown that *n*-alkane band in the fuel oil range (*n*-C₁₀-*n*-C₂₄) was no longer present, whereas all other compound classes such as nor-pristane, pristane and phytane are evident within the residual oil at the same sampling site (i.e. the West Falmouth site, Reddy et al., 2002). These latest results suggest that these compounds will be very useful petroleum biomarkers in understanding the distribution pattern of traffic-emitted aerosol components. In addition, steroid skeletons have been widely used as an indicator of diagenesis and the biological origin (biomarker) of organic matter (Jasper, 1993; Huang and Meinschein, 1976; Simoneit, 1984; Venkatesan et al., 2003). Steroids are also source tracers for biogenic material in complex mixtures of dissolved and particulate matter in the geosphere, especially in the marine environment (Brault and Simoneit, 1988 and Wang et al., 2004).

2.3 Cluster analysis & receptor models

2.3.1 Cluster analysis (CA)

Cluster analysis (CA), also called segmentation analysis or taxonomy analysis, seeks to identify homogeneous subgroups of cases in a population. That is, cluster analysis seeks to identify a set of groups which both minimise within-group variation and maximise between-group variation. In this study, CA was conducted using SPSS 13.0 for Windows. CA techniques may be *hierarchical* (i.e. the resultant classification has an increasing number of nested classes) or *non-hierarchical* (i.e. *k*-means clustering). *Hierarchical clustering* allows users to select a definition of distance, then select a linking method of forming clusters, then determine how many clusters best suit the data. *Hierarchical clustering* methods do not require pre-set knowledge of the number of groups. Two general methods of *hierarchical clustering* methods are available: divisive and agglomerative. The divisive technique start by assuming a single group, partitioning that group into subgroups, partitioning these subgroups further into subgroups and so on until each object forms its own subgroup. The agglomerative techniques start with each object describing a subgroup, and then combine like subgroups into more inclusive subgroups until only one group remains. In either case, the results of the application of the clustering technique are best described using a dendrogram or binary tree. The objects are represented as nodes in the dendrogram and the branches illustrate when the cluster method joins subgroups containing that object. The length of the branch indicates the distance between the subgroups when they are joined.

After selecting the *hierarchical clustering* method, it is important to select the clustering algorithm (i.e. the rules which govern between which point distances are measured to determine cluster membership). There are many methods available, the criteria used differ and hence different classifications may be obtained for the same data. Five algorithms, available within SPSS, are (i) average linkage clustering, (ii) complete linkage clustering, (iii) single linkage clustering, (iv) within

groups clustering and (v) Ward's method. Average linkage clustering is defined as the dissimilarity between clusters and calculated using cluster average values. The most common method to calculate an average is UPGMA (Un-weighted Pair-Groups Method Average). Complete linkage clustering (Maximum or Furthest-Neighbour Method) can be described as the dissimilarity between two groups is equal to the greatest dissimilarity between a member of cluster i and a member of cluster j . This method tends to produce very tight clusters of similar cases. On the other hand, single linkage clustering can be simply explained, as the dissimilarity between two clusters is the minimum dissimilarity between members of two clusters. This method has been widely employed in numerical taxonomy. Besides, it is crucial to note that within groups clustering is similar to UPGMA except clusters are fused so that within clusters variances is minimized. This tends to produce tighter clusters than the UPGMA method. Finally, Ward's Method is assessed by calculating the total sum of squared deviations from the mean of a cluster. The criterion for fusion is that it should produce the smallest possible increase in the error sum of squares.

2.3.2 Receptor models

Receptor models can be categorized into two types, namely, Chemical Mass Balance (CMB) and multivariate models. The most widely used multivariate models are principal component analysis (PCA), positive matrix factorization (PMF), and UNMIX model. CMB predicts the contribution of different sources to measured target compound concentrations in atmosphere by means of an inverse variance weighted least-square linear regression, (Watson *et al.*, 2001). The concept of CMB model, based on the principle of mass conservation, assumes that the total concentration of chemical species, C_i , at the receptor site, is the sum of the contributions from all sources j which emit species i .

$$C_i = \sum_{j=1}^p \alpha_{ij} \times f_{ij} \times S_j$$

Equation 8

where S_j is the fractional mass contribution of source j to the pollutant of target compound in the atmosphere, f_{ij} is the fraction of chemical species i in the emission from source j , for p sources. α_{ij} is the coefficient of fractionation used to correct uncertainties in f_{ij} between the source and the atmosphere, (Watson *et al.*, 1990 and Engelbrecht *et al.*, 2002).

Unlike other receptor models, which extract source compositions from the data, CMB model assumptions are based on: (i) compositions of source emissions are constant over the period of ambient and source sampling, (ii) chemical species do not react with each other, (iii) all sources with a potential for contributing to the receptor have been identified and have had their emissions characterized, (iv) the number of sources or source categories is less than or equal to the number of species, (v) the source profiles are linearly independent of each other, and (vi) the uncertainties are random, uncorrelated, and normally distributed, (CMB8 Applications and Validation Protocol for PM_{2.5} and VOCs announced by Desert Research Institute US). CMB have been widely used to assess sources of air pollutants because it: (i) theoretically yields the most likely solutions based on chemical source profiles, (ii) uses all available chemical measurements, (iii) estimates the uncertainty of the source contributions based on resolution of both the ambient concentrations and source profiles, (iv) provides greater influence to chemical species with higher resolution in both the source and receptor

measurements than to species with lower resolution. However, the major weaknesses of the CMB are its difficulty to account for non-stable compounds and incapability to identify those sources that have similar contributions. Moreover, CMB requires chemical source profiles as fingerprints for source apportionment of environmental pollutant.

The fundamental principles of various chemical methods for receptor modeling, including chemical mass balance (CMB) and multivariate method, have been review in detail (Gordon, 1988; Watson, 1994). Factor analysis offers the advantages of not requiring prior knowledge of the chemical composition and size distribution of emissions from specific sources (source profiles) but has the drawback of being mathematically indeterminate, allowing a wide range of possible solutions even when it is applied to relatively simple simulated data sets. In urban atmosphere, which is composed by many potential and diverse sources, PCA has been chosen by many workers for source apportionment. This technique has been widely applied to source apportionment of particulate pollutants, especially trace metals, and more recently, PAHs. In order to identify sources, multivariate receptor modeling can be applied to the observed target compound data. Multivariate approaches are based on the idea that the time dependence of a chemical species at the receptor site will be the same for species from the same source. Chemical species are measured in a large number of samples gathered at a single receptor site over time. Species of similar variability are grouped together in a minimum number of factors that explain the variability of data set. It is assumed that each factor is associated with a source or source type. However, the method has some limitations in that it can recognize at most only about eight individual source categories in any study, and poor discrimination of closely related source categories is commonly found. A further disadvantage of multivariate factor analysis is that large numbers of ambient air samples must be collected and analyzed (usually at least 50) and the statistically independent source tracers are required for each major source type.

In contrast to CMB model, multivariate techniques such as PCA are preferable since they require no qualitative insight of the sources of certain chemical species, and thus overcome the limitations of CMB, (Rachdawong et al., 1998 and Park et al., 2005). The aim of PCA is to identify the major sources of air pollutant emissions and to select statistically independent source tracers, (Bruno et al., 2001; Miller et al., 2002 and Gou et al., 2003). All variables are expressed in standardized form with a mean of 0 and a standard deviation of 1. The total variance therefore equals the total number of variables, and the variance of each factor expressed as a fraction of the total variance is referred to as the eigenvalue. If a factor has a low eigenvalue, then it is contributing little to the explanation of variances in the variables and may be ignored. PCA is generally used when the research purpose is data reduction (i.e. to reduce the information in many measured variables into a smaller set of components). PCA seeks a linear combination of variables such that the maximum variance is extracted from the variables. It then removes this variance and seeks a second linear combination that explains the maximum proportion of the remaining variance, and so on. This is called the principal axis method and results in orthogonal (uncorrelated) factors. Thus, the largest combination, accounting for most of the variance, becomes principal component 1 (PC1), the second largest accounts for the next largest amount of variances and becomes principal component 2 (PC2), and so on.

Over a period of about 10 years the combination of interest driven by regulations with advances in instrumental analytical analysis and the wide availability of computers resulted in the innovative field of source apportionment/receptor modeling. The first applications of a receptor model using factor analysis were done by Hopke *et al.* (1977) and Garrenstrom *et al.* (1977). The first Ph.D. thesis on multivariate air quality receptor modeling was that of Henry (1977). This work made explicit the connection between the statistical and physical models underlying multivariate receptor models for the first time. Finally, the initial development of UNMIX was fulfilled by Henry and Hidy (1979), who discovered physically significant air quality patterns in the first multivariate analysis of an air quality data set that combined pollutant gas concentrations, particulate composition, and meteorological variables.

UNMIX is a multivariate receptor modeling package that inputs observations of particulate composition and seeks to find the number, composition, and contributions of the contributing sources or source types. This model also produces estimates of the uncertainties in the source compositions. UNMIX uses a generalization of the self-modeling curve resolution method developed by Henry *et al.* (1997). Using only ambient data, UNMIX outputs the following information: (i) number of sources, (ii) composition of each source, (iii) source contributions to each sample, (iv) uncertainties in the source compositions, and (v) apportionment of the average total mass, if total mass is included in the model. The major advantages of the UNMIX are described as follows: (i) no assumptions about the number or compositions of sources are needed, (ii) no assumptions or knowledge of errors in the data are needed, and (iii) UNMIX automatically correct source compositions for effects of chemical reactions. A major difference between UNMIX and PMF is that UNMIX does not make explicit use of errors or uncertainties in the ambient concentrations. This is not to imply that the UNMIX approach regards data uncertainty as unimportant, but rather that the UNMIX model results implicitly incorporate error in the ambient data. Assume that N air quality samples are analyzed for n species, which come from m sources. If these species are conservative, then mass balance on each species requires that

$$C_{i,j} = \sum_{k=1}^m a_{jk} S_{ik} + errors$$

Equation 9

Where C_{ij} is the concentration of the j^{th} ($j=1, \dots, n$) species in the i^{th} sample ($i=1, \dots, N$), a_{jk} is the mass fraction of species j in source k ($k=1, \dots, m$), and S_{ik} is the total mass of material from source k in the i^{th} sample. In the parlance of receptor modeling, the a_{jk} are the source compositions, and the S_{ik} are the source contributions. The equation above includes errors, which may be the results of analytical uncertainty and variations in the sources' composition. The existence of errors profoundly complicates solution of the mixture problem, which is an ill-posed problem in that there are an insufficient number of constraints to define a unique solution. Several attempts to define a unique solution had been made by adding the obvious constraints of non-negativity of the source contribution and narrowing down the range of possible solutions based on physical knowledge of the sources (Henry *et al.*, 1994, 2003 and 2005). However, the question remains under what conditions can a unique solution be found using only the data without a priori knowledge. To answer this question, the

graphical approach had been introduced for solving the mixture problem. The main idea is to reduce the dimension of the problem by projection generalizes to any number of species and sources. Fig. 4 illustrates the single source case in which all the data points lie, except for errors, on a ray coming from origin. The direction of the ray is determined by the composition of the source. If $[p_1, p_2, p_3]$ is any point on the line, and $[a_1, a_2, a_3]$ is the source composition then $[p_1, p_2, p_3] = k[a_1, a_2, a_3]$. Since the ratio of each element relative to all others in the source composition, the mixture problem can be solved for the single source case, except that the source composition is only determined up to a multiplicative constant. In the case of two sources, as demonstrated in Fig. 5, the data are distributed in a plane through the origin. The problem is to find the vectors (or points) that represent the source composition. There are two possible choices for the source vectors namely (i) the source composition vectors of the two sources must lie in the same plane as the data and (ii) the source vectors must also be non-negative (Henry *et al.*, 2002). This further limits the data points to lie on the plane between the two rays defined by the two source compositions. If one source is missing from some of the data points then these data points will lie along a ray defined by the composition of the single, remaining source. These data points will be distributed so that an edge is apparent (see Fig. 5) and a line drawn along that edge will give the relative source composition, just as in the single source case.

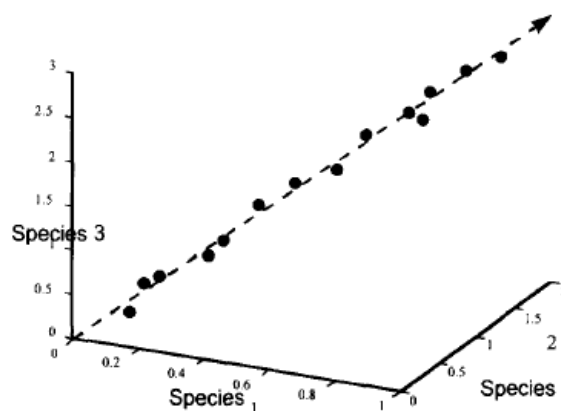


Figure 4. Plot for the one source, three species case showing the data points lying along the ray defined by the source composition (Henry *et al.*, 1997).

However, if there are three or more sources, then the points with one source missing have two or more sources present, and it is not so simple to determine the source compositions. As illustrated in Fig. 6, all the data points are composed of three sources of three species. In this case the points with one source missing are located on the planes defined by the rays through the remaining two sources. While this can be difficult to visualize those remaining two sources in a three-dimensional plot, a projection from the origin into a plane as demonstrated in Fig. 5 enables the location of the source vectors much easier to see. In most cases of environmental data, however, data points are composed of more than three sources and many more than three species. In this case the generalization to more than three dimensions requires the concepts of a hyperplane and simplex. A hyper-plane is the

generalization of a plane. For instance, a plane in 3-space is two dimensional, so a hyper-plane in n -space has dimension $n-1$. Thus, the process of reducing dimensions of the data points in UNMIX is to find the edges in the data (i.e. finding hyper-planes that define a simplex). Finally, UNMIX uses these edges to find the source points in data set.

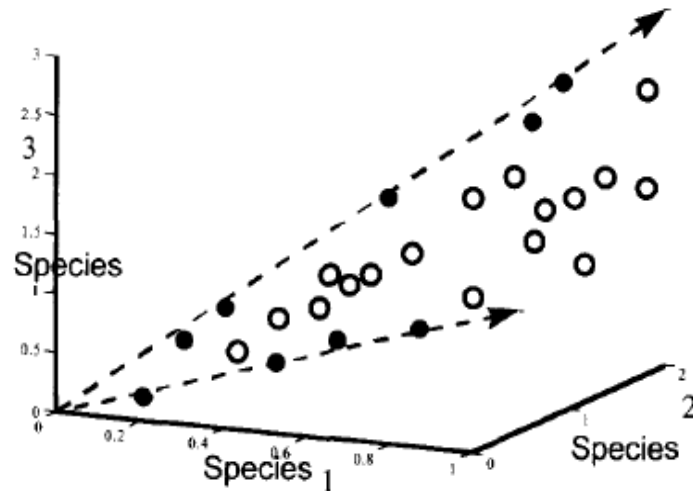


Figure 5. Plot for the two sources, three species case showing the data points lying in the plane defined by the two source composition rays. The solid circles are edge points, which have one source missing or low. The edges defined by these points give the relative source composition for the two sources (Henry *et al.*, 1997).

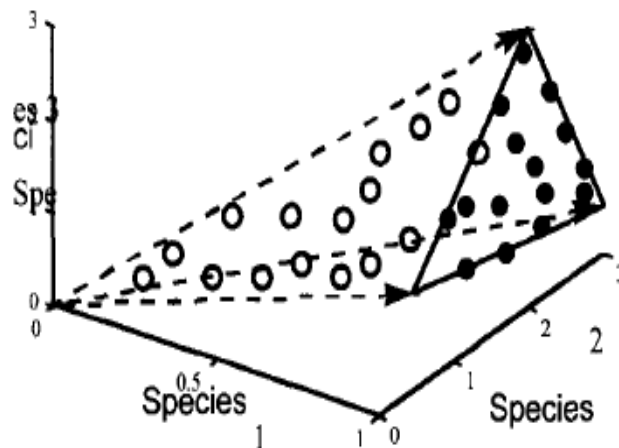


Figure 6. Plot for the three sources, three species case showing the data points (open circles) and the projection of the data points from the origin to the plane Species 1 = 1 (solid circles). Among the projected points, the edge points are easy to identify (Henry *et al.*, 1997).

3. DISCUSSION & CONCLUSION

Despite of considerably large number of studies focusing on tsunami impact onshore, little is known about their geomorphologic imprints offshore. In order to gain more insights on return periods of both earthquake and tsunami hazard, it is therefore crucial to study past tsunami events by carefully investigate offshore tsunami deposits. There remain substantial difficulties, however, in discriminating between deposits triggered by tsunamis and those caused by extreme events such as hurricane/Indian Ocean monsoon (IOM) and/or other sedimentary processes. Hence, it is important to emphasize that the term of “tsunami deposit” is that it defines deposits that have created by numerous distinctive geological processes that are not necessarily specific to marine deposits formed during the tsunami 'backwash' phase (Shanmugam, 2006; Shiki and Yamazaki, 2008). Tipmanee et al (2012) attempted to use PAHs as a chemical proxy to trace the transport of land-derived materials caused by the tsunami backwash to better understand how it may have affected the distribution of sedimentary deposition throughout the seabed of Khao Lak coastal areas. The article provides interesting application of diagnostic binary ratios of PAHs from coastal sediments and marine deposits in tsunami 2004 affected coastal area of Thailand. The application of PAHs as a chemical proxy to identify tsunami backwash patterns is interesting and very challenging, however, there are several concerns and questions that need clarification as well as some of the following points for a thorough reconsideration of the proposed concept.

- As the tsunami wave approaches the shoreline its wavelength become shorter and horizontal water velocity increases. It carries large amount of marine sediments to inundated land. After reaching its maximum run-up, the backwash phenomenon is occurred and responsible for channelized and erosions in specific places. The mixture of marine sediments, beach sediments, minor part of eroded terrestrial soils and eroded older sediments from backwash channels are transported back to the sea as high density flows, part is transferred as suspension load as well as simultaneously mobilization of marine sediments. Hence, it is most likely that offshore tsunami deposits contain both terrestrial signatures and re-deposited marine sediments. In normal conditions terrestrial component may be delivered to the sea bottom as well. However, this phenomenon will take longer time than the “tsunami backwash”, which the debris flow is very fast and sediments are buried rapidly then the "terrestrial set of PAH signatures" might be hypothetically preserved.
- It is also important to emphasize that not only “tsunami wave” but also “monsoon wave” can transfer terrigenous components from land to deposit in sea bottom. Therefore, it is crucial to consider the difference in nature of "tsunami wave" and "monsoon wave". While monsoon prolongs for several hours with relatively lower magnitude of power, the tsunami wave occurred in a greater magnitude of power but shorter in backwash time (i.e. several minutes). The tsunami deposit tends to contain "suspended particle", whereas the monsoon-derived sediments typically are produced through "bed-load transport". In these particular cases, two types of hypothesis can be considered;

Hypothesis I (Difference in transportation pattern)

It is well known that different types of PAHs exist in different sizes of particles (Kukkonen and Landrum, 1996; Wang et al., 2001). Since tsunami waves are capable of transport all particle sizes of terrestrial sediments via suspended load transport, it is most likely that tsunami deposit will have a different "distribution pattern of PAHs" from those of monsoon derived sediments.

Hypothesis II (Difference in erosion time)

Tsunami backwash occurred in relatively short time scale of minutes whereas the inundation of monsoon prolonged for several hours. Differences in "time dimension" cause the fractionization of PAHs due to its differences in term of "water solubility". For instance, Phe tends to have a higher water solubility than B[a]P (Lu et al., 2008). The longer the erosion, the higher amount of Phe will dissolve into backwash water in comparison with B[a]P. As a result, the monsoon derived deposit will contain Phe more than B[a]P. However, this fractionization effect will not happen in the case of tsunami deposit. Firstly, the tsunami involved only three large waves. Once the waves had passed and receded the event was over. Therefore, both Phe and B[a]P will be washed back by tsunami wave simultaneously without providing any time for the fractionization effect. For these reasons, the fingerprint of terrestrial PAHs may hypothetically be well preserved and possibly be a better proxy than conventional terrigenous biomarker "lignin" (Tareq et al., 2004), which is highly sensitive to microdegradation procedure due to its weak chemical structure in comparison with PAHs.

- Fingerprinting reflects the chemical characteristics of various source emissions of the sediment samples collected at any receptor. Because a simple ratio of two or three PAHs is sensitive to both photolysis and chemical/biological degradation and may be insufficient to identify PAH emission sources at fixed monitoring sites, the best strategy to investigate the impact of backwash tsunami is the use of the entire PAH profiles. Hence, the establishment of PAHs profile of individual "end member" is therefore essentially crucial.
- It is well known that Ret can be used as indicators of "wood combustion" (Gonçalves et al., 2011). During the bonfire night episode, the highest contributions of individual PAH came from Fl, Ac, Ret, B[b+j+k]F, Ind, B[g,h,i]P, while alkane concentrations was following the decrease order of $C_{29} > C_{24} > C_{27} > C_{22}$. The *chain-saw-distribution* of alkanes was evident at the range of C_{23} to C_{31} during the bonfire night episode, suggesting a strong signal of biomass burnings (Pongpiachan, 2013a). The contribution of diesel engine to atmospheric PAHs concentrations, especially those of Fl and Phe, has been widely investigated for many years (Williams *et al.*, 1986). It is well known that diesel fuel is relatively rich in PAHs and most of them are alkylated PAHs compared to that of the parent PAHs. Several factors like diesel-engine type and engine operating conditions reflect the ratio of MePhe/Phe in urban air. For example, the relatively high MePhe/Phe ratio was found when the combustion and exhaust temperatures were low (Barbella et al., 1989). Takada et al (1991) and Westerholm et al (1992) reported the values of MePhe/Phe ratios exhausted from diesel engine vehicle, bus and petrol engine vehicle as 5.5, 4.8 and 0.7 respectively. It is worth mentioning that the

- MePhe/Phe ratio of 5.5 was the average of five types of diesel engine ranging from 1500 cc to 14000 cc running without engine load and at a constant speed of 3000 rpm. In order to enhance the reliability of using PAHs as proxy of tsunami backwash deposits, one should consider the analysis of Ret, MePhe and Phe as well as the employment of *chain-saw-distribution* of alkanes and CPI index. In addition, it is also important to use cholestanes and hopanes as alternative biomarkers to distinguish “typical marine sediments” from “tsunami backwash deposits”.
- The representative of the “tsunami backwash” group as discussed by Tipmanee et al (2012) is not as far as approximately 25 km from the shoreline. Special signal found in this group could just be a particular dominant source, not necessary to be tsunami backwash signal. The results generated from binary ratios of PAHs, HCA coupled with PCA results obtained from Tipmanee et al (2012) were only surface sediments and there is no direct and strong evidence that the source of PAHs resulted from the tsunami in 2004. It could increase the strength if there are dated core sediment samples and showed the temporal distribution in this area. Furthermore, there are uncertainties in the estimation of source contribution by using PCA and UNMIX. Further source apportionment techniques such as a positive matrix factorisation (PMF) and a chemical mass balance (CMB) model should be conducted to increase the reliability of source contributions.
-

ACKNOWLEDGEMENTS

This work was performed with the approval of Deutsche Forschungsgemeinschaft (DFG) and National Research Council of Thailand (NRCT). The authors acknowledge the Research Center of National Institute of Development Administration (NIDA), Thailand for financial support.

REFERENCES

- Allard, B., Rager, M.N., and Templier, J., 2002: Occurrence of high molecular weight lipids (C80+) in the trilaminar outer cell walls of some freshwater microalgae. A reappraisal of algaenan structure. *Org. Geochem.*, 33, 789-801, 2002.
- Atwater, B.F., 1987: Evidence for great Holocene earthquakes along the outer coast of Washington State. *Science.*, 236, 942-4, 1987.
- Baek, S.O., Goldstone, M.E., and Kirk, P.W., 1991: Phase distribution and particle size dependency of polycyclic aromatic hydrocarbons in the urban atmosphere. *Chemosphere.*, 22, 503-20, 1991a.
- Baek, S.O., Field, R.A., Goldstone, M.E., Kirk, P.W., Lester, J.N., and Perry, R., 1991b: A review of atmospheric polycyclic aromatic hydrocarbons: sources, fate and behavior. *Water, Air, and Soil Pollution.*, 60, 279-300, 1991b.
- Barbella, R., Ciajolo, A., Anna, D.A., and Bertoli, C., 1989: Effect of fuel aromaticity on diesel emissions. *Combust. Flame.*, 77(3-4), 267-77, 1989.
- Belicka, L.L., Macdonald, W.R., Yunker, B.M., and Harvey, R.H., 2004: The role of depositional regime on carbon transport and preservation in Arctic Ocean sediments. *Mar. Chem.*, 86, 65-88, 2004.
- Benson, B. E., Grimm, K. A., and Clague, J. J.: Tsunami deposits beneath tidal marshes on northwestern Vancouver Island British Columbia. *Quaternary. Res.*, 48, 192-204, 1997.
- Blokker P., van Bergen P. F., Pancost R. D., Collinson M. E., Sinninghe Damst J. S., and de Leeuw J. W.: The chemical structure of *Gloeocapsomorpha prisca* microfossils: implication for their origin. *Geochim. Cosmochim. Acta.*, 65, 885-900, 2001.
- Bondevik, S., Sevendsen, J. I., and Mangerud, J.: Tsunami sedimentary facies deposited by the Storegga tsunami in shallow marine basins and coastal lakes, western Norway. *Sedimentology.*, 44, 1115-31, 1997.
- Boonyatumanond, R., Murakami, M., Wattayakorn, G., Togo, A., and Takada, H.: Sources of polycyclic aromatic hydrocarbons (PAHs) in street dust in a tropical Asian mega-city, Bangkok, Thailand. *Sci. Tot. Environ.*, 384 (1-3), 420-32, 2007.
- Brasser, L. J.: Polycyclic aromatic hydrocarbon concentrations in the Netherlands. *VDI-Berichete Nr.*, 348, 171-80, 1980.
- Brault, M., and Simoneit, T.R.B.: Steroid and triterpenoid distributions in bransfield strait sediments: Hydrothermally-enhanced diagenetic transformations. *Org. Geochem.*, 13(4-6), 697-705, 1988.

Bray, E.E., and Evans, E.D.: Distribution of n-paraffins as a clue to recognition of source beds. *Geochim. Cosmochim. Acta.*, 22, 2-15, 1961.

Bruno, P., Caselli, M., Curri, L.M., Genga, A., Striccoli, R., and Traini, A.: Chemical characterisation of ancient pottery from south of Italy by Inductively Coupled Plasma Atomic Emission Spectroscopy (ICP-AES): Statistical multivariate analysis of data. *Anal. Chim. Acta.*, 410(1-2), 193-202, 2000.

Bryant, E.: *Tsunami. The Underrated Hazard*: Cambridge, 320, 2001.

Burns, K.A., and Teal, J.M.: The West Falmouth oil spill: hydrocarbons in the salt marsh ecosystem. *Est. Coast. Mar. Sci.*, 8, 349-60, 1979.

Cantalamessa, G., and Di Celma, C.: Sedimentary features of tsunami backwash deposits in a shallow marine Miocene setting, Mejillones Peninsula, northern Chile. *Sediment. Geol.*, 178, 259 – 73, 2005.

Cautreels, W., and Van Cauwenburghe, K.: Experiments on the distribution of organic pollutants between airborne particulate matter and the corresponding gas phase. *Atmos. Environ.*, 12, 1133-41, 1978.

Chetwittayachan, T., Shimazaki, D., and Yamamoto, K.: A comparison of temporal variation of particle-bound polycyclic aromatic hydrocarbons (pPAHs) concentration in different urban environments: Tokyo, Japan, and Bangkok, Thailand. *Atmos. Environ.*, 36 (12), 2027-37, 2002.

Choowong, M., Murakoshi, N., Hisada, K., Charusiri, P., Daorerk, V., Charoentitirat, T., Chutakositkanon, V., Jankaew, K., and Kanjanapayont, P.: Erosion and deposition by the 2004 Indian Ocean tsunami in Phuket and Phang-nga Provinces, Thailand. *J. Coastal. Res.*, 23(5), 1270–76, 2007.

Choowong, M., Murakoshi, N., Hisada, K., Charusiri, P., Charoentitirat, T., Chutakositkanon, V., Jankaew, K., Kanjanapayont, P., and Phantuwongraj, S.: 2004 Indian Ocean tsunami inflow and outflow at Phuket, Thailand. *Mar. Geol.*, 248(3–4), 179–92, 2008a.

Choowong, M., Murakoshi, N., Hisada, K., Charoentitirat, T., Charusiri, P., Phantuwongraj, S., Wongkok, P., Choowong, A., Subsayjun, R., Chutakositkanon, V., Jankaew, K., and Kanjanapayont, P.: Flow conditions of the 2004 Indian Ocean tsunami in Thailand inferred from capping bedforms and sedimentary structures. *Terra. Nova.*, 20, 141–9, 2008b.

Choowong, M., Phantuwongraj, S., Charoentitirat, T., Chutakositkanon, V., Yumuang, S., and Charusiri, P.: Beach recovery after 2004 Indian Ocean tsunami from Phang-nga, Thailand. *Geomorphology.*, 104, 134–42, 2009.

Chagué-Goff, C., Schneider, J.L., Goff, J.R., Dominey-Howes, D., and Strotz, L.: Expanding the proxy toolkit to help identify past events—Lessons from the 2004 Indian Ocean Tsunami and the 2009 South Pacific Tsunami. *Earth. Sci. Rev.*, 107, 107–22, 2011.

Dawson, A.G., Long, D., and Smith, D.E.: The Storegga slides: Evidence from eastern Scotland for a possible tsunami. *Mar. Geol.*, 82, 271-6, 1988.

Dawson, A.G., Foster, I. D. L., Shi, S., Smith, D.E., and Long, D.: The identification of tsunami deposits in coastal sediment sequences. *Sci. Tsunami. Hazards.*, 9, 73-82, 1991.

Dawson, A.G.: Linking tsunami deposits, submarine slides and offshore earthquakes. *Quaternary Intern.*, 60, 119 – 26, 1999.

Dawson, A.G., and Shaozong, S.: Tsunami Deposits. *Pure. Appl. Geophys.*, 157, 875 – 97, 2000.

Department of Mineral Resources, 2005. Goehazard Mitigation: How to survive a tsunami, 34 p.

Diesing, M., Kubicki, A., Winter, C., and Schwarzer, K.: Decadel scale stability of sorted bedforms, German Bight, Southeastern North Sea. *Cont. Shelf. Res.*, 26, 902 – 16, 2006.

Duan, J., Bi, X., Tan, J., Sheng, G., and Fu, J.: The differences of the size distribution of polycyclic aromatic hydrocarbons (PAHs) between urban and rural sites of Guangzhou, China. *Atmos. Environ.*, 78, 190-203, 2005.

Einsele, G.: Event stratigraphy: recognition and interpretation of sedimentary event horizons. In: Doyle, P. and Bennett, M.R. (eds.). *Unlocking the stratigraphic record: advances in modern stratigraphy*, 145 – 193, 1998.

Engelbrecht, P.J., Swanepoel, L., Chow, C.J., Watson, G.J., and Egami, T.R.: The comparison of source contributions from residential coal and low-smoke fuels, using CMB modelling, in South Africa. *Environ. Sci. Pol.*, 5(2), 157-67, 2002.

EPA Appendix A to 40 CFR, Part 423–126 Priority Pollutants Available from: <http://www.epa.gov/region01/npdes/permits/generic/prioritypollutants.pdf>, (2003).

Fang, M., Wan, T., and Kwan, J.: Characterization of the organic compounds in the aerosols of Hong Kong-identification, abundance, origin and toxicity. *Research Center Publication.*, 21-96, 1996.

Fang, M., Zheng, M., Wang, F., To, K.L., Jaafar, A.B., and Tong, S.L.: The solvent extractable organic compounds in Indonesia biomass burning aerosols – Characterisation studies. *Atmos. Environ.*, 33, 783-95, 1999.

Fang, G.C., Chang, C.N., Wu, Y.S., Fu, P.P.C., Yang, I.L., and Chen, M.H.: Characterization, identification of ambient air and Road dust polycyclic aromatic hydrocarbons in central Taiwan, Taichung. *Sci. Tot. Environ.*, 366(2-3), 729-38, 2006.

- Ferrini, V.L., and Flood, R.D.: A comparison of Rippled Scour Depressions identified with multibeam sonar: Evidence of sediment transport in inner shelf environments. *Cont. Shelf. Res.*, 25, 1979–95, 2005.
- Fisher, R.V.: Flow transformation in sediment gravity flows. *Geology.*, 11, 273 – 4, 1983.
- Freeman, D.J., and Cattell, F.C.R.: Wood-burning as a source of atmospheric polycyclic aromatic hydrocarbons. *Environ. Sci. Technol.*, 24, 1581-5, 1990.
- Garrenstrom, D.P., Perone, P.S., and Moyers, L.J.: Application of pattern recognition and factor analysis for characterization of atmospheric particulate composition in southwest desert atmosphere. *Environ. Sci. Technol.*, 10, 795-800, 1977.
- Gelfenbaum, G., and Jaffe, B.: Erosion and sedimentation from the July 17, 1998 Papua New Guinea tsunami. *Pure. Appl. Geophys.*, 160, 1969-99, 2003.
- Gogou, A., Stratigakis, N., Kanakidou, M., and Stephanou, E.: Organic aerosol in Eastern Mediterranean: component source reconciliation by using molecular markers and atmospheric back trajectories. *Org. Geochem.*, 25, 79-96, 1996.
- Gogou, I. A., Bouloubassi, I., and Stephanou, G.E.: Marine organic geochemistry of the Eastern Mediterranean: 1. Aplyphatic and polyaromatic hydrocarbons in Cretan Sea surficial sediments. *Mar. Chem.*, 68(4), 265-82, 2000.
- Gordon, G.E.: Receptor models. *Environ. Sci. Technol.*, 22, 1132–42, 1988.
- Gonçalves, C., Alves, C., Fernandes, A. P., Monteiro, C., Tarelho, L., Evtyugina, M., and Pio, C.: Organic compounds in PM_{2.5} emitted from fireplace and woodstove combustion of typical Portuguese wood species. *Atmos. Environ.*, 45 (27), 4533-45, 2011.
- Gou, H., Lee, C.S., Ho, F.K, Wang, X.M., and Zou, C.S.: Particle-associated polycyclic aromatic hydrocarbons in urban air of Hong Kong. *Atmos. Environ.*, 37, 5307–17, 2003.
- Grantham, P. J., and Douglas, A. G.: The nature and origin of sesquiterpenoids in some Tertiary fossil resins. *Geochim. Cosmochim. Acta.*, 44, 1801-10, 1980.
- Gusiakov, V.K.: Tsunami generation potential of different tsunamigenic regions in the Pacific. *Mar. Geol.*, 215, 3 – 9, 2005.

Harrison, R. M., Smith, D. J. T., and Luhana, L.: Source Apportionment of Atmospheric Polycyclic Aromatic Hydrocarbons Collected from an Urban Location in Birmingham, U.K. *Environ. Sci. Technol.*, 30(3), 825-32, 1996.

Harrison, R.M., Smith, D.J.T., Pio, C.A., and Castro, L.M.: Comparative receptor modeling study of airborne particulate pollutants in Birmingham (United Kingdom), Coimbra (Portugal) and Lahore (Pakistan). *Atmos. Environ.*, 31, 3309-21 1997.

Harrison, M.R., Tilling, R., Callèn Romero, S.M., Harrad, S., and Jarvis, K.: A study of trace metals and polycyclic aromatic hydrocarbons in the roadside environment. *Atmos. Environ.*, 37, 2391-402, 2003.

Hedberg, H. D.: Significance of high-wax oils with respect to genesis of petroleum. *Am. Assoc. Petrol. Geol. Bull.*, 52(5), 736-50, 1968.

Henry, C.R., and Hidy, M.G.: Multivariate analysis of particulate sulfate and other air quality variables by principal components-Part I: Annual data from Los Angeles and New York. *Atmos. Environ.*, 3, 1581-96, 1979.

Henry, C.R., Lewis, C., and Collins, J.: Vehicle-related hydrocarbon source compositions from ambient data: The GRACE/SAFER method. *Environ. Sci. Technol.*, 28, 823-32, 1994.

Henry, C.R.: Multivariate receptor modeling by *N*-dimensional edge detection. *Chemom. Intell. Lab. Syst.*, 65, 179-89, 2002.

Henry, C.R.: Multivariate receptor modelling by *N*-dimensional edge detection, *Chemom. Intell. Lab. Syst.*, 65(2), 179-89, 2003.

Henry, C.R.: Duality in multivariate receptor models, *Chemom. Intell. Lab. Syst.*, 77(1-2), 59-63, 2005.

Holba, A. G., Dzou, L. I. P., Masterson, W. D., Hughes, W. B., Huizinga, B. J., Singletary, M. S., Moldowan, J. M., Mello, M. R., and Tegelaar, E.: Application of 24-norcholestanes for constraining source age of petroleum. *Org. Geochem.*, 29(5-7), pp.1269-83, 1998a.

Holba, A. G., Tegelaar, E. W., Huizinga, B. J., Moldowan, J. M., Singletary, M. S., McCaffrey, M. A., and Dzou, L. I. P.: 24-norcholestanes as age-sensitive molecular fossils. *Geology.*, 26(9), 783-6, 1998b.

Hopke, K.P., Gladney, S.E., Gordon, E.G., Zoller, H.W., and Jones, G.A.: The use of multivariate analysis to identify sources of selected elements in the Boston urban aerosol. *Atmos. Environ.*, 10, 1015-25, 1977.

Huang, Y.W., and Meinschein, G.W.: Sterols as source indicators of organic materials in sediments. *Geochimica et Cosmochimica Acta.*, 40(3), 323-30, 1976.

International Agency for Research on Cancer (1983) IARC Monographs on the evaluation of the carcinogenic risk of chemicals to man, Vol.32: Polycyclic aromatic hydrocarbons, Part 1: Chemical, environmental and experimental data. IARC, Lyon, France.

International Agency for Research on Cancer (1984) IARC Monographs on the evaluation of the carcinogenic risk of chemicals to man, Vol.34: Polycyclic aromatic hydrocarbons, Part 3: Industrial exposures in aluminium production, coal gasification, coke production, and iron and steel founding. IARC, Lyon, France.

International Agency for Research on Cancer (1985) IARC Monographs on the evaluation of the carcinogenic risk of chemicals to man, Bitumens, coal-tars and derived products, shale-oils and soots. Monograph No 35, IARC, Lyon, France.

International Agency for Research on Cancer (1987) IARC Monographs on the evaluation of the carcinogenic risk of chemicals to man, Supplement, IARC, Lyon, France.

Jasper, P.J., and Gagosian, B.R.: The relationship between sedimentary organic carbon isotopic composition and organic biomarker compound concentration. *Geochim. Cosmochim. Acta.*, 57 (1), 167-86, 1993.

Kalaitzoglou, M., Terzi, E., and Samara, C.: Patterns and sources of particle-phase aliphatic and polycyclic aromatic hydrocarbons in urban and rural sites of western Greece. *Atmos. Environ.*, 38, 2545-60, 2004.

Kavouras, G.I., Lawrence, J., Koutrakis, P., Stephanou, G.E., and Oyola, P.: Measurement of particulate aliphatic and polynuclear aromatic hydrocarbons in Santiago de Chile: Source reconciliation and evaluation of sampling artifacts. *Atmos. Environ.*, 33(30), 4977-86, 1999.

Kendall, M., Hamilton, S. R., Watt, J., and Williams, D. I.: Characterisation of selected speciated organic compounds associated with particulate matter in London. *Atmos. Environ.*, 35, 2483-95, 2001.

Killops, S. D., Carlson, R. M. K., and Peters, K. E.: High-temperature GC evidence for the early formation of C₄₀+ n-alkanes in coals. *Org. Geochem.*, 31, 589-97, 2000.

Kukkonen, J., and Landrum, P. F.: Distribution of organic carbon and organic xenobiotics among different particle-size fractions in sediments. *Chemosphere.*, 32 (6), 1063-76, 1996.

Le Roux, J.P., and Vargas, G.: Hydraulic behaviour of tsunami backflows: Insights from their modern and ancient deposits. *Environ. Geol.*, 49, 65 – 75, 2005.

Li, C., Fu, J., Sheng, G., Bi, X., Hao, Y., Wang, X., and Mai, B.: Vertical distribution of PAHs in the indoor and outdoor PM_{2.5} in Guangzhou, China. *Build. Environ.*, 40, 327–39, 2005.

Lim, H. L., Harrison, M. R., and Harrad, S.: The contribution of traffic to atmospheric concentrations of polycyclic aromatic hydrocarbons. *Environ. Sci. Technol.*, 33, 3538-42, 1999.

Lu, G. N., Dang, Z., Tao, X. Q., Yang, C., and Yi, X. Y.: Estimation of water solubility of polycyclic aromatic hydrocarbons using quantum chemical descriptors and partial least squares. *Mol. Inform.*, 27(5), 618-26, 2008.

Mainwaring, S. J., and Stirling, D. M.: A study of the size distribution and concentrations of polynuclear hydrocarbons in Melbourne air. In “Proceedings of the 7th International Clean Air”, 1981.

Mei, Z., Ming, F., and Fuwang, K.L.: Characterization of the solvent extractable organic compounds in PM_{2.5} aerosols in Hong Kong. *Atmos. Environ.*, 34(17), 2691-702, 2000.

Miller, L.S., Anderson, J.M., Daly, P.E., and Milford, B.J.: Source apportionment of exposures to volatile organic compounds. I. Evaluation of receptor models using simulated exposure data. *Atmos. Environ.*, 36(22), 3629-41, 2002.

Moldowan, J. M., Fago, F. J., Lee, C. Y., Jacobson, S. R., Watt, D. S., Slougui, N.E., Jeganathan, A., and Young, D. C.: Sedimentary 24-n-propylcholestanes, molecular fossils diagnostic of marine algae. *Science.*, 247, 309-12, 1990.

Motelay, A., Harner, T.M., Shoeib, M., Diamond, M., Stern, G., and Rosenberg, B.: Using passive air samplers to assess urban-rural trends for persistent organic pollutants and polycyclic aromatic hydrocarbons. 2. Seasonal trends for PAHs, PCBs and Organochlorine Pesticides. *Environ. Sci. Technol.*, 39, 5763-73, 2005.

Mudge, S.M.: Reassessment of the hydrocarbons in Prince William Sound and the Gulf of Alaska: Identifying the source using Partial Least-Squares. *Environ. Sci. Technol.*, 36, 2354-60, 2002.

Murray, A.B., and Thielert, E.R.: A new hypothesis on exploratory model for the formation of large-scale inner shelf sediment sorting and “rippled scour depressions”. *Cont. Shelf. Res.*, 24, 295 – 315, 2004.

Nielsen, T.: Traffic contribution of polycyclic aromatic hydrocarbons in the center of a large city. *Atmos. Environ.*, 30(20), 3481-90, 1996.

Nitttrouer, C.A., and Wright, L.D.: Transport of particles across continental shelves. *Rev. Geophys.*, 32, 85–113, 1994.

Ohura, T., Amagai, T., Sugiyama, T., Fusaya, M., and Matsushita, H.: Characteristics of particle matter and associated polycyclic aromatic hydrocarbons in indoor and outdoor air in two cities in Shizuoka, Japan. *Atmos. Environ.*, 38, 2045–54, 2004.

Ondov, M.J., Kelly, R.W., Holland, Z.J., Lin, C.Z., and Wight, A.S.: Tracing fly ash emitted from a coal-fired power plant with enriched rare-earth isotopes: An urban scale test. *Atmos. Environ. Part B.*, 26(4), 453–62, 1992.

Ourisson, G., and Albrecht, P.: Hopanoids 1. Geohopanoids: the most abundant natural products on Earth? *Acc. Chem. Res.*, 25, 398–402, 1992.

Paasivirta, J., Sinkkonen, S., Mikkelsen, P., Rantio, T., and Wania, F.: Estimation of vapor pressures, solubilities and Henry's law constants of selected persistent organic pollutants as functions of temperature. *Chemosphere*, 39(5), 811–32, 1999.

Park, S.S., and Kim, J.Y.: Source contributions to fine particulate matter in an urban atmosphere. *Chemosphere.*, 59(2), 217–26, 2005.

Pierson, R.W., and Brachaczek, W.W.: Particulate matter associated with vehicles on the road II. *Aerosol. Sci. Technol.*, 2, 1–40, 1993.

Pinegina, T.K., and Bourgeois, J.: Historical and paleo-tsunami deposits on Kamchatka, Russia: long-term chronologies and long-distance correlations. *Nat. Hazard. Earth. Sys. Sci.*, 1, 177–85, 2001.

Pongpiachan, S., Thamanu, K., Ho, K.F., Lee, S.C., and Sompongchaiyakul, P.: Predictions of gas-particle partitioning coefficients (K_p) of polycyclic aromatic hydrocarbons at various occupational environments of Songkhla province, Thailand. *Southeast Asian J. Trop. Med.*, 40 (6), 1377–94, 2009.

Pongpiachan, S., Thumanu, K., Na Pattalung, W., Hirunyatrakul, P., Kittikoon, I., Ho, F. K., and Cao, J. J.: Diurnal variation and spatial distribution effects of Sulfur Speciation in Aerosol Samples as Assessed by X-ray Absorption Near-edge Structure (XANES). *J. Anal. Methods. Chem.*, Article ID 696080, 10 pages, doi:10.1155/2012/696080, 2012a.

Pongpiachan, S., Thumanu, K., Kositanont, C., Schwarzer, K., Prietzel, J., Hirunyatrakul, P., and Kittikoon, I.: Parameters Influencing Sulfur Speciation in Environmental Samples Using Sulfur K-Edge X-Ray Absorption Near-Edge Structure (XANES). *J. Anal. Methods. Chem.*, Article ID 659858, 12 pages, doi: 10.1155/2012/659858, 2012b.

Pongpiachan, S.: Fingerprint of Carcinogenic Semi-Volatile Organic Compounds (SVOCs) during Bonfire Night. *Asian. Pac. J. Cancer. Prev.*, 14(5), 3243-54, 2013a.

Pongpiachan, S.: Vertical distribution and potential risk of particulate polycyclic aromatic hydrocarbons in high buildings of Bangkok, Thailand. *Asian. Pac. J. Cancer. Prev.*, 14(3), 1865-77, 2013b.

Pongpiachan, S.: Diurnal Variation, Vertical Distribution and Source Apportionment of Carcinogenic Polycyclic Aromatic Hydrocarbons (PAHs) in Chiang-Mai, Thailand. *Asian. Pac. J. Cancer. Prev.*, 14(3), 1851-63, 2013c.

Pongpiachan, S., Thumanu, K., Na Phatthalung, W., Tipmanee, D., Kanchai, P., Feldens, P., and Schwarzer, K.: Using Fourier Transform Infrared (FTIR) to Characterize Tsunami Deposits in Near-Shore and Coastal Waters of Thailand. *Sci. Tsu. Haz.*, 32 (1), 39-57, 2013a.

Pongpiachan, S., Thumanu, K., Tanthanuch, W., Tipmanee, D., Kanchai, P., Schwarzer, K., and Tancharakorn, S.: Sedimentary features of tsunami backwash deposits as assessed by micro-beam synchrotron X-Ray Fluorescence (μ -SXRF) at the Siam Photon Laboratory. *Sci. Tsu. Haz.*, 32 (2), 96-115, 2013b.

Pongpiachan, S., Choochuay, C., Hattayanone, M., and Kositanont, C.: Temporal and spatial distribution of particulate carcinogens and mutagens in Bangkok, Thailand. *Asian. Pac. J. Cancer. Prev.*, 14(3), 1879-87, 2013c.

Pongpiachan, S., Ho, K. F., and Cao, J.: Estimation of Gas-Particle Partitioning Coefficients (K_p) of Carcinogenic Polycyclic Aromatic Hydrocarbons by Carbonaceous Aerosols Collected at Chiang-Mai, Bangkok and Hat-Yai, Thailand. *Asian. Pac. J. Cancer. Prev.*, 14(4), 3369-84, 2013d.

Pongpiachan, S., Tipmanee, D., Deelaman, W., Muprasit, J., Feldens, P., and Schwarzer, K.: Risk assessment of the presence of polycyclic aromatic hydrocarbons (PAHs) in coastal areas of Thailand affected by the 2004 tsunami. *Mar. Pollut. Bulletin.*, In Press, 2013e.

Prince, R.C., Elmendoft, D.L., Lute, R.J., and Hsu, C.E.: $17\alpha(H), 21\beta(H)$ -hopanes as a conserved internal marker for estimating the biodegradation of crude oil. *Environ. Sci. Technol.*, 28, 142-5, 1994.

Rachdawong, P., Christensen, R.E., and Chi, S.: Source identification of PCBs in sediments from the Milwaukee Harbor Estuary, USA. *Water. Sci. Technol.*, 37(6-7), 199-206, 1988.

Ramdahl, T.: Retene- a molecular marker of wood combustion in ambient air. *Nature.*, 306, 580-2, 1983.

Ramdahl, T., and Becher, G.: Characterization of polynuclear aromatic hydrocarbon derivatives in emissions from wood and cereal straw combustion. *Analytica. Chimica. Acta.*, 144(1), 83-91, 1982.

Ramdahl, T., and Møller, M.: Chemical and biological characterization of emissions from a cereal straw burning furnace. *Chemosphere.*, 12(1), 23-4, 1983.

Reddy, M.C., Eglinton, I.T., Hounshell, A., Xu, K.W., Gaines, B.R., and Frysinger, S.G.: The West Falmouth oil spill after thirty years: The persistence of petroleum hydrocarbons in marsh sediments. *Environ. Sci. Technol.*, 36 (22), 4754-60, 2002.

Rogge, W. F., Mazurek, M. A., Hildemann, L. M., and Cass, G. R., and Simoneit, B.R.T.: Quantification of urban organic aerosols at a molecular level: identification, abundance and seasonal variation. *Environ. Sci. Technol.*, 27A, 1309-30, 1993.

Rohmer, M., Bouvier-Nav, P., and Ourisson, G.: Distribution of hopanoid triterpenes in prokaryotes. *J. Gen. Microbiol.*, 130, 1137-50, 1984.

Ruchirawat, M., Mahidol, C., Tangjarukij, C., Pui-ock, S., Jensen, O., Kampeerawipakorn, O., Tuntaviroon, J., Aramphongphan, A., and Autrup, H.: Exposure to genotoxins present in ambient air in Bangkok, Thailand — particle associated polycyclic aromatic hydrocarbons and biomarkers. *Sci. Tot. Environ.*, 287 (1-2), 121-32, 2002.

Ruchirawat, M., Navasumrit, P., Settachan, D., Tuntaviroon, J., Buthbumrung, N., and Sharma, S.: Measurement of genotoxic air pollutant exposures in street vendors and school children in and near Bangkok. *Toxicol. Appl. Pharm.*, 206 (2), 207-14, 2005.

Ruchirawat, M., Settachan, D., Navasumrit, P., Tuntawiroon, J., and Autrup, H.: 2007. Assessment of potential cancer risk in children exposed to urban air pollution in Bangkok, Thailand. *Toxicol. Lett.*, 168 (3), 200-9, 2007.

Salma, I., Maenhaut, W., Dubtsov, S., Zemplén-Papp, E., and Záray, G.: Impact of phase out of leaded gasoline on the air quality in Budapest. *Microchemical Journal.*, 67(1-3), 127-33, 2000.

Sanderson, G.E., Raqbi, A., Vyskocil, A., and Farant, P.J.: Comparison of particulate polycyclic aromatic hydrocarbon profiles in different regions of Canada. *Atmos. Environ.*, 38, 3417-29, 2004.

Scheffers, A., and Kelletat, D.: Sedimentologic and geomorphologic tsunami imprints worldwide – a review. *Earth. Sci. Rev.*, 63, 83 – 92, 2003.

Schwarzer, K., Diesing, M., Larson, M., Niedermeyer, R.O., Schumacher, W., and Furmanczyk, K.: Coastline evolution at different time scales. - Examples from the southern Baltic Sea (Pomeranian Bight) – *Mar. Geol.*, 194, 79 – 101, 2003.

Shanmugam, G.: The Tsunamite problem. *J. Sediment. Res.*, 76, 718–30, 2006.

Shi, S., Dawson, A.G., and Smith, D.E.: Coastal tsunami sedimentation processes. In: CEA/DASE (eds.). *Proceedings of the International Conference on Tsunamis*, Paris, France, May 26 – 28, 43 – 55, 1998.

Shiki, T., and Yamazaki, T.: The term 'Tsunamiite'. In Shiki T. *Tsunamiites: features and implications*. *Developments in Sedimentology*. Elsevier. p. 5. ISBN 978-0-444-51552-0. 2008.

Simoneit, B.R.T.: Organic matter of the troposphere—III. Characterization and sources of petroleum and pyrogenic residues in aerosols over the western United States. *Atmos. Environ.*, 18, 51–67, 1984.

Stenberg, U., and Alsberg, T.: Capillary GC-MS analysis of PAH emissions from combustion of peat and wood in hot water boiler. *Chemosphere.*, 8, 487-96, 1979.

Summons, R. E., Jahnke, L. L., and Roksandic, Z.: Carbon isotope fractionation in lipids from methanotrophic bacteria: relevance for interpretation of the geological record of biomarkers. *Geochim. Cosmochim. Acta.*, 58, 2853-63, 1994a.

Szczuciński, W., Niedzielski, P., Rachlewicz, G., Sobczyński, T., Ziola, A., Kowalski, A., Lorenc, S., and Siepak, J.: Contamination of tsunami sediments in a coastal zone inundated by the 26 December 2004 tsunami in Thailand. *Environ. Geol.*, 49 (2), 321-31, 2005.

Szczuciński, W., Chaimanee, N., Niedzielski, P., Rachlewicz, G., Saisuttichai, D., Tepsuwan, T., Lorenc, S., and Siepak, J.: Environmental and geological impacts of the 26 December 2004 tsunami in coastal zone of Thailand—overview of short and long-term effects. *Pol. J. Environ. Stud.*, 15 (5), 793–810, 2006.

Szczuciński, W., Niedzielski, P., Kozak, L., Frankowski, M., Ziola, A., and Lorenc, S.: Effects of rainy season on mobilization of contaminants from tsunami deposits left in a coastal zone of Thailand by the 26 December 2004 tsunami. *Environ. Geol.*, 53 (2), 253-64, 2007.

Takada, H., Onda, T., Harada, M., and Ogura, N.: Distribution and sources of polycyclic aromatic hydrocarbons (PAHs) in street dust from the Tokyo Metropolitan area. *Sci. Total. Environ.*, 107, 45-69, 1991.

Tarek, A.T.A., and Bernd, R.T.S.: Lipid geochemistry of surficial sediments from the coastal environment of Egypt I. Aliphatic hydrocarbons — characterization and sources. *Mar. Chem.*, 54(1-2), 135-58, 1996.

Tareq, S. M., Tanaka, N., and Ohta, K.: Biomarker signature in tropical wetland: lignin phenol vegetation index (LPVI) and its implications for reconstructing the paleoenvironment. *Sci.Tot. Environ.*, 324 (1–3), 91-103, 2004.

Tipmanee, D., Deelaman, W., Pongpiachan, S., Schwarzer, K. and., Sompongchaiyakul, P. Using Polycyclic Aromatic Hydrocarbons (PAHs) as a chemical proxy to indicate Tsunami 2004 backwash in Khao Lak coastal area, Thailand. *Nat. Hazards Earth Syst. Sci.*, 12, 1441–51, 2012.

Tsapakis, M., and Stephanou, G.E.: Polycyclic aromatic hydrocarbons in the atmosphere of the Eastern Mediterranean. *Environ. Sci. Technol.*, 39, 6854-90, 2005.

Vargas, G., Ortlieb, L., Chapron, E., Valdes, J., and Marquardt, C.: Paleoseismic inferences from a high-resolution marine sedimentary record in northern Chile (23° S). *Tectonophysics*, 399, 381 – 98, 2005.

Venkatesan, I.M., Ruth, E., Rao, S.P., Nath, N.B., and Rao, R.B.: Hydrothermal petroleum in the sediments of the Andaman Backarc Basin, Indian Ocean. *Applied Geochemistry*., 18(6), 845-61, 2003.

Volkman, J.K.: Sterols in microorganisms. *Appl. Microbiol. Biotechnol.*, 60, 496-506, 2003.

Wang, L.R., Brassell, C.S., Scarpitta, C.S., Zheng, P.M., Zhang, C.S., Hayde, R.P., and Muench, M.L.: Steroids in sediments from Zabuye Salt Lake, western Tibet: diagenetic, ecological or climatic signals? *Org. Geochem.*, 35(2), 157-68, 2004.

Wang, X. C., Zhang, Y. X., and Chen, R. F.: Distribution and Partitioning of Polycyclic Aromatic Hydrocarbons (PAHs) in Different Size Fractions in Sediments from Boston Harbor, United States. *Mar. Pollut. Bullet.*, 42 (11), 1139-49, 2001.

Watson, G.J., Robinson, F.N., Chow, C.J., Henry, C.R., Kim, M.B., Pace, G.T., Meyer, L.E., and Nguyen, Q.: The USEPA/DRI chemical mass balance receptor model, CMB 7.0. *Environ. Soft.*, 5(1), 38-49, 1990.

Watson, J.G., Chow, J.C., Lu, Z., Fujita, E.M., Lowenthal, D.H., and Lawson, D.R.: Chemical mass balance source apportionment of PM₁₀ during the Southern California air quality study. *Aerosol. Sci. Technol.*, 21, 1-36, 1994.

Watson, G.J., Chow, C.J., and Fujita, M.E.: Review of volatile organic compound source apportionment by chemical mass balance. *Atmos. Environ.*, 35(9), 1567-84, 2001.

Westerholm, R., Almen, J., Li, H., Rannug, U., and Rosen, A.: Exhaust emissions from gasoline-fuelled light duty vehicles operated in different driving conditions: a chemical and biological characterization. *Atmos. Environ.*, 26B, 79-90, 1992.

Williams, T.P., Bartle, D.K., and Andrews, E.G.: The relationship between polycyclic aromatic compounds in diesel fuels and exhaust particulates. *Fuel*., 65(8), 1150-8, 1986.

Yunker, B.M., Macdonald, W.R., Vingarzan, R., Mitchell, H.R., Goyette, D., and Sylvestre, S.: PAHs in the Fraser River basin: a critical appraisal of PAH ratios as indicators of PAH source and composition. *Org. Geochem.*, 33, 489-515, 2002.

Yunker, B.M., and Macdonald, W.R.: Petroleum biomarker sources in suspended particulate matter and sediments from the Fraser River Basin and Strait of Georgia, Canada. *Org. Geochem.*, 34, 1525-41, 2003.

Zakaria, P.M., Okuda, T., and Takada, H.: Polycyclic aromatic hydrocarbon (PAHs) and Hopanes in Stranded Tar-balls on the coasts of Peninsular Malaysia: Applications of biomarkers for identifying sources of oil pollution. *Mar. Pollut. Bulletin.*, 42(12), pp.1357-1366, 2001.

Zheng, M., Fang, M., Wang, F., and To, K.L.: Characterization of the solvent extractable organic compounds in PM_{2.5} aerosols in Hong Kong. *Atmos. Environ.*, 34, 2691-702, 2000.

Zundel, M., and Rohmer, M.: Hopanoids of the methylotrophic bacteria *Methylococcus capsulatus* and *Methylomonas* sp. As possible precursors of C₂₉ and C₃₀ hopanoid chemical fossils. *FEMS. Microbiol. Lett.*, 28(1), 61-4, 1985a.

Zundel, M., and Rohmer, M.: Prokaryotic triterpenoids 1.3-methylhopanoids from *Acetobacter* sp. and *Methylococcus capsulatus*. *Eur. J. Biochem.*, 150, 23-7, 1985b.

Zundel, M., and Rohmer, M.: Prokaryotic triterpenoids 3. The biosynthesis of 2b-methylhopanoids and 3b-methylhopanoids of *Methylobacterium organophilum* and *Acetobacter pasteurianus* spp. *Eur. J. Biochem.*, 150, 35-9, 1985c.

APPENDIX. TABLES

Table 1. Physiochemical properties of PAHs

Congeners	MW (g/mol)	MP (°C)	BP (°C)	P_s	P_L	Log K_{ow}	H	Log K_{OA}
Ace	154.2	96	277.5	0.3	1.52	3.92	12.17	6.23
Ac	150.2	92	265-275	0.9	4.14	4.00	8.40	6.47
Fl	166.2	116	295	0.09	0.72; 0.79 ^a	4.18	7.87	6.68
Phe	178.2	101	339	0.02	0.11; 0.06	4.57	3.24	7.45
1-MePh	192.3	123	359			5.14		
An	178.2	216	340	1.00E-03	7.78E-02	4.54	3.96	7.34
					1.19E-02; 8E-03			
Pyr	202.3	156	360	6.00E-04	03	5.18	0.92	8.61
Flu	202.3	111	375	1.23E-03	8.72E-03	5.22	1.04	8.60
B[a]F	216.3	187	407			5.40		
B[b]F	216.3	209	402			5.75		
							6.50E-02	
Chry	228.3	255	448	5.70E-07	1.07E-04	5.86	1.20E-02	10.44
Tri	228.3	199	438	2.30E-06	1.21E-04	5.49	02	10.80
p-terp	230.1	213		4.86E-06		6.03		
B[a]								
A	228.3	160	435	2.80E-05	6.06E-04	5.91	0.58	9.54
							4.60E-02	
B[a]P	252.3	175	495	7.00E-07	2.13E-05	6.04	02	10.77
B[e]P	252.3	178		7.40E-07	2.41E-05		0.02	
							3.00E-03	
Per	252.3	277	495	1.40E-08		6.25	03	12.17
B[b]F	252.3	168	481			5.80		
B[j]F	252.3	166	480					
							1.60E-02	
B[k]F	252.3	217	481	5.20E-08	4.12E-06	6.00	7.50E-02	11.19
B[g,h,i]P	268.4	277			2.25E-05	6.50	02	11.02
D[a,h]A	278.4	267	524	3.70E-10	9.16E-08	6.75		
Cor	300.4	>350	525	2.00E-10		6.75		

Source: <http://www.es.lanacs.ac.uk/ecerg/kcjgroup/5.html>

MP (°C) Melting Point

BP (°C) Boiling Point

P_s Vapour pressure of solid substance

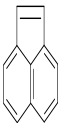
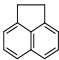
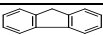
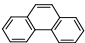
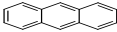
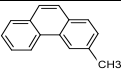
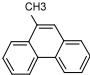
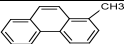
P_L Vapour pressure of subcooled liquid

K_{ow} Octanol-water partition coeffic

H Henry 's Law Constant

K_{oa} Octanol-air partition coefficient

Table 2. Chemical structures of PAHs

Congener	Abbreviation	M.W. [g]	Chemical Structure
Acenaphthylene	Ac	152	
Acenaphthene	Ace	154	
Fluorene	Fl	166	
Phenanthrene	Phe	178	
Anthracene	An	178	
3-Methyl Phenanthrene	3-MePhe	192	
9-Methyl Phenanthrene	9-MePhe	192	
1-Methyl Phenanthrene	1-MePhe	192	

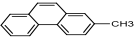
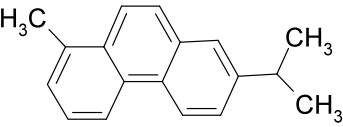
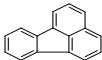
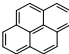
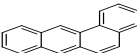
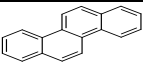
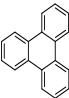
2-Methyl Phenanthrene	2-MePhe	192	
1-methyl-7-isopropyl phenanthrene (Retene)	Ret	234	
Fluoranthene	Fluo	202	
Pyrene	Py	202	
Benz[<i>a</i>]anthracene	B[<i>a</i>]A	228	
Chrysene	Chry	228	
Triphenylene	Tri	228	

Table 3. Chemical structures of alkanes.




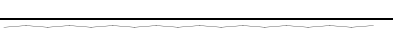
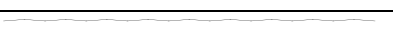

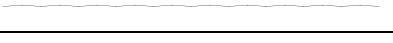
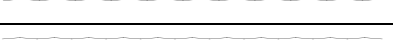

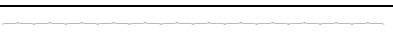

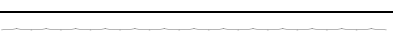

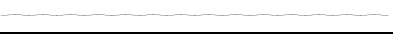
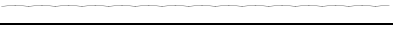
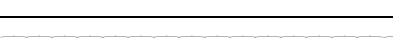
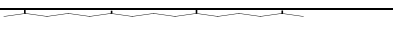
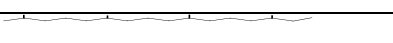
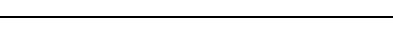


Congener	Abbreviation	M.W. [g]	Chemical Structure
Tetradecane	C ₁₄	198	
Pentadecane	C ₁₅	212	
Hexadecane	C ₁₆	226	
Heptadecane	C ₁₇	268	
Octadecane	C ₁₈	254	
Nonadecane	C ₁₉	268	
Eicosane	C ₂₀	282	
Heniacosane	C ₂₁	296	
Docosane	C ₂₂	310	
Tricosane	C ₂₃	324	
Tetracosane	C ₂₄	338	
Pentacosane	C ₂₅	352	
Hexacosane	C ₂₆	366	
Heptacosane	C ₂₇	380	
Octacosane	C ₂₈	394	
Nonacosane	C ₂₉	408	
Triacontane	C ₃₀	422	
Hentriacontane	C ₃₁	436	
Dotriacontane	C ₃₂	450	
Pristane	PC ₁₉	268	
Phytane	PC ₂₀	282	

Table 4. Chemical structures of hopanes.

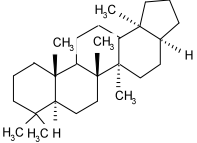
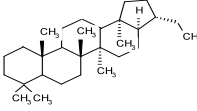
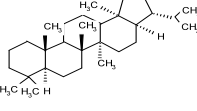
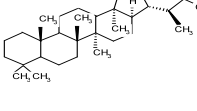
Congener	Abbreviation	M.W. [g]	Chemical Structure
17 α (H)-22,29,30-Trisnorhopane	22,29,30-trisnorhopane (th)	370	
17 α (H),21 β (H)-30-Norhopane	17,21,ab-30-norhopane (nh)	398	
17 α (H),21 β (H)-Hopane	17,21,ab-hopane (hop)	412	
17 α (H),21 β (H)-22R-Homohopane	22R-17,21ab-30-homohopane (homo)	426	

Table 5. Chemical structures of cholestanes.

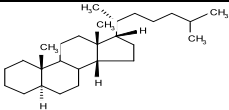
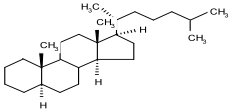
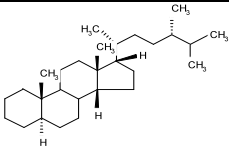
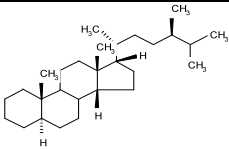
Congener	Abbreviation	M.W. [g]	Chemical Structure
$\alpha\beta\beta$ 20R-Cholestane	20R-abb-cholestane (abbC)	372	
$\alpha\alpha\alpha$ 20R-Cholestane	20R-aaa-cholestane (aaaC)	372	
$\alpha\beta\beta$ 20R 24S-Methylcholestane	20R-abb-methylcholestane (MC)	386	
$\alpha\beta\beta$ 20R 24R-Ethylcholestane	20R-abb-ethylcholestane (EC)	400	

Table 6. ΣPAH concentrations in different regions

Location	Sample Type	ΣPAHs [ng m ⁻³]	Reference
UK (London,Bounds Green)	TSP	4.27 (0.23-27.87)	Kendall et al., 2001
UK (London, St Paul)	TSP	7.24 (1.04-32.04)	Kendall et al., 2001
Indonesia (Pudu)	PM ₁₀	26.5 (7-46)	Fang et al., 1999
Greece (Rural Area)	TSP	1.1 (0.2-2.0)	Gogou et al., 1996
Greece (Heraklion)	TSP	17.4 (3.2-44.9)	Gogou et al., 2000
Portugal (Forest)	TSP	0.5 (0.1-0.9)	Kavouras et al., 1999
China (Hong Kong)	PM _{2.5}	9.6 (0.7-12.2)	Zheng et al., 2000
China (Guangzhou)	TSP	73.7 (32.5-153.7)	Duan et al., 2005
Canada (Urban)	TSP	2.35 (1.86-2.83)	Sanderson et al., 2004
Eastern Mediterranean	TSP	0.7 (0.3-1.6)	Tsapakis and Stephanou, 2005
Canada (Toronto)	P+V	36.5 (11.5-61.4)	Motelay et al., 2005
Traffic, Hong Kong	PM _{2.5}	33.96	Gou et al., 2003
Industrial, Hong Kong	PM _{2.5}	16.72	Gou et al., 2003
Industrial (indoor), Shizuoka, Japan	PM _{2.5}	1.6–23.7	Ohura et al., 2004
Industrial (outdoor), Shizuoka, Japan	PM _{2.5}	1.1–29.5	Ohura et al., 2004
Pastureland (open) Taichung, Taiwan	PM _{2.5}	74.47	Fang et al., 2006
Temple (semi-open) Taichung, Taiwan	PM _{2.5}	284.91	Fang et al., 2006
Traffic Guangzhou, China	PM _{2.5}	57.89	Li et al., 2005
Residential Guangzhou, China	PM _{2.5}	27.06	Li et al., 2005

Table 7. Biological and/or environmental interpretation of *n*-alkanes

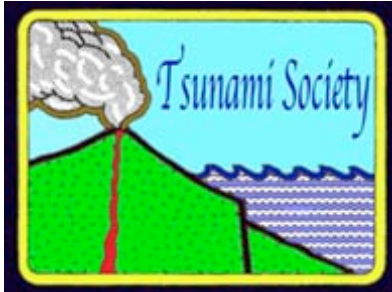
Biomarker	Biological and/or environmental interpretation	References
Outstanding concentrations of n15, n17 and n19 in early Paleozoic rocks	Marine phytoplankton of uncertain affinity, probably an alga, identified in Cambrian Devonian sediments but most prominent in Ordovician.	Blokker <i>et al.</i> , 2001
<i>n</i> -C ₂₇ with OEP ¹	Estonian kukersite is a typical source Waxes derived from higher plants, terrestrial input, post-Silurian age	Hedberg, 1968
<i>n</i> -C ₄₀	Predominantly degradation products of aliphatic macromolecules such as algaenan (marine, lacustrine), cutan and suberan (terrestrial, plant derived)	Allard <i>et al.</i> , 2002 Killops <i>et al.</i> , 2000

Table 8. Biological and /or environmental interpretation of hopanes

Biomarker	Biological and/or environmental interpretation	References
C ₃₀ -hopanes	Diverse bacterial lineages, few eukaryotic species (e.g. some cryptogams, ferns, mosses, lichens, filamentous fungi, protests)	Rohmer <i>et al.</i> , 1984
Extended C ₃₁ to C ₃₅ hopanes (homohopanes)	Diagnostic for bacterial, biosynthesis appears to be restricted to lineages that are not strictly anaerobic	Ourisson and Albrecht, 1992, Rohmer <i>et al.</i> , 1984
Extended C ₃₂ to C ₃₆ 3b-methylhopanes	Diagnostic for some microaerophilic proteobacteria (certain methylotrophs, methanotrophs, acetic acid bacteria)	Zundel and Rohmer., 1985a, 1985b, 1985c.
28,30-dinorhopane, 25,28,30-trinorhopane	Often prominent in sediments from euxinic environment	Grantham <i>et al.</i> , 1980

Table 9. Biological and /or environmental interpretation of cholestanes

Biomarker	Biological and/or environmental interpretation	References
24-norcholestane (C ₂₆)	Possible diatom origin, high concentrations relative to 27-norcholestane indicate	Holba <i>et al.</i> , 1998a and 1998b
Cholestane	Cretaceous or younger crude oil In aquatic sources probably almost exclusively derived from diverse eukaryotes	Volkman, 2003
24- <i>n</i> -propylcholestane	Pelagophyte algae, a biomarker for marine conditions with few exceptions	Moldowan <i>et al.</i> , 1990
4-Methylcholestane and 4,4-dimethylcholestane	Diverse eukaryotic sources, high concentrations likely indicate a dinoflagellates origin	Summons <i>et al.</i> , 1994



**MARINE CONGLOMERATE AND REEF MEGACLASTS AT MAURITIUS ISLAND:
Evidences of a tsunami generated by a flank collapse of the
PITON DE LA Fournaise volcano, Reunion Island?**

R. Paris^{1,2}, K. Kelfoun^{1,2}, T. Giachetti³

¹Clermont Université, Université Blaise Pascal, BP 10448, F-63000 Clermont-Ferrand, France

*Corresponding author : r.paris@opgc.univ-bpclermont.fr

²CNRS, UMR 6524, Magmas et Volcans, F-63038 Clermont-Ferrand, France

³Department of Earth Science, Rice University, Houston, TX 77005, USA

ABSTRACT

Tsunamis related to volcano flank collapse are typically a high-magnitude, low frequency hazard for which evaluation and mitigation are difficult to address. In this short communication, we present field evidences of a large tsunami along the southern coast of Mauritius Island ca. 4400 years ago. Tsunami deposits described include both marine conglomerates and coral boulders up to 90 m³ (> 100 tons). The most probable origin of the tsunami is a flank collapse of Piton de la Fournaise volcano, Réunion Island.

Keywords: *tsunami deposits; volcano flank failure; Mauritius Island; Reunion Island*

1. INTRODUCTION

Massive flank failures of volcanic edifices are evidenced by large submarine complexes of debris and scars both onshore and offshore. Although these low-frequency but high magnitude hazards are well documented on the geological point of view, there are still uncertainties on their rheology and timing (e.g. multistage or en masse), especially in the case of large-volume failures affecting ocean islands. These events have the potential to generate giant tsunami waves, but numerical models and hazard assessment are limited by uncertainties on the volume, velocity and rheology of the falling mass (e.g. Giachetti et al., 2011). The largest lateral collapse of an island volcano recorded in historical times ($\sim 5 \text{ km}^3$) took place during the 1888 eruption of Ritter Island (New Guinea), producing 10-15 m high waves all around Bismarck Sea (Ward and Day, 2003). The most recent tsunami caused by flank collapse occurred in December 2002 at Stromboli volcano. Despite its small volume ($17 \times 10^6 \text{ m}^3$), the landslide produced a tsunami with a maximum run-up of 8 m on the coasts of Stromboli, but had limited far-field effects (Maramai et al., 2005).

The scarcity of observations encourages geologists to find proxies for reconstructing past tsunamis generated by volcano flank failures. A promising proxy is the identification and characterisation of tsunami deposits, i.e. deposits left inland by tsunami waves. Marine conglomerates found at unusually high elevations in Hawaii (Moore and Moore, 1984, 1988; Moore et al., 1994; Moore, 2000; Rubin et al., 2000; McMurtry et al., 2004), Cape Verde (Paris et al., 2011) and the Canary Islands (Paris et al., 2004; Pérez Torrado et al., 2006) are often interpreted as being the result of giant tsunami waves generated by massive flank failures of volcanic islands. Nevertheless, some of the units or facies of such conglomerates at Lanai and Molokai (Hawaii) were also interpreted as uplifted coastal and shallow marine deposits (Grigg and Jones, 1997; Felton 2002; Felton et al., 2006; Crook and Felton, 2008). The coral-bearing deposits studied by McMurtry et al. (2004) at Kohala, on the island of Hawaii, are less controversial than the Lanai and Molokai deposits, since the subsidence of this island is well established (e.g. Moore, 1971). Considering the subsidence rate and the present-day maximum elevation of the deposits (61 m a.s.l.), the run-up of the tsunami is estimated to be higher than 400 m. The tsunami conglomerate described by Pérez-Torrado et al. (2006) on Gran Canaria (Canary Islands) is attached to the slopes of a valley, and is found up to an altitude of 188 m. A massive flank failure on the eastern coast of Tenerife is the most probable source of this tsunami (Güímar failure $\sim 0.83 \text{ Ma}$, $\sim 44 \text{ km}^3$: Carracedo et al., 2011; Giachetti et al., 2011). Similar tsunami conglomerates were described by Paris et al. (2011) in Cape Verde and interpreted as an evidence of a flank collapse of Fogo volcano ~ 90 -100 kyrs ago.

The distinction between tsunami conglomerates and other rocky coast deposits relies on a suite of sedimentological, morphological and chronological criteria (Stearns, 1978; Moore and Moore, 1984, 1988; Moore et al., 1994; Shiki and Yamasaki, 1996; Moore, 2000; Rubin et al., 2000; Le Roux et al., 2004; McMurtry et al., 2004; Le Roux and Vargas, 2005; Pérez-Torrado et al., 2006; Paris et al., 2011). Tsunami conglomerates are typically attached to the topography and preserved at different elevations, whereas emerged marine deposits typically show great lateral continuity along elevated terraces. The elevation of these marine terraces fall within the range of sea-level changes (highstands), though vertical motions (uplift) must also be taken into account. Marine deposits display a large

variety of sedimentary facies corresponding to specific shoreface to backshore environments. At the contrary, tsunami conglomerates result in a mixing of offshore, coastal and subaerial sediments. Marine bioclasts found in tsunami deposits are never in live or growth position. The internal stratification, or organisation, in subunits is not a key-feature of tsunami deposits, but together with clast-fabrics it can indicate successive inflows (landward imbrication) and outflows (seaward imbrication). In terms of mean grain size and thickness, landward fining and thinning may occur in tsunami conglomerates, but this alone cannot be considered as a unique diagnostic criteria. More convincing is the identification of rip-up clasts of the substratum in the lower part of a marine conglomerate, attesting for an erosive emplacement.

2. RÉUNION ISLAND AS A POSSIBLE SOURCE OF TSUNAMIS IN THE INDIAN OCEAN

Réunion Island represents a possible source of tsunamis in the Indian Ocean, as more than 40 failures from the flanks of Piton des Neiges and Piton de la Fournaise shield volcanoes occurred during the last 2 Myrs (Labazuy 1996, Oehler et al., 2004). A large eastward (seaward) ground displacement was recorded by InSAR monitoring during the April 2007 eruption at Piton de la Fournaise (Augier et al., 2009), which is one of the more active volcanoes in the world. The last major flank failure of Piton de la Fournaise volcano may have occurred ca. 4500 years ago (Bachelery & Mairine, 1990; Labazuy, 1996). Numerical simulations of different scenarios of flank collapses were realised by Kelfoun et al. (2010). As an example of worst-case scenario, a 10 km³ landslide on the eastern flank of Piton de la Fournaise volcano would generate waves up to 80 m high at the southern coast of Mauritius Island, which is located 170 km ENE of Réunion Island (Fig. 1).



Fig. 1. Sampling sites along the southern coast of Mauritius Island (Indian Ocean) and location of the Beau Champ marine conglomerate (in yellow), interpreted as an evidence of tsunami.

With the aim of identifying sedimentary evidences of past tsunamis, we surveyed the southern coast of Mauritius Island. In order to avoid confusion with deposits left inland by earthquake-induced tsunamis and cyclones, we have not considered coastal deposits and focused on evidences of marine inundation in terrestrial environments. Both Mauritius and Réunion islands were impacted by the 1883 Krakatau, 2004 Sumatra and 2010 Mentawai tsunamis, but wave runups were respectively below 7 m, 3 m and 2 m a.s.l. (Okal et al., 2006; Sahal et al., 2011; Sahal and Morin, 2012). Cyclone deposits are observed at altitudes always lower than 3 m (Montaggioni, 1978).

3. MARINE CONGLOMERATE IN MAURITIUS ISLAND

The most convincing evidence of tsunami inundation at high grounds is a marine conglomerate found between 10 and 15 m a.s.l. at several locations near Beau Champ (20°30'28"S / 57°26'19"E). The conglomerate is 20-45 cm thick, intercalated in a reddish lateritic soil at a depth of -50 to -80 cm from one section to another (Fig. 2).

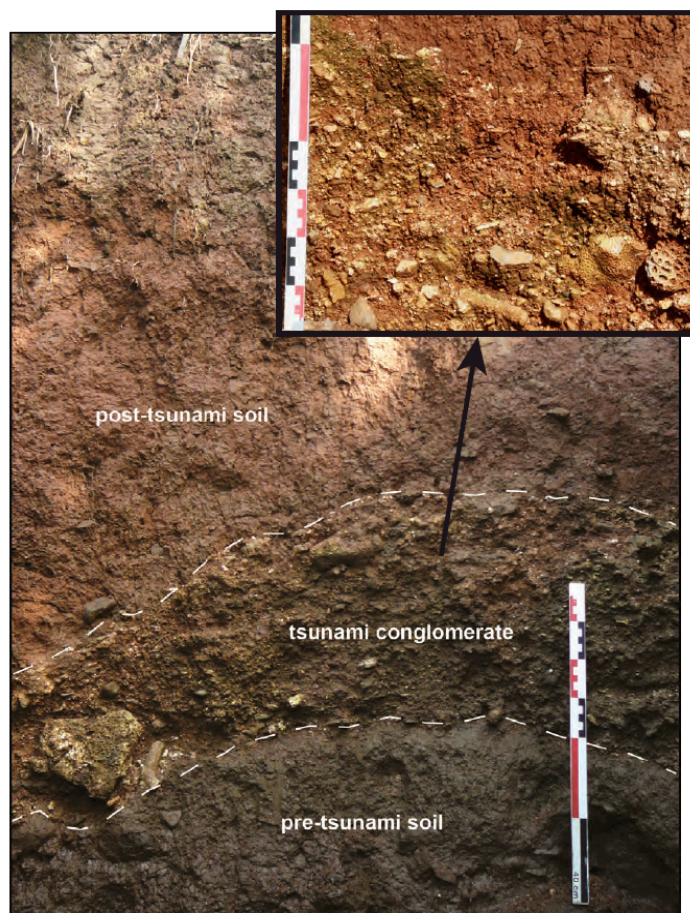


Fig. 2. Tsunami conglomerate (coral and shells fragments) at a depth of 70 cm near Beau Champ (altitude 11 m a.s.l.). Note the irregular and sharp contacts with soils below and above the event unit. The marine conglomerate is composed of corals (both branching forms and brain corals) and shell fragments (bivalves and gastropods). A ^{14}C age of 4425 ± 35 BP was obtained on a coral branch (this work).

It is very poorly sorted and its composition reflects a mixing of two sediment sources: (1) marine bioclasts such as debris of corals (branching forms and brain corals), gastropods, and fragments of shells, and (2) fragments of volcanic rocks and minerals, from sand-size to pebbles. The mean thickness and grain size of the conglomerate fines landward. Basal contact with the underlying paleo-soil is erosive. The ^{14}C age of 4425 ± 35 BP obtained on a coral branch (*Poznan Radiocarbon Laboratory, Poland*) represents a minimum age for the conglomerate, since it is not determined if the coral dated was alive or dead before being transported landward. Due to many similarities with the criteria mentioned above, the marine conglomerate found at Beau Champ could represent an evidence of tsunami in Mauritius ca. 4400 years ago.

4. REEF-MEGACLASTS AT UNUSUAL ALTITUDES

The marine conglomerate described in this study is not the only sedimentary evidence of tsunami in Mauritius Island. Reef megaclasts were previously described by Montaggioni (1978) at unusual altitudes (3-40 m) for marine deposits (i.e. not linked to sea level high stands) along the coasts of Mauritius and Rodrigues islands. Uncalibrated ^{14}C and U/Th ages of these blocks range between 3730 ± 100 BP and 6200 ± 800 BP (Montaggioni 1978). Diversity of the sedimentary facies and random orientation of the blocks (e.g. overturned) show that they were not in growth position and could not correspond to in-situ remnants of old reefs. Most of these reef fragments are located between 3 and 15 m, but L. Montaggioni also mentioned a 2 m^3 *Porites* dome at 40 m a.s.l. (Coin de Mire, northern coast). The largest megaclast (100 m^3) was found at 4 m a.s.l. near Tamarin (western coast). Between Montaggioni's observations and our survey (April 2010) some of these megaclasts have been destroyed, and tsunami evidence is getting more or more erased by new buildings. A 90 m^3 coral megaclast dated 5220 ± 150 BP (uncalibrated) by Montaggioni (1978) was found preserved close to the marine conglomerate at Beau Champ (Fig. 3). The long axis of the block is oriented N140°, tangent to a flow coming from the southwest.

Many studies demonstrated that elongated boulders moved by tsunamis tend to dispose their long axis tangent to flow direction (e.g. Mastronuzzi and Sansò, 2000; Whelan and Kelletat, 2005; Goto et al., 2007; Paris et al., 2009; Etienne et al., 2011). Considering its dimensions and assuming a density of 1.2 g/cm^3 , this megaclast (length: 7 m; width: 5 m; height: 1.5-4 m) requires flow velocities higher than 3.6 m/s to be transported, if we assume that the block was already detached from its substratum, and 8.0 m/s if joint-bounded on the outer reef (based on equations proposed by Nandasena et al., 2011). Same calculations for the 100 m^3 megaclast in Tamarin yields minimum flow velocities between 5 m/s (free block) and 16.7 m/s (joint-bounded) if we assume a density of 1.8 g/cm^3 (beach rock). It is actually impossible to state if the megaclasts considered here were already detached from their substratum (e.g. by cyclonic swells or previous tsunamis) or joint-bounded.

Rough estimates of flow depth can then be proposed considering the minimum flow velocities and different values of Froude numbers $\text{Fr} = U / (gh)^{0.5}$, where U is the flow velocity, g is the acceleration due to gravity and h is the flow depth). Fr is a non-dimensional number that describes whether a flow is supercritical (>1), critical ($=1$), or subcritical (<1). For a tsunami, Fr varies spatially and temporally.

Tsunami flow is usually subcritical, with Fr ranging typically from 0.6 to 1, but supercritical conditions can be expected at the leading front, with Fr up to 2. Assuming that the reef megaclasts were joint-bounded and that $Fr = 1.5$ at the wave's front, flow depth estimates range between 3 m (Beau Champ megaclast) and 13 m (Tamarin megaclast). For $Fr = 1$ and $Fr = 0.5$, flow depth increases respectively to 28 m and 110 m.



Fig. 3. Reef megaclast near Beau Champ, dated 5220 ± 150 BP (uncalibrated) by Montaggioni (1978). Assuming a density of 1.2 g/cm^3 and a volume of 90 m^3 , the block has a mass > 100 tons.

5. ORIGIN OF THE TSUNAMI DEPOSITS IN MAURITIUS ISLAND

Sedimentary evidences of tsunami were found preserved on the southern coast of Mauritius Island, at altitudes ranging between 10 and 15 m (up to 40 m if we include coral boulders previously mentioned by Montaggioni, 1978). The most suitable source of tsunamis with wave heights higher than 3 m in Mauritius is a flank failure in Réunion Island ca. 4.4 kyrs, which is located 170 km WSW

of the southern coast of Mauritius. The size and altitude of the reef megaclasts and conglomerate found in Mauritius do not necessarily require very large waves to be emplaced and deposited at an altitude of 15 m. However, the characteristics of sediments transported and deposited by tsunamis do not only depend on flow characteristics but also on the kind and size of sediments available (e.g. limited by the maximum size of reef megaclasts available). We were not able to find evidences of smaller reef clasts at altitudes higher than 15 m, but they might have been remobilised by post-tsunami erosion or destroyed by farming. Szczuciński (2011) reinvestigated the 2004 Indian Ocean tsunami deposits along the Andaman coast of Thailand four years after the tsunami. He found that in about 50% of the sites, the deposits were not preserved, and when preserved, their internal structure was often blurred by bioturbation. Extrapolating these observations over a period of 4000 years suggests that the marine conglomerate found at Beau Champ is clearly the relict of a wider formation which was reworked soon after the tsunami. Destruction of vegetation by the tsunami would have enhanced slope erosion, especially in such a humid tropical environment.

When trying to link the sedimentary evidences of a tsunami to its physical characteristics (flow velocity, depth), other uncertainties are related to the source mechanisms. In the case of a flank failure, the way the collapsing mass is released (velocity, in one go or multistage) is a key parameter in the determination of the characteristics of the resulting tsunami, as confirmed by numerical simulations (e.g. Kelfoun et al., 2010; Giachetti et al., 2011; Paris et al., 2011). The rheology chosen to simulate the landslide propagation (e.g. frictional or constant retarding stress) has only a second-order impact on the produced waves (Giachetti et al., 2011, 2012). Hunt et al. (2012) studied distal turbidites around the Canary Islands and proposed that some volcano flank failures are multistage retrogressive failures, separated by short gaps, and thus have a lower tsunamigenic potential compared to failures in one go. The youngest debris avalanche complex identified on the eastern flank of the Piton de la Fournaise volcano (Râle Poussé) is also sub-organised in three different units (Labazuy, 1996; Oehler et al., 2004): the first unit ($< 10 \text{ km}^3$) would correspond to the main failure, followed by two phases of reworking implying lower volumes (Oehler et al., 2004).

6. CONCLUSIONS

Sedimentary evidences of tsunami inundation are preserved along the southern coast of Mauritius Island. The more convincing deposits were found near Beau Champ, where reef megaclasts described by Montaggioni (1978) are associated with a marine conglomerate at altitudes ranging between 10 and 15 m a.s.l. This is far higher than the altitudes usually reached by earthquake-induced tsunamis (e.g. 2004 Indian Ocean tsunami), cyclone and marine high stand deposits along this coast. The most probable source for this tsunami is a flank failure of Piton de la Fournaise volcano in Réunion Island, which is located 170 km WSW of Mauritius. The age of the marine conglomerate ($< 4400 \text{ ka}$) is concordant with the age of the last flank failure at Fournaise volcano (ca. 4500 ka). However, it is actually difficult to propose an inverse model of the failure (volume, fall velocity, in one go or multistage) from the characteristics of the tsunami deposits (e.g. maximum altitude, size of the reef megaclasts).

ACKNOWLEDGEMENTS

The authors are particularly grateful to Lucien Montaggioni for providing documents on reef megaclasts, to Eyjafjöll volcano (Iceland) for postponing our survey, to Mauritian samosas cooked in oil (the most dangerous ones) and to the Mauritian police. This work was funded by French ANR (*Agence Nationale de la Recherche*) program “Young Scientist” 2008 – project VITESSS (Volcano-Induced Tsunamis: Sedimentary Signature and numerical Simulation) whose leader is Raphaël Paris. This is Laboratory of Excellence *ClerVolc* contribution n° X.

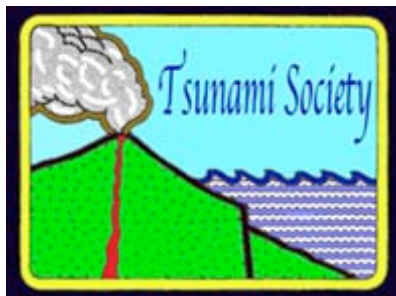
REFERENCES

- AUGIER, A., FROGER, J.L., CAYOL, V., BYRDINA, S., SOURIOT, T., STAUDACHER, T. (2009), Understanding the April 2007 eruption at Piton de la Fournaise, Réunion Island, from ENVISAT-ASAR and ALOS-PALSAR satellite data. *International Lithosphere Program Joint Task Force Meeting*, Clermont-Ferrand, France, 05-09/10/2009.
- BACHÉLERY, P., MAIRINE, P. (1990), Evolution volcano-structurale du Piton de la Fournaise depuis 0.53 Ma. In: Lénat J.F. (Ed.), *Le volcanisme de la Réunion, monographie*. Centre de Recherches en Volcanologie, Clermont-Ferrand, France, 213–242.
- CARRACEDO, J.C., GUILLOU, H., NOMADE, S., RODRÍGUEZ BADIOLA, E., PÉREZ TORRADO, F.J., RODRÍGUEZ GONZÁLES, A., PARIS, R., TROLL, V.R., WIESMAIER, S., DELCAMP, A., FERNÁNDEZ TURIEL, J.L. (2011), Evolution of ocean island rifts: the northeast rift-zone of Tenerife, Canary Islands. *Geological Society of America Bulletin* 123, 562–584.
- CROOK, K.A.W., FELTON, E.A. (2008), Sedimentology of rocky shorelines : 5. The marine samples at +326m from ‘Stearns swale’ (Lanai, Hawaii) and their paleo-environmental and sedimentary process implications. *Sedimentary Geology* 206, 33–41.
- ETIENNE, S., BUCKLEY, M., PARIS, R., NANDASENA, N.A.K., CLARK, K., STROTZ, L., CHAGUÉ-GOFF, C., GOFF, J., RICHMOND, B. (2011), The use of boulders for characterising past tsunamis: lessons from the 2004 Indian Ocean and 2009 South Pacific tsunamis. *Earth-Science Reviews* 107, 76–90.
- FELTON, E.A. (2002), Sedimentology of rocky shorelines : 1. A review of the problem, with analytical methods, and insights gained from the Hulopoe Gravel and the modern rocky shoreline of Lanai, Hawaii. *Sedimentary Geology* 152, 221–245.
- FELTON, E.A., CROOK, K.A.W., KEATING, B.H., KAY, E.A. (2006), Sedimentology of rocky shorelines : 4. Coarse gravel lithofacies, molluscan biofacies, and the stratigraphic and eustatic records in the type area of the Pleistocene Hulopoe Gravel, Lanai, Hawaii. *Sedimentary Geology* 184, 1–76.
- FRITZ, H.M., BORRERO, J.C., SYNOLAKIS, C.E., YOO, J. (2006), 2004 Indian Ocean tsunami flow velocity measurements from survivor videos. *Geophysical Research Letters* 33, L24605.

- GIACHETTI, T., PARIS, R., KELFOUN, K., PÉREZ TORRADO, F.J. (2011), Numerical modelling of the tsunami triggered by the Güimar debris avalanche, Tenerife (Canary Islands): comparison with field-based data. *Marine Geology* 284, 189-202.
- GIACHETTI, T., PARIS, R., KELFOUN, K., ONTOWIRJO, B. (2012), Tsunami hazard related to a flank collapse of Anak Krakatau Volcano, Sunda Strait, Indonesia. *Geological Society, London, Special Publications* 361, 79-90.
- GOTO, K., CHAVANICH, S.A., IMAMURA, F., KUNTHASAP, P., MATSUI, T., MINOURA, K., SUGAWARA, D., YANAGISAWA, H. (2007), Distribution, origin and transport process of boulders deposited by the 2004 Indian Ocean tsunami at Pakarang Cape, Thailand. *Sedimentary Geology* 202, 821-837.
- GRIGG, R.W., JONES, A.T. (1997), Uplift caused by lithospheric flexure in the Hawaiian archipelago, as revealed by elevated coral deposits. *Marine Geology* 141, 11-25.
- HUNT, J.E., WYNN, B.W., MASSON, D.G., TALLING, P.E., TEAGLE, D.A.H. (2011), Sedimentological and geochemical evidence for multistage failure of volcanic island landslides: a case-study from Icod landslide on north Tenerife, Canary Islands. *G3: Geochemistry, Geophysics and Geosystems* 12(1).
- KELFOUN, K., GIACHETTI, T., LABAZUY, P. (2010), Landslide-generated tsunamis at Reunion Island. *Journal of Geophysical Research*, F04012.
- LABAZUY, P. (1996), Recurrent landsliding events on the submarine flanks of Piton de la Fournaise volcano (Reunion Island). In: McGuire, W.J., Jones, A.P., Neuberg, J. (Eds.), Volcano instability on the Earth and other planets. *Geological Society, London, Special Publications* 110, 293-306.
- LE ROUX, J.P., GÓMEZ, C., FENNER, J., MIDDLETON, H. (2004), Sedimentological processes in a scarp-controlled rocky shoreline to upper continental slope environment, as revealed by unusual sedimentary features in the Neogene Coquimbo Formation, north-central Chile. *Sedimentary Geology* 165, 67-92.
- LE ROUX, J.P., VARGAS, G. (2005), Hydraulic behavior of tsunami backflows: insight from their modern and ancient deposits. *Environmental Geology* 49, 65-75.
- MASTRONUZZI, G., SANSÒ, P. (2000), Boulders transport by catastrophic waves along the Ionian coast of Apulia (southern Italy). *Marine Geology* 170, 93-103.
- MCMURTRY, G.M., FRYER, G.J., TAPPIN, D.R., WILKINSON, I.P., WILLIAMS, M., FIETZKE, J., GARBE-SCHOENBERG, D., WATTS, P. (2004), Megatsunami deposits on Kohala volcano, Hawaii, from flank, collapse of Mauna Loa. *Geology* 32 (9), 741-744.
- MONTAGGIONI, L. (1978), *Recherches géologiques sur les complexes récifaux de l'archipel des Mascareignes (Océan Indien Occidental)*. Thèse d'Etat, Université d'Aix-Marseille, France.
- MOORE, A.L. (2000), Landward fining in onshore gravel as evidence for a late Pleistocene tsunami on Molokai, Hawaii. *Geology* 28 (3), 247-250.
- MOORE G.W., MOORE J.G. (1988), Large-scale bedforms in boulder gravel produced by giant waves in Hawaii. *Geological Society of America Special Paper* 229, 101-110.
- MOORE, J.G. (1971), Relationship between subsidence and volcanic load, Hawaii. *Bulletin Volcanologique* 34, 562-576.

- MOORE J.G., MOORE G.W. (1984), Deposit from a giant wave on the island of Lanai, Hawaii. *Science* 226, 1312-1315.
- MOORE, J.G., BRYAN, W.B., LUDWIG, K.R. (1994), Chaotic deposition by a giant wave, Molokai, Hawaii. *Geological Society of America Bulletin* 106, 962-967.
- NANDASENA, N.A.K., PARIS, R., TANAKA, N. (2011), Reassessment of hydrodynamic equations to initiate boulder transport by high energy events (storms, tsunamis). *Marine Geology* 281, 70-84.
- NANDASENA, N.A.K., SASAKI, Y., TANAKA, N. (2012), Modeling field observations of the 2011 Great East Japan tsunami: efficacy of artificial and natural structures on tsunami mitigation. *Coastal Engineering* 67, 1-13.
- OEHLER, J.-F., LABAZUY, P., LÉNAT, J.F. (2004), Recurrence of major flank landslides during the last 2–Ma—history of Réunion Island. *Bulletin of Volcanology* 66, 585–598.
- OKAL, E. A., SLADEN, A., AND OKAL, E.A. (2006), Rodrigues, Mauritius, and Réunion islands field survey after the December 2004 Indian Ocean tsunami. *Earthquake Spectra* 22, 241–261.
- PARIS, R., PÉREZ TORRADO, F.J., CABRERA, M.C., SCHNEIDER, J.L., WASSMER, P., CARRACEDO, J.C. (2004), Tsunami-induced conglomerates and debris flow deposits on the western coast of Gran Canaria (Canary Islands). *Acta Vulcanologica* 16(1), 133-136.
- PARIS, R., WASSMER, P., SARTOHADI, J., LAVIGNE, F., BARTHOMEUF, B., DESGAGES, E., GRANCHER, D., BAUMERT, P., VAUTIER, F., BRUNSTEIN, D., GOMEZ, C. (2009), Tsunamis as geomorphic crises: Lessons from the December 26, 2004 tsunami in Lhok Nga, West Banda Aceh (Sumatra, Indonesia). *Geomorphology* 104, 59-72.
- PARIS, R., GIACHETTI, T., CHEVALIER, J., GUILLOU, H., FRANK, N. (2011), Tsunami deposits in Santiago Island (Cape Verde archipelago) as possible evidence of a massive flank failure of Fogo volcano. *Sedimentary Geology* 239, 129-145.
- PÉREZ TORRADO, F.J., PARIS, R., CABRERA, M.C., SCHNEIDER, J.L., WASSMER, P., CARRACEDO, J.C., RODRIGUEZ SANTANA, A., SANTANA, F. (2006), The Agaete tsunami deposits (Gran Canaria): evidence of tsunamis related to flank collapses in the Canary Islands. *Marine Geology* 227 (1-2), 137-149.
- RUBIN, K.H., FLETCHER III, C.H., SHERMAN, C. (2000), Fossiliferous Lana'i deposits formed by multiple events rather than a single giant tsunami. *Nature* 408, 675-681.
- SAHAL, A., MORIN, J. (2012), Effects of the October 25th, 2010 Mentawai tsunami in La Réunion Island (France): observations and crisis management. *Natural Hazards* 62, 1125–1136.
- SAHAL, A., MORIN, J., SCHINDELÉ, F., LAVIGNE, F. (2011), A catalog of tsunamis in La Réunion island from August 27th, 1883 to October 26th, 2010. *Science of Tsunami Hazards* 30, 178–190.
- SHIKI, T., YAMAZAKI, T. (1996), Tsunami-induced conglomerates in Miocene upper bathyal deposits, Chita Peninsula, central Japan. *Sedimentary Geology* 104, 175-188.
- SPIESKE, M., WEISS, R., BAHLBURG, H., ROSKOSCH, J., AMIJAYA, H. (2010), The TsuSedMod inversion model applied to the deposits of the 2004 Sumatra and 2006 Java tsunami and implications for estimating flow parameters of palaeo-tsunami. *Sedimentary Geology* 224, 29-37.

- STEARNS, H.T. (1978), *Quaternary shorelines in the Hawaiian Islands*. Bernice P. Bishop Museum Bulletin 237, 57.
- SZCZUCIŃSKI, W. (2012), The post-depositional changes of the onshore 2004 tsunami deposits on the Andaman Sea coast of Thailand. *Natural Hazards* 60, 115-133.
- WHELAN, F., KELLETAT, D. (2005), Boulder deposits on the southern Spanish Atlantic coast: possible evidence for the 1755 AD Lisbon tsunami? *Science of Tsunami Hazards* 23, 25-38.



ISSN 8755-6839

SCIENCE OF TSUNAMI HAZARDS

Journal of Tsunami Society International

Volume 32

Number 4

2013

Copyright © 2013 - TSUNAMI SOCIETY INTERNATIONAL

TSUNAMI SOCIETY INTERNATIONAL, 1741 Ala Moana Blvd. #70, Honolulu, HI 96815, USA.

WWW.TSUNAMISOCIETY.ORG